

STATUS OF THESIS

Title of thesis

Fully Decoupled Controller Models for Voltage Source Converter
based High Voltage DC Transmission

I AHMED MAHJOUR AHMED MAHJOUR

Hereby allow my thesis to be placed at the Information Resource Center (IRC) of
Universiti Teknologi PETRONAS (UTP) with the following conditions:

1. The thesis becomes the property of UTP.
2. The IRC of UTP may make copies of the thesis for academic purposes only.
3. This thesis is classified as

Confidential

Non-confidential

If this thesis is confidential, please state the reason:

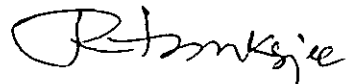
The contents of the thesis will remain confidential for _____ years.

Remarks on disclosure:

Endorsed by



AHMED MAHJOUR AHMED
Universiti Teknologi PETRONAS
Bandar Seri Iskandar, Tronoh, 31750
Perak, Malaysia
Date: 27/7/2009



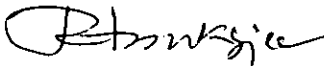
RAVINDRA N. MUKERJEE
Universiti Teknologi PETRONAS
Bandar Seri Iskandar, Tronoh, 31750
Perak, Malaysia
Date: 27/7/2009

UNIVERSITI TEKNOLOGI PETRONAS

Approval by Supervisor (s)

The undersigned certify that they have read, and recommend to The Postgraduate Studies Programme for acceptance, a thesis entitled "**Fully Decoupled Controller Models of Voltage Source Converter Based High Voltage DC Transmission**" submitted by (**Ahmed Mahjoub Ahmed**) for the fulfillment of the requirements for the degree of Master of Science in Electrical and Electronics Engineering.

Date: _____

Signature : 

Main Supervisor : Dr. Ravindra N. Mukerjee

Date : 27/7/2009

UNIVERSITI TEKNOLOGI PETRONAS

**Fully Decoupled Controller Models for Voltage Source Converter based High
Voltage DC Transmission**

By

Ahmed Mahjoub Ahmed Mahjoub

A THESIS

SUBMITTED TO THE POSTGRADUATE STUDIES PROGRAMME
AS A REQUIREMENT FOR THE
DEGREE OF MASTER OF SCIENCE
IN ELECTRICAL AND ELECTRONICS ENGINEERING

BANDAR SERI ISKANDAR,

PERAK

JULY, 2009

DECLARATION

I hereby declare that the thesis is based on my original work except for quotations and citations which have been duly acknowledge. I also declare that it has not been previously or concurrently submitted for any other degree at UTP or other institutions.

Signature : Ahmed

Name : Ahmed Mahjoub Ahmed Mahjoub

Date : 27/7/2009

ACKNOWLEDGEMENTS

First of All, I would like to express my gratitude and appreciation to my advisor Dr. Ravindra Nath Mukerjee. He was always there for me. His support, encouragement, valuable assistance, and unwavering patience rescued me from frustration and guided me throughout my research. Without his excellent guidance it would have been impossible to finish this work. His very positive influence on my professional development will be carried forward into my future career.

I would like to thank my parents, my sisters, and my brothers for their endless support. They gave me courage and strength to never give up. They provided me sturdy motivation and strong emotional and moral support which I have needed throughout my life.

Special thanks are extended to my colleagues at Electrical and Electronic Engineering Department. They have been very friendly and gracious which provided me an excellent study environment.

At the end, I would like to thank my friends for their consistent support, help, and encouragement.

Ahmed Mahjoub Ahmed Mahjoub
Universiti Teknologi PETRONAS, JULY 2009

ABSTRACT

VSC-HVDC has two distinct advantages over its earlier generation thyristor based High Voltage DC transmission. Synchronous voltage source is not required to commute against, for its operation and it does not suffer from commutation failures under adverse conditions in interfacing ac system. These two properties make it amenable to wider application areas. To make it adapt to operational conditions imposed on it in various applications, its controller parameters need to be assessed and tuned through extensive simulation studies. To facilitate this, two alternative controllers viz. a fully decoupled controller model and also an instantaneous theory based fully decoupled hybrid controller model are developed in the thesis. The decoupling is achieved by exploiting similarity transformation in both the controllers. In the first controller model, the Park's currents and voltages are directly obtained from the measured network variables and the reference park's currents for the inner current loop are obtained from the instantaneous measured power. In the second one, both the feedback as well as reference Park's currents for the inner current loop are obtained from the Clarke's variables. An AC system interfacing electronics based power transmission or distribution network experiences non-sinusoidal voltage and current waveforms. Instantaneous power theory being suitable for steady as well as transient states, is used for handling measured inputs. The performance of the models is assessed through SIMULINK Power system Blockset aided simulations on a VSC-HVDC link interfacing an ac system, having normal fault level, low fault level and also witnessing a single line to ground fault on its rectifier transformer primary side.

ABSTRAK

VSC-HVDC mempunyai dua kelebihan semenjak awal pengeluaran tiristor berasaskan penghantaran A. T. Voltan Tinggi. Sumber voltan segerak tidak memerlukan penukartertiban untuk proses operasinya dan juga ia tidak mendatangkan sebarang kesan jika penukartertiban gagal untuk berfungsi pada keadaan dimana proses pengantaramuka sistem a.u. tidak begitu baik. Kelebihan-kelebihan ini telah memberi peluang kepada para penyelidik untuk mengkaji dengan lebih terperinci bidang ini. Dua alternatif model pengawal iaitu pengawal penyahgandingan penuh dan pengawal hybrid penyahgandingan penuh diperkenalkan di dalam tesis ini. Penyahgandingan terhasil apabila kaedah tranformasi yang sama digunakan pada kedua-dua pengawal tersebut. Dalam model pengawal yang pertama, voltan dan arus Park boleh diperolehi secara terus dengan mengukur boleh ubah rangkaian. Rujukan arus gelung Park pula diperolehi dengan mengukur kuasa pada ketika itu. Bagi model pengawal yang kedua pula, kedua-dua suapbalik dan juga rujukan arus gelung Park diperolehi terus dari boleh ubah Clarke. Elektronik pengantaramuka sistem a.u. adalah berasaskan kepada penghantaran kuasa atau rangkaian pengagihan ketika bentuk gelombang voltan dan arus yang tidak sinus berlaku. Untuk proses pengukuran pula, masukan yang digunakan adalah berasaskan teori kuasa ketika yang sesuai untuk status tetap dan juga beralun. Pencapaian model-model tersebut diukur melalui simulasi VSC-HVDC pautan pengantaramuka sistem a.u. yang mengalami tahap kerosakan yang normal, rendah dan juga kerosakan satu fasa ke bumi pada bahagian utama pengubah penerus. Perisian yang digunakan untuk simulasi tersebut adalah perisian SIMULINK Power System Blockset.

TABLE OF CONTENTS

ACKNOWLEDGEMENT	v
ABSTRACT.....	vi
ABSTRAK.....	vii
TABLE OF CONTENTS.....	viii
LIST OF FIGURES	x
LIST OF TABLES	xi
CHAPTER ONE: INTRODUCTION.....	1
1.1 Introduction.....	1
1.2 Objective of the Research	2
1.3 Outline of the Thesis of Thesis	2
1.4 List of Publications	3
CHAPTER TWO: LITERATURE REVIEW... ..	4
2.1 Introduction	4
2.2 VSC-HVDC Transmission System.....	6
2.2.1 Components of VSC-HVDC	7
2.3 Operation of VSC-HVDC	11
2.4 Applications of VSC-HVDC	13
2.5 Instantaneous Power Theory.....	16
2.6 Related Research.....	18
2.7 Conclusion	21
CHAPTER THREE: CONTROLLERS OF VSC-HVDC SYSTEM	22
3.1 Introduction.....	22

3.2 State Space Model of VSC-HVDC.....	23
3.3 Decoupling the State Variables	31
3.4 Fully Decoupled Controller Models	33
3.4.1 d-q Controller.....	33
3.4.2 Hybrid Controller.....	40
3.5 Conclusion	44
CHAPTER FOUR: MODEL VALIDATION	46
4.1 Introduction.....	46
4.2 Power System Blockset.....	46
4.3 VSC-HVDC Transmission System Model	47
4.3.1 Outer Loop Controller.....	48
4.3.2 Inner Current Loop Controller.....	50
4.4 Comparative Performance Assessment of d-q Controller	51
4.5 Comparative Performance Assessment of Hybrid Controller	57
4.6 Conclusion	62
CHAPTER FIVE: CONCLUSION AND FUTURE WORK	63
5.1 Conclusion	63
5.2 Contributions of the Research	64
5.3 Future work.....	64
REFERENCES	65
APPENDICES	69
Appendix A.....	69
Appendix B	72
Appendix C.....	79
Appendix D.....	102

LIST OF TABLES

Table 4.1 System Descriptions	51
Table 4.2: Scenario Description of d-q Controller.....	52
Table 4.3: Scenario Description of Hybrid Controller.....	57

LIST OF FIGURES

Figure 2.1: Components of Conventional HVDC transmission system	5
Figure 2.2: Capacitor Commutated Converter.....	5
Figure 2.3: Components of VSC-HVDC transmission system.....	7
Figure 2.4: Converter Topologies of VSC-HVDC	8
Figure 2.5: P-Q Diagram for VSC-HVDC	12
Figure 2.6: Three-phase Instantaneous active power.....	17
Figure 2.7: Physical meaning of the instantaneous real and reactive powers.....	18
Figure 3.1: VSC-HVDC Power Circuit and Measurement Scheme	23
Figure 3.2: Inter-Relationship between Frames of References for VSC-HVDC.....	24
Figure 3.3: VSC-HVDC Rectifier d-q Controller.....	39
Figure 3.4: VSC-HVDC Inverter d-q Controller	39
Figure 3.5: VSC-HVDC Rectifier Hybrid Controller.....	43
Figure 3.6: VSC-HVDC Inverter Hybrid Controller	44
Figure 4.1: VSC-HVDC Transmission System Model.....	47
Figure 4.2: AC Network Bus Voltages - Rectifier Side d-q Controller.....	53
Figure 4.3: AC Network Bus Voltages - Inverter Side d-q Controller	53
Figure 4.4: Real Power Flow into DC Link -Rectifier Side d-q Controller.....	54
Figure 4.5: Reactive Power Flow into DC Link- Rectifier Side d-q Controller	54
Figure 4.6: DC Link Voltage Measured on Inverter Side d-q Controller.....	55
Figure 4.7: AC network Phase voltages – Single Line to Ground Fault near Rectifier Transformer Primary d-q Controller.....	56
Figure 4.8: Modulation Index – Rectifier Side d-q Controller	56
Figure 4.9: AC Network Bus Voltage - Rectifier Side Hybrid Controller	58
Figure 4.10: AC Network Bus Voltage - Inverter Side Hybrid Controller.....	58
Figure 4.11: Real Power Flow into DC Link -Rectifier Side Hybrid Controller.....	59

Figure 4.12: Reactive Power Flow into DC Link- Rectifier Side Hybrid Controller	59
Figure 4.13: DC Link Voltage Measured on Inverter Side Hybrid Controller	60
Figure 4.14: Reactive Power Flow into DC Link- Inverter Side Hybrid Controller	61
Figure 4.15: Modulation Index – Rectifier Side Hybrid Controller	61

CHAPTER ONE: INTRODUCTION

1.1 Introduction

Voltage Source Converter based High-voltage direct current transmission (VSC-HVDC) a high power electronics based technology, provides (i) economical alternatives to ac transmission for long-distance bulk power delivery from remote sources, (ii) immunity against network congestion or loop flow on parallel paths facilitating power trading, and (iii) is useful as asynchronous link to provide a firewall against propagation of cascading outages in one network crossing over to another network. It also facilitates interconnection of ac systems in the lower and middle power range [1].

VSC-HVDC has two distinct advantages over its earlier generation thyristor based HVDC transmission. Synchronous voltage source is not required to commutate against, for its operation and voltage source converters (VSC) do not suffer from commutation failures under adverse conditions in interfacing ac system, allowing fast recoveries from nearby ac faults [1, 2]. These two properties make it amenable to wider application areas.

Thyristor based HVDC requires switching for polarity reversal. VSC-HVDC transmission reverses power through reversal of current direction rather than voltage polarity, facilitating power reversal at an intermediate tap point independent of the main power flow direction, required in Multi-terminal HVDC systems.

An ac system interfacing electronics based power transmission or distribution network experiences non-sinusoidal voltage and current waveforms. Events in an ac power network may prompt variation in fault level at the interface point or some amount of system unbalance or even initiation of transients. Since VSC-HVDC controller performance depends on the accuracy in the measured values of currents and voltages and the reference values of the currents derived there from, it is important to use a

measurement processing technique appropriate for the non-sinusoidal waveforms and transients. Instantaneous power theory is used in this thesis for not only obtaining the measured values of the real and reactive powers, but also for deriving reference values of the currents used in the inner current control loop. A fully decoupled controller model exploiting similarity transformation is also developed. The performance of the model is assessed through simulations on a VSC-HVDC link interfacing an ac system.

1.2 Objective of the Research

The main objectives of the research are as follows:

- To developed the controller dynamic model for VSC-HVDC.
- To gauge performance of the controller dynamic model for VSC-HVDC, when subjected to AC grid disturbances.

1.3 Outline of the Thesis

Chapter 2 reviews an HVDC link and describes essential subsystems in a VSC-HVDC transmission link, discusses the advantages and the applications of VSC-HVDC. And also mention briefly about instantaneous power theory. Earlier research in VSC-HVDC link controllers are also summarized in this chapter.

Chapter 3 develops the state space model of a VSC-HVDC link controller. Two fully decoupled controller models are developed. In the first model, the reference values of the currents for inner current loop are estimated from the d-q transformed values of the phase voltages and currents measured at the interface bus. In the second one, instantaneous power theory is first used to obtain Clarke's voltages and currents and then the reference values of the currents for inner current loop are derived from these values.

Chapter 4 assesses the performance of a composite power system incorporating the developed controllers in a VSC-HVDC link interfacing an ac system. For performance assessment of the first, viz. d-q controller, the SIMULINK based simulations are carried out on a composite system with the ac system having Normal fault level, low fault level and witnessing a single line to ground fault on rectifier transformer primary side. The second one viz. the hybrid controller, performance is assessed with the interfacing ac system having normal fault level.

Chapter 5 draws conclusions, contributions, and mentions some directions for future work.

1.4 List of publications

1. **Ahmed Mahjoub** and Ravindra Mukerjee, "Modeling of Controller for Voltage Sourced Converter based HVDC Transmission System", 2nd IEEE International Conference on Power and Energy (PECon 08), Johor Baharu, Malaysia, pp. 849–854, December 2008.
2. Ravindra N. Mukerjee and **Ahmed Mahjoub**, "A Fully Decoupled Controller Model for VSC-HVDC Transmission System", Elsevier Electric Power Systems Research. Manuscript # EPSR-D-09-00189.
3. Ravindra N. Mukerjee and **Ahmed Mahjoub**, "Instantaneous Power Theory Based Fully Decoupled Controller Model for VSC-HVDC Transmission System", European Transactions on Electrical Power. Manuscript# ETEP-09-0125.

CHAPTER TWO: LITERATURE REVIEW

2.1 Introduction

High-voltage direct current transmission (HVDC), a high power electronics based technology provides more economical alternative to ac transmission for long-distance bulk power delivery from remote sources such as hydroelectric, pit head power plants or large scale wind farms and long submarine cable transmission. HVDC lines and cables are less expensive and have lower losses than those for three-phase ac transmission.

Because of their controllability, HVDC links offer firm capacity without limitation due to network congestion or loop flow on parallel paths. Higher power transfers are achievable without distance limitation on HVDC cable systems using fewer cables than with ac systems having charging current. Rapid drop-off takes place in cable capacity over distance in ac transmission due to considerable reactive component of charging current. Although, this can be compensated by intermediate shunt compensation for underground cables, it is not practical to do so for submarine cables.

With HVDC transmission systems, interconnections can be made between asynchronous networks for more economic or reliable operation. Often, these interconnections use back-to-back converters. The asynchronous links act as a firewall against propagation of cascading outages in one network from crossing over to another network.

Thyristor based HVDC transmission schemes utilize line commutated current source converters. Such converters require a synchronous voltage source in order to operate.

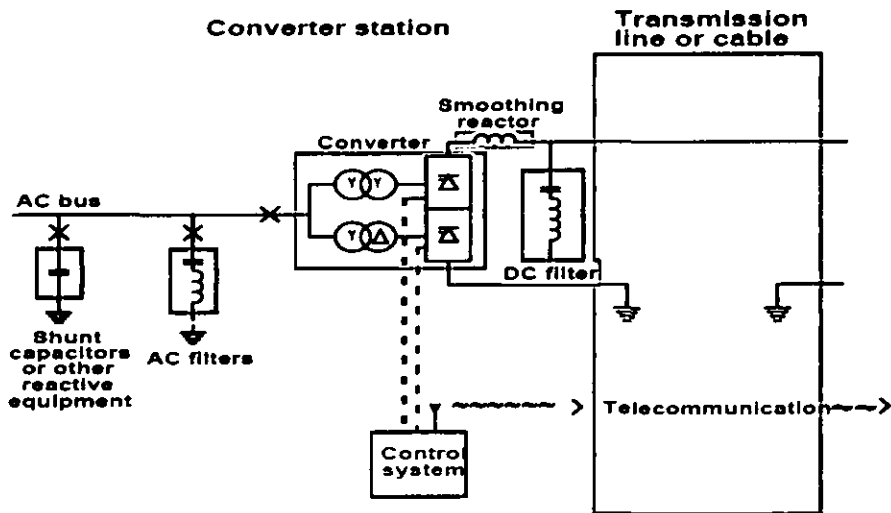


Figure 2.1: Components of Conventional HVDC Transmission Systems

For weak ac system back-to-back applications, converters are provided with series capacitors connected between the valves and the transformers, known as capacitor-commutated converters (CCC) [3, 4].

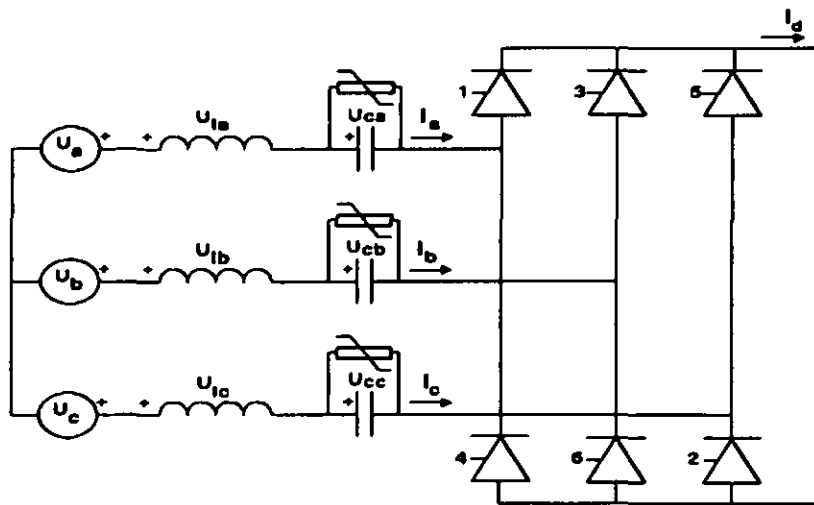


Figure 2.2: Capacitor commutated converter

The series capacitor provides some of the converter reactive power compensation requirements with load current and provides part of the commutation voltage improving voltage stability. CCC configuration allows higher power ratings in areas where the ac network is close to its voltage stability limit.

A conventional HVDC can only operate with ac systems having appropriate short circuit power, as thyristor converters always require reactive power, which varies according to the active power being transferred. Consequently, switched capacitor banks and static var compensators are required to supply reactive power demand of the converter stations. Thyristor converters also suffer from commutation failures during adverse ac system conditions or maloperation of the firing controls [5].

2.2 VSC-HVDC Transmission System

HVDC transmission using self commutated IGBT based voltage source converters (VSC-HVDC) uses Pulse Width Modulation (PWM) with relatively high switching frequencies to get high speed control of both active and reactive power, making it possible to generate ac output voltage with any desired phase angle or amplitude instantly. AC voltage is created by switching very fast between two fixed voltages. The desired fundamental frequency voltage is created through low pass filtering of the high frequency pulse modulated voltage. Up to a certain limit, any phase angle or amplitude can be created by changing the PWM pattern [6, 7]. Higher switching frequency components permit use of pulse width modulation technology together with simple converter topology and reduced filter size.

IGBT being a MOS-device, power need for the control of the component is very low. Due to a switching frequency that is considerably higher than the ac system power frequency, the wave shape of the converter is controlled to be very sinusoidal resulting in reduced harmonic generation and elimination of low order harmonics. Harmonic

interference of VSC converter is rather small compared to the conventional line commutated converters in thyristor based HVDC. Series connection of many semiconductors with good voltage distribution even at switching frequencies in kHz range is possible, to achieve a high HVDC link voltage [8–10].

2.2.1 Components of VSC-HVDC

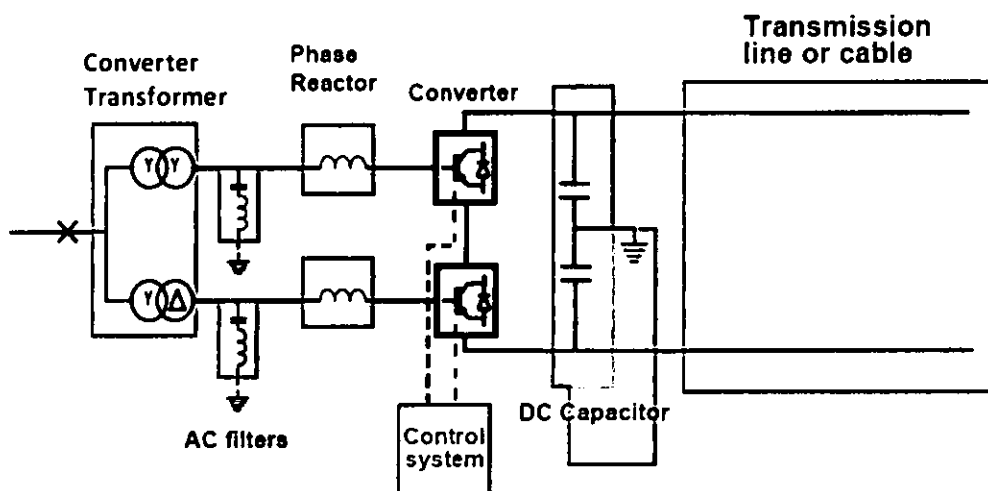
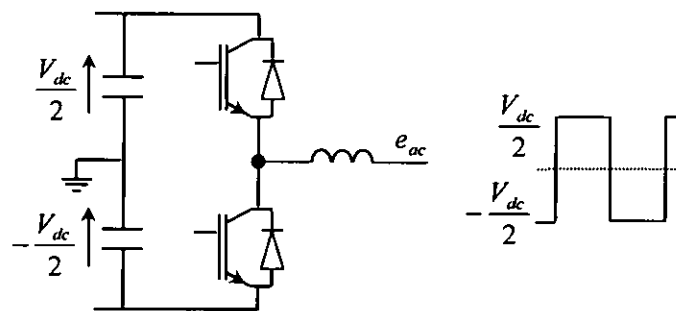


Figure 2.3: Components of VSC- HVDC transmission system

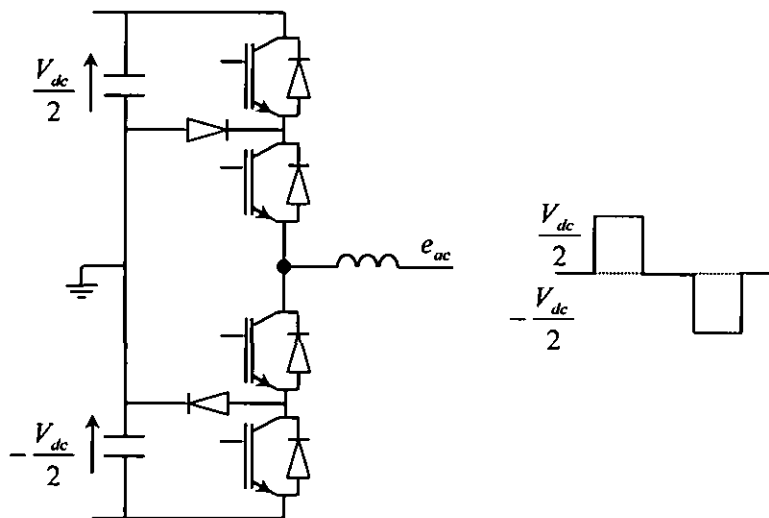
Converter topologies

VSC-HVDC transmission system employs forced commutated, voltage sourced converters with IGBT valves. IGBT is a development of the MOSFET, in which removal of current from the gate switches off the through current, thereby allowing power to be switched on or off throughout an ac cycle. This provides a means of controlling currents in relation to the voltage in ac systems. Thus, VARs may be generated or absorbed. Current injection into ac systems for power-flow control is achieved using these devices. Natural Ac output waveform of a VSC is determined by the topology of the converter [11–14]. Two main categories of topology appropriate for dc power transmission exist,

viz. Two-Level topology or Three-Level topology. The Two-Level converter is simple circuit arrangement. It has been widely used in many applications for a wide range of power level. The schematic of one phase of a Two-Level converter is given in Figure 2.4(a). As shown, it is capable of generating the two-voltage levels $+0.5 V_{dc}$ and $-0.5 V_{dc}$.



(a) One phase of a two-level converter



(b) One phase of a three-level converter

Figure 2.4: Converter topologies of VSC-HVDC

The three-level converter consists of four valves in on arm and additional diodes. Figure 2.4(b) shows one phase of a three-level converter and the output three-voltage levels $+ 0.5 V_{dc}$, 0 and $- 0.5 V_{dc}$. However, the more complex converter and higher investment costs make a two-level converter preferred. Currently device of valve is IGBT which can be turned off under short-circuit conditions, has high switching speed capability, requires low control power and permits active control of the voltage cross the device [15].

DC capacitor

DC capacitor is connected to the terminals of the VSC to provide energy storage on the dc side, acting as a dc voltage source which is necessary for the dynamic operation of the system. Capacitor must have low inductance and is placed close to VSC valve to minimize stray inductance in the commutating loop. Capacitance must be large enough to limit harmonic ripple to design limits; ripple depends on direct current amplitude and on the switching strategy, long pulses of high current cause more ripple, and voltage variations during faults in ac networks also need to be taken into account.

Converter reactor

Converter reactor provides constant fundamental frequency impedance for the control of the VSC active and reactive power output, and it provides a high frequency blocking filter between the ac converter and the ac network. It limits rate of rise of short-circuit currents.

AC harmonic filter

Like all power electronic converters, VSCs generate harmonic voltages and currents on the ac and dc sides. Harmonics generated depend on: Operation topology (i.e. 6-pulse or

12-pulse), using a 12-pulse converter to reduce the additional current and voltage harmonics, filtering required for 6-pulse converter, i.e., 5th and 7th on the ac side and 6th on the dc side. This is because although these harmonic currents still flow through the valves and the transformer windings, they are 180° out of phase and cancel out on the primary side.

The high switching frequency of the IGBTs is advantageous to reduce harmonic generation. However, operation loss of the converters increase in direct proportion to the switching frequency applied. High operational losses not only reduce the power of a VSC-HVDC transmission system, they also warm up the converter power electronics and thus might reduce the fundamental power transfer capability.

Ground

The ground reference for the VSC may be made at the mid-point of the dc capacitor via high impedance. This has the advantage of limiting current flow during ground faults on the dc side.

Transformer

In general, the converters are connected to the ac system by means of transformers. The most important functions of the transformers are to provide a reactance between Ac converter and ac system beneficial for harmonics and to transform the voltage of the ac system to a level appropriate for the converter.

DC lines

The dc link may be a cable or overhead line having two conductors. DC cable can take significant advantage of the fixed polarity of the dc voltage.

VSC-HVDC converter station can comprise of either voltage-sourced converters or current-sourced converters (CSC). Whereas the CSCs' are robust, the VSCs' have higher efficiency, low initial cost, and smaller physical size. Voltage-sourced converter is preferred over CSC, since with CSC both power and control circuits are more complex. Filter capacitors are required at the ac terminals of a CSC to improve output ac current waveform quality, thus adding to cost. CSC requires switches of sufficient reverse voltage withstand capability such as Gate-Turn-off thyristors, capable of blocking voltages of both polarities in off-state. Alternatively, series diode is required with each switch, resulting in increased cost and conduction losses. CSC also requires smoothing dc inductors across the three-phase bridge terminals, which are generally larger and more expensive than capacitors used in voltage-sourced converters [16, 17].

IGBT module commercially available is more suitable for voltage-source PWM converter, since a free-wheeling diode is connected in anti-parallel with each IGBT. Thus the IGBT does not need to be provided with the built-in reverse voltage blocking capability, bringing in more flexibility to device design, a compromise between switching losses and short-circuit capability.

2.3 Operation of VSC-HVDC

The operational requirements imposed on VSC-HVDC link keep on varying, depending on the changes in interfacing ac network operating conditions at its sending and receiving ends. Normal power transfer in forward direction, reverse power transfer, sending end and/or receiving end ac network short circuit capacity low due to network fault, dc line witnessing fault, are some of the operating conditions, the VSC may have to encounter. The converter phase angle can be used for the active power control. A VSC operates as a rectifier when ac voltage of the converter u_{ac} phase lags the ac network voltage e_{ac} i.e. $\delta_{ac} > 0$. The active power flows into VSC from ac system in this case.

$$p_{ac} = \frac{e_{ac} u_{ac}}{x_{ac}} \sin \delta_{ac} \quad (2.1)$$

The voltage magnitude can be used to control reactive power. The converter provides reactive power support to the ac network, when the converter ac voltage $|u_{ac}|$ is higher than the ac network voltage $|e_{ac}|$.

$$Q_{ac} = \frac{e_{ac}^2}{x_{ac}} - \frac{e_{ac} u_{ac}}{x_{ac}} \cos \delta_{ac} \quad (2.2)$$

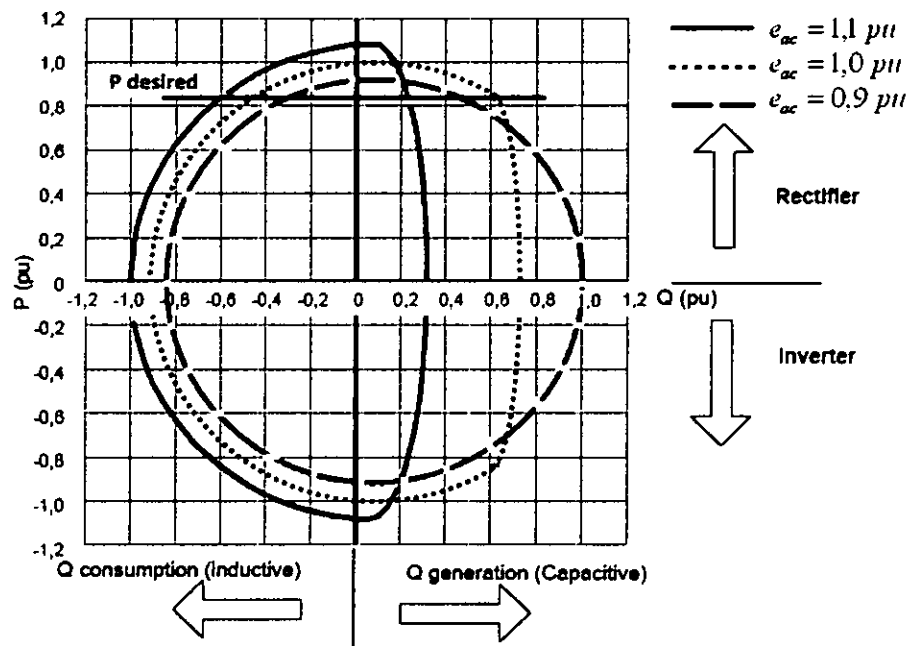


Figure 2.5: P-Q diagram for VSC-HVDC

Figure 2.5 illustrates the characteristic variation in active power, P , and reactive power, Q , capability of a VSC-HVDC link as a function of ac system voltage, measured at the network interfacing point. The reactive power delivery to the network increases with decreasing network voltage [18]. Similarly, the converter reactive power absorption

increases with increasing network voltage. For a given ac system voltage, the converter can be operated at any point within the P-Q circle, as required.

Through control of modulation index and the phase shift between network voltage and converter input voltage on the sending end side and /or between converter output voltage and the network voltage on the receiving end side, the operational requirements are met by modifying the instant and duration of conduction of the IGBT switches of the VSC converters. The change in PWM pattern enables this. The change in PWM pattern realized through the controller provided with decision logics, enables change in fundamental frequency voltage phase angle and the fundamental frequency voltage magnitudes of the converters and hence the required change in active and reactive power flows. However, for ensuring appropriate design, extensive simulation tests on the composite system incorporating its controllers, need to be carried out.

VSC with PWM can operate in all four quadrants of PQ-plane as shown in Figure 2.5, i.e. it can operate as rectifier or inverter at variable frequency and at the same time absorb or supply reactive power to the ac network. Reactive power can also be controlled at each terminal independent of the dc transmission voltage level. This control capability gives total flexibility to place converters anywhere in the ac network since there is no restriction on minimum network short circuit capacity. HVDC transmission and reactive power compensation with VSC technology has attributes beneficial to overall system performance.

2.4 Applications of VSC-HVDC

Forced commutation with VSC even permits black start. In a VSC the current can be switched on and off by controlling the semiconductor valves, there is no need for a network to commutate against. The converter can be used as virtual synchronous generator. VSC technology thus, can supply passive networks i.e. areas which lack

enough power in the rotating machines implying too low short circuit power, thus, improving power quality of the weak system. VSC-HVDC can also feed power into passive networks with no local power generation. It enables fast control of active and reactive power independently of each other with high bandwidth and provides reactive power or voltage support to an area independently of the active power transmitted, if rating of the converter permits the total apparent power. Active power flow can be quickly reversed enabling short term transactions in the electric power trading. It can also be used for the dynamic compensation of power transmission systems, providing increased transient stability and improved damping. It can ensure good behaviour of the system variables in response to positive and negative active power steps and can be used in Back-to-back schemes [19].

Forced commutation, dynamic voltage control and black start capability allow VSC-HVDC to serve isolated loads on islands over long distance submarine cables without any need for running expensive local generation. VSC converters can operate at variable frequency providing power efficiently to large high voltage drives such as compressors or pumps on offshore oil or gas platforms from shore, thus eliminating the need of more expensive, less efficient higher emission offshore power production. Interconnections between asynchronous networks are often at their periphery, where networks tend to be weak for the desired power transfer. The dynamic voltage support and improved voltage stability offered by VSC-HVDC permits higher power transfers without need for ac system reinforcement. VSC converters do not suffer from commutation failures, allowing fast recoveries from nearby ac faults. Absence of minimum power or current restrictions facilitates reverse power flow and economic power schedules.

VSC-HVDC underground transmission circuits can be placed on dual-use right-of-way to bring in power as well as provide voltage support, allowing an economical power supply without compromising reliability. Large remote wind generation arrays

require a collector system, reactive power support for doubly fed induction generators and power evacuation facility. VSC based HVDC transmission allows efficient land use, use of submarine cables and provides reactive power support to the wind generation complex. VSC-HVDC transmission reverses power through reversal of current direction rather than voltage polarity, facilitating power reversal at an intermediate tap point independently of the main power flow direction in Multi-terminal HVDC systems. However, thyristor based HVDC requires switching for polarity reversal.

VSC-HVDC may be the only viable choice for long distance, bulk power delivery, asynchronous interconnections, long submarine cable crossings, economic underground power transmission without distance limitations, offshore power applications, resource diversification, congestion relief, and replacement of reliability-must-run generation and mitigation of voltage instability. Controllability of VSC-HVDC facilitates it to operate under constant power, ac voltage control and frequency control modes, enabling it to be radially interconnected to an electric distribution system having feed from synchronous generation. Thus, a remote wind generation in-feed can be connected to an electric distribution system as embedded or distributed generation using a VSC-HVDC link operating in parallel with the upstream electric utility sources.

VSC-HVDC has STATCOM functionality, enabling it to continuously adjust reactive power support to an ac system to control ac bus voltage and improve system stability. It facilitates interconnection of AC systems in the lower and middle power range. The dynamic support of the ac voltage at each converter terminal improves the voltage stability and increases the transfer capability of the sending and receiving end ac systems. VSC-HVDC being an asynchronous link and connecting a wind farm in-feed to an electric distribution system as distributed generation can isolate the power system from the wind power fluctuations. Voltage in the wind farm is also not affected by changes of the voltage in the ac network, caused by switching actions or remote faults.

A VSC-HVDC link supplying power to (i) an electric distribution network with or without embedded generation and interfacing directly with the loads having varying characteristics, (ii) an industrial electric distribution system having feed from the onsite generation or (iii) serving as asynchronous link between two ac systems, often has to adjust itself to avoid oscillations under changing operating conditions. To suppress these oscillations, design and operational strategy of controllers in a VSC-HVDC plays a significant role.

2.5 Instantaneous Power Theory

The development of power electronics devices and their associated converters has brought new boundary conditions to the energy flow problem. This is not exactly because is new , but because these converters and the way they generate reactive power and harmonic components have made it clear that conventional approaches to the analysis of power are not sufficient in terms of taking average or rms values of variables. Therefore, time-domain analysis has evolved as a new manner to analyse and understand the physical nature of the energy flow in a nonlinear circuit. The theories that deal with instantaneous power can be mainly classified into the following two groups. The first one is developed based on the transformation from the *a-b-c* phases to three-orthogonal axes, called the *p-q* theory or instantaneous power theory. The second one is done directly on the *a-b-c* phase, called the *abc* theory. In this thesis, the first theory is our concern [20].

The instantaneous power theory is based on a set of instantaneous power defined in the time domain. No restrictions are imposed on the voltage and current waveform, and it can be applied to three-phase systems with or without a neutral wire for three-phase generic voltage and current waveforms. Thus, it is valid not only in the steady state, but also in the transient state. This theory is very efficient and flexible in designing controllers for power conditioners based on power electronics devices.

Other traditional concepts of power are characterized by treating a three-phase system as three single-phase circuits. The instantaneous power theory first transforms voltages and currents from the a-b-c to $\alpha\beta 0$ coordinates, and then defines instantaneous power on these coordinates. Hence, this theory always considers the three-phase system as a unit, not a superposition or sum of the three single-phase circuits.

The instantaneous power theory is defined in three-phase systems with or without a neutral conductor. Three instantaneous powers – the instantaneous zero-sequence power p_0 , the instantaneous real power p , and the instantaneous imaginary power q – are defined from the instantaneous phase voltages and line currents on the $\alpha\beta 0$ axes as

$$\begin{bmatrix} p \\ q \\ p_0 \end{bmatrix} = \begin{bmatrix} v_\alpha & v_\beta & 0 \\ v_\beta & -v_\alpha & 0 \\ 0 & 0 & v_0 \end{bmatrix} \begin{bmatrix} i_\alpha \\ i_\beta \\ i_0 \end{bmatrix} \quad (2.3)$$

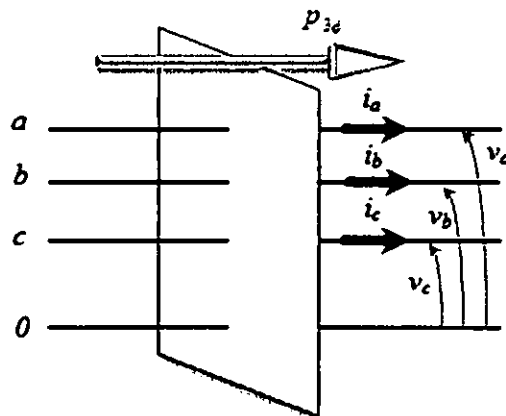


Figure 2.6: Three-phase instantaneous active power

There are no zero-sequence current components in three-phase, three-wire systems, that is, $i_0=0$. In this case, only the instantaneous powers defined on the $\alpha\beta$ axes

exist. Hence, in three-phase, three-wire systems, the instantaneous real power p represents the total energy flow per time unity in terms of $\alpha\beta$ components.

In this case

$$p_{3\phi} = p \quad (2.4)$$

The instantaneous reactive power q is proportional to the quantity of energy that is being exchanged between the phases of the system. It does not contribute to the energy delivered to the load, and also the energy oscillating the source and the load at any time.

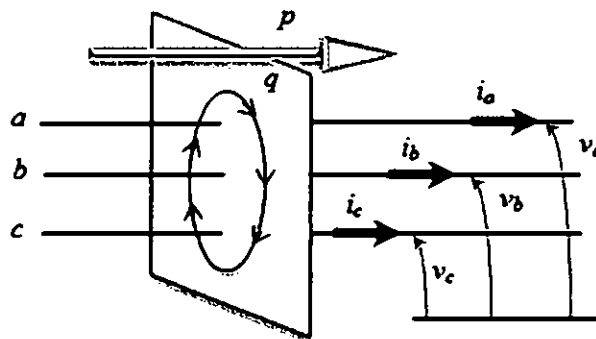


Figure 3.7: Physical meaning of the instantaneous real and reactive powers

2.6 Related Research

To facilitate dynamic simulation of a composite power system incorporating a VSC-HVDC link and thereby assess performance of a controller supervising PWM module for ultimate firing control of the IGBT valves, models for the VSC-HVDC controllers were developed by several authors [21–25]. The control system in a VSC-HVDC comprises a fast inner current controller controlling the ac current within the converter's current carrying capability limit and a number of outer loop controllers providing reference

values of current to the inner current controller, for the control strategy chosen at the rectifier or the inverter end. The outer controllers could be dc voltage controller, active power controller, reactive power controller and the frequency controller. Not all the outer controllers are used at the same time. However, one of the two converters must control the link dc voltage to achieve active power balance between the power entering the rectifier end and leaving the inverter end.

In reference [21], state model $\dot{x} = Ax + Bu$ is developed with currents in direct and quadrature axes of a synchronously rotating reference frame as state variables and using d-q transformed equivalent of the source side circuit of the VSC converter, originally framed in a-b-c frame of reference. Synchronously rotating d-axis is assumed to be leading the phase 'a' by a transformation angle θ , derived through a phase locked loop. Decoupled control rule for the current state variables or the inner current controller is obtained by defining the feedback loop and the PI compensation. The inner current controller loop is implemented in d-q frame. However, control law for determining the converter source side reference voltage variables u_d and u_q still need cross-coupled terms. Converter source side voltages and the dc link voltage V_{dc} , determine the amplitude and angle modulation indices. The measured real and reactive power on the network side is assessed using the Clarke's variables viz. instantaneous voltage and current vectors.

In reference [22], strategy is similar as in Reference [21], except that a one-sample delay is implemented in the inner current controller for slow current control and a smith predictor is used in the current controller to compensate for the time delay for fast current control. The inner current control loop is implemented in d-q frame. The dead beat current control is achieved through proportional control of the current error. However, to wipe-off the steady state current error, integral part can also be added. The measured values of the d-q transformed currents are derived from the real and reactive power computed after transforming the voltages and the currents acquired in a-b-c reference frame to rotating d-q frame. The computation of converter source side reference

voltage variables u_d and u_q need i_q and i_d respectively, and in that sense use coupled expressions. These reference voltages are transformed to the a-b-c frame via Clarke's transformation.

Reference [23] follows somewhat similar strategy as in References [21] and [22]. Fundamental frequency model in terms of d-q variables is formed through transformation from a-b-c frame to switching reference frame and then to dq0 frame. The inner current loop is once again implemented in d-q frame. The current components are decoupled. However, computation of d component of converter source side terminal voltage needs q component of current and similarly, computation of q component of converter source side voltage needs d component of current and hence the model is like the earlier two models in this respect. Like in [21] converter source side voltages and the dc link voltage V_{dc} , determine the amplitude and angle modulation indices.

In References [24] and [25] converter source side phase voltages in a-b-c frame are transformed into Clarke's components. The components are then identified and separated into positive and negative sequence voltages. While positive sequence voltage is subjected to a counter clockwise d-q transformation, the negative sequence voltage is transformed to a clockwise d-q transformation. This is to transform both of them into dc components during filtering, so as to avoid any phase shift. The two filtered components are then used to compute an accurate mean value of the source voltage during the sample period, specifically witnessing ac system disturbances.

Reference values of the active and reactive parts of the converter currents in rotating d-q frame are supplied from the outer power loop. The outer loop on the rectifier side includes a PI-control of the dc link voltage and a forward feed of the d-component of the reference value derived from the outer power loop of the inverter side, thus facilitating change of the ordered active current without influencing the dc link voltage.

The inner current loop is implemented in d-q frame, wherein the current errors are computed using the measured d-q currents and two sample delayed reference currents. This is to avoid failure of the dead-beat current control during normal ac network. Dead-beat current control works satisfactorily with strong ac network interfacing the VSC-HVDC. The reference value of the converter source side voltages are transformed to a-b-c frame, before feeding the PWM block with amplitude and angle modulation indices as inputs.

2.7 Conclusion

This chapter introduces High Voltage Direct Current (HVDC), describes VSC-HVDC transmission system, explains the advantages and the applications of VSC-HVDC, and presents a critical review of the related research in the area of VSC-HVDC link controllers.

CHAPTER THREE: CONTROLLERS OF VSC-HVDC SYSTEM

3.1 Introduction

The control system in a VSC-HVDC comprises of a fast inner current loop controlling the ac current within the converter's current carrying capability limit and a number of outer loops providing reference values of the current to the inner current controller, for the control strategy chosen at the rectifier or the inverter end. The outer controllers could be dc voltage controller, active power controller, reactive power controller and the frequency controller. Not all the outer controllers are used at the same time. However, one of the two converters must control dc link voltage for active power balance between the power entering the rectifier and leaving the inverter [22].

This chapter develops a fully decoupled controller for the inner current loop. Two fully decoupled controller models are developed. In the first (d-q) model, the reference values of the currents for the inner current loop are estimated using the d-q transformed values of the phase voltages and currents measured at the interface bus. In the second (Hybrid) one, instantaneous power theory is first used to obtain Clarke's voltages and currents from the measured phase values and then the reference values of the currents for inner current loop are derived from these Clarke's components. Instantaneous power theory, park transformation, and similarity transformation are used to develop the controller models.

The models developed are valid for both rectifier as well as inverter sides of a dc link. Both real and reactive power is controlled on the rectifier side. DC link voltage and the reactive power are controlled on the inverter side.

3.2 State Space Model of VSC-HVDC

The schematic of VSC-HVDC is shown in Figure 3.1. VSC-HVDC converter stations are connected by a dc link, wherein each converter consists of three phases of two-level converters and each phase contains two switching devices with anti-parallel diodes.

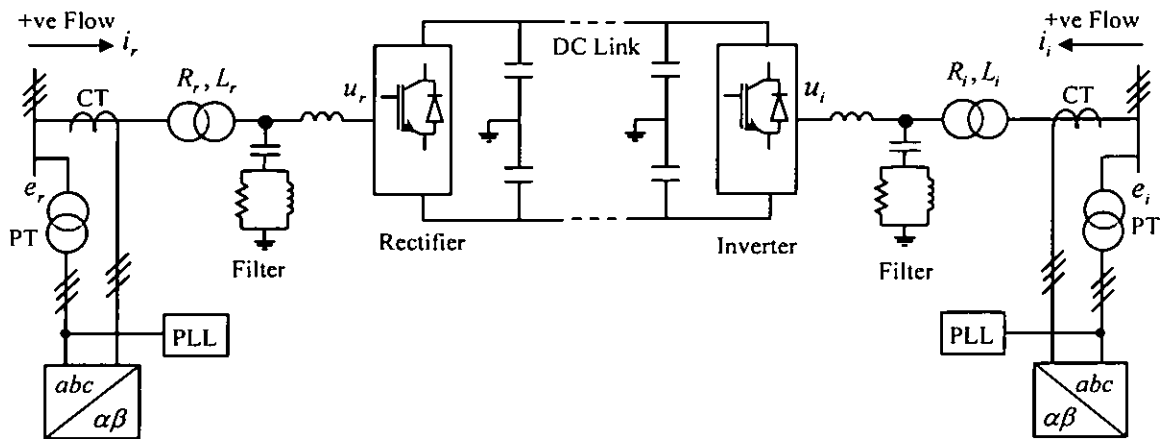


Figure 3.1: VSC-HVDC Power Circuit and Measurement Scheme

Assuming flows from the network to the converters at both rectifier and the inverter ends to be positive as shown in Figure 3.1, the voltage and current relationships at the network side of the respective coupling transformers are given by:

$$e_r^{abc} = R_r i_r^{abc} + L_r \frac{di_r^{abc}}{dt} + u_r^{abc} \quad (3.1)$$

$$e_i^{abc} = R_i i_i^{abc} + L_i \frac{di_i^{abc}}{dt} + u_i^{abc} \quad (3.2)$$

where e_r^{abc} , e_i^{abc} are the ac network voltages, i_r^{abc} , i_i^{abc} are the ac network currents and u_r^{abc} , u_i^{abc} are the ac converter voltages, on rectifier and inverter ends respectively.

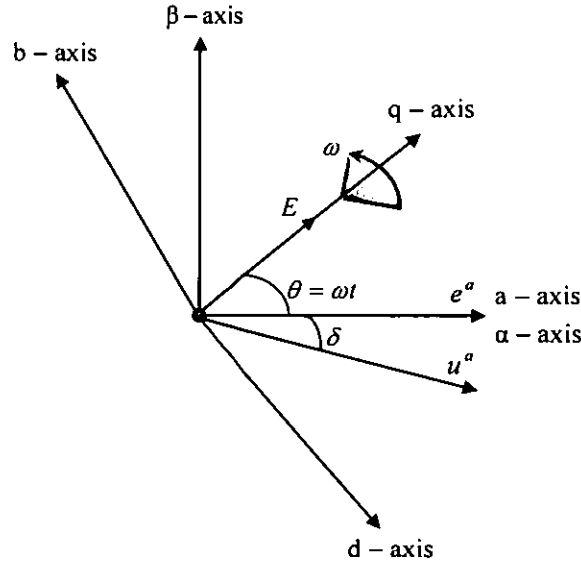


Figure 3.2: Inter-relationship between frames of references for VSC-HVDC

Transforming the equations in a-b-c frame of reference to a synchronously rotating reference frame as shown in Figure 3.2, equations (3.1) and (3.2) become

$$T_{dq0}^{-1} e_r^{dq0} = R_r T_{dq0}^{-1} i_r^{dq0} + L_r \frac{d(T_{dq0}^{-1} i_r^{dq0})}{dt} + T_{dq0}^{-1} u_r^{dq0} \quad (3.3)$$

$$T_{dq0}^{-1} e_i^{dq0} = R_i T_{dq0}^{-1} i_i^{dq0} + L_i \frac{d(T_{dq0}^{-1} i_i^{dq0})}{dt} + T_{dq0}^{-1} u_i^{dq0} \quad (3.4)$$

where, T_{dq0} is the Park's transformation and T_{dq0}^{-1} is the inverse Park's transformation with reference to Figure 3.2. These are given as

$$T_{dq0} = \frac{2}{3} \begin{bmatrix} \sin \theta & \sin(\theta - 120^\circ) & \sin(\theta + 120^\circ) \\ \cos \theta & \cos(\theta - 120^\circ) & \cos(\theta + 120^\circ) \\ \frac{1}{2} & \frac{1}{2} & \frac{1}{2} \end{bmatrix}$$

$$T_{dq0}^{-1} = \begin{bmatrix} \sin \theta & \cos \theta & 1 \\ \sin(\theta - 120^\circ) & \cos(\theta - 120^\circ) & 1 \\ \sin(\theta + 120^\circ) & \cos(\theta + 120^\circ) & 1 \end{bmatrix}$$

Pre multiplying both sides by T_{dq0} , and expanding the 2nd term on the right hand side, equations (3.3) and (3.4) can be written as

$$e_r^{dq0} = R_r i_r^{dq0} + L_r \left(\frac{di_r^{dq0}}{dt} + T_{dq0} \frac{dT_{dq0}^{-1}}{dt} i_r^{dq0} \right) + u_r^{dq0} \quad (3.5)$$

$$e_i^{dq0} = R_i i_i^{dq0} + L_i \left(\frac{di_i^{dq0}}{dt} + T_{dq0} \frac{dT_{dq0}^{-1}}{dt} i_i^{dq0} \right) + u_i^{dq0} \quad (3.6)$$

Noting that in equation (3.5) and (3.6),

$$T_{dq0} \frac{d}{dt} T_{dq0}^{-1} = \frac{2}{3} \begin{bmatrix} \sin \omega t & \sin(\omega t - 120^\circ) & \sin(\omega t + 120^\circ) \\ \cos \omega t & \cos(\omega t - 120^\circ) & \cos(\omega t + 120^\circ) \\ \frac{1}{2} & \frac{1}{2} & \frac{1}{2} \end{bmatrix} \begin{bmatrix} \omega \cos \omega t & -\omega \sin \omega t & 0 \\ \omega \cos(\omega t - 120^\circ) & -\omega \sin(\omega t - 120^\circ) & 0 \\ \omega \cos(\omega t + 120^\circ) & -\omega \sin(\omega t + 120^\circ) & 0 \end{bmatrix}$$

$$T_{dq0} \frac{dT_{dq0}^{-1}}{dt} = \omega \begin{bmatrix} 0 & -1 & 0 \\ 1 & 0 & 0 \\ 0 & 0 & 0 \end{bmatrix} \quad (3.7)$$

Equations (3.5) and (3.6), by substituting equation (3.7) and after simplification can be written as

$$\begin{bmatrix} e_r^d \\ e_r^q \\ e_r^0 \end{bmatrix} = R_r \begin{bmatrix} i_r^d \\ i_r^q \\ i_r^0 \end{bmatrix} + L_r \frac{d}{dt} \begin{bmatrix} i_r^d \\ i_r^q \\ i_r^0 \end{bmatrix} + \omega_r L_r \begin{bmatrix} 0 & -1 & 0 \\ 1 & 0 & 0 \\ 0 & 0 & 0 \end{bmatrix} \begin{bmatrix} i_r^d \\ i_r^q \\ i_r^0 \end{bmatrix} + \begin{bmatrix} u_r^d \\ u_r^q \\ u_r^0 \end{bmatrix} \quad (3.8)$$

$$\begin{bmatrix} e_i^d \\ e_i^q \\ e_i^0 \end{bmatrix} = R_i \begin{bmatrix} i_i^d \\ i_i^q \\ i_i^0 \end{bmatrix} + L_i \frac{d}{dt} \begin{bmatrix} i_i^d \\ i_i^q \\ i_i^0 \end{bmatrix} + \omega_i L_i \begin{bmatrix} 0 & -1 & 0 \\ 1 & 0 & 0 \\ 0 & 0 & 0 \end{bmatrix} \begin{bmatrix} i_i^d \\ i_i^q \\ i_i^0 \end{bmatrix} + \begin{bmatrix} u_i^d \\ u_i^q \\ u_i^0 \end{bmatrix} \quad (3.9)$$

where ω_r , ω_i are the angular velocity corresponding to the rated system frequency on rectifier and inverter sides respectively.

Assuming balanced operation of interfacing ac network signifying, absence of zero axis components, the d-q transformed versions of equations (3.1) and (3.2) are

$$\frac{1}{L_r} \begin{bmatrix} e_r^d \\ e_r^q \end{bmatrix} = \begin{bmatrix} \frac{R_r}{L_r} & 0 \\ 0 & \frac{R_r}{L_r} \end{bmatrix} \begin{bmatrix} i_r^d \\ i_r^q \end{bmatrix} + \begin{bmatrix} 0 & -\omega_r \\ \omega_r & 0 \end{bmatrix} \begin{bmatrix} i_r^d \\ i_r^q \end{bmatrix} + \frac{d}{dt} \begin{bmatrix} i_r^d \\ i_r^q \end{bmatrix} + \frac{1}{L_r} \begin{bmatrix} u_r^d \\ u_r^q \end{bmatrix} \quad (3.10)$$

$$\frac{1}{L_i} \begin{bmatrix} e_i^d \\ e_i^q \end{bmatrix} = \begin{bmatrix} \frac{R_i}{L_i} & 0 \\ 0 & \frac{R_i}{L_i} \end{bmatrix} \begin{bmatrix} i_i^d \\ i_i^q \end{bmatrix} + \begin{bmatrix} 0 & -\omega_i \\ \omega_i & 0 \end{bmatrix} \begin{bmatrix} i_i^d \\ i_i^q \end{bmatrix} + \frac{d}{dt} \begin{bmatrix} i_i^d \\ i_i^q \end{bmatrix} + \frac{1}{L_i} \begin{bmatrix} u_i^d \\ u_i^q \end{bmatrix} \quad (3.11)$$

Equations (3.10) and (3.11), with currents along d-q axes i_r^d , i_r^q and i_i^d , i_i^q as state variables, can be written in state space form $\dot{x} = Ax + Bu$ as

$$\frac{d}{dt} \begin{bmatrix} i_r^d \\ i_r^q \end{bmatrix} = \begin{bmatrix} -\frac{R_r}{L_r} & \omega_r \\ -\omega_r & -\frac{R_r}{L_r} \end{bmatrix} \begin{bmatrix} i_r^d \\ i_r^q \end{bmatrix} + \frac{1}{L_r} \begin{bmatrix} e_r^d - u_r^d \\ e_r^q - u_r^q \end{bmatrix} \quad (3.12)$$

$$\frac{d}{dt} \begin{bmatrix} i_i^d \\ i_i^q \end{bmatrix} = \begin{bmatrix} -\frac{R_i}{L_i} & \omega_i \\ -\omega_i & -\frac{R_i}{L_i} \end{bmatrix} \begin{bmatrix} i_i^d \\ i_i^q \end{bmatrix} + \frac{1}{L_i} \begin{bmatrix} e_i^d - u_i^d \\ e_i^q - u_i^q \end{bmatrix} \quad (3.13)$$

AC network voltages on rectifier and inverter ends of the dc link are assumed to be

$$\begin{bmatrix} e_r^a \\ e_r^b \\ e_r^c \end{bmatrix} = E_r \begin{bmatrix} \cos \omega_r t \\ \cos(\omega_r t - 120^\circ) \\ \cos(\omega_r t + 120^\circ) \end{bmatrix} \quad (3.14)$$

$$\begin{bmatrix} e_i^a \\ e_i^b \\ e_i^c \end{bmatrix} = E_i \begin{bmatrix} \cos \omega_i t \\ \cos(\omega_i t - 120^\circ) \\ \cos(\omega_i t + 120^\circ) \end{bmatrix} \quad (3.15)$$

where E_r , E_i are the peak values of ac network voltage on rectifier and inverter sides. Ac network voltage on rectifier side in equation (3.14) can be written as

$$T_{dq0}^{-1} \begin{bmatrix} e_r^d \\ e_r^q \\ e_r^0 \end{bmatrix} = E_r \begin{bmatrix} \cos \omega_r t \\ \cos(\omega_r t - 120^\circ) \\ \cos(\omega_r t + 120^\circ) \end{bmatrix}$$

Pre-multiplying both sides by T_{dq0}

$$T_{dq0} T_{dq0}^{-1} \begin{bmatrix} e_r^d \\ e_r^q \\ e_r^0 \end{bmatrix} = E_r T_{dq0} \begin{bmatrix} \cos \omega_r t \\ \cos(\omega_r t - 120^\circ) \\ \cos(\omega_r t + 120^\circ) \end{bmatrix}$$

$$\begin{bmatrix} e_r^d \\ e_r^q \\ e_r^0 \end{bmatrix} = \frac{2}{3} E_r \begin{bmatrix} \sin \omega t & \sin(\omega t - 120^\circ) & \sin(\omega t + 120^\circ) \\ \cos \omega t & \cos(\omega t - 120^\circ) & \cos(\omega t + 120^\circ) \\ \frac{1}{2} & \frac{1}{2} & \frac{1}{2} \end{bmatrix} \begin{bmatrix} \cos \omega_r t \\ \cos(\omega_r t - 120^\circ) \\ \cos(\omega_r t + 120^\circ) \end{bmatrix}$$

$$\begin{bmatrix} e_r^d \\ e_r^q \\ e_r^0 \end{bmatrix} = \begin{bmatrix} 0 \\ E_r \\ 0 \end{bmatrix} \quad (3.16)$$

Similar equation for the inverter side is

$$\begin{bmatrix} e_i^d \\ e_i^q \\ e_i^0 \end{bmatrix} = \begin{bmatrix} 0 \\ E_i \\ 0 \end{bmatrix} \quad (3.17)$$

Assuming balanced operation of interfacing ac network signifying, absence of zero axis components, the d-q transformed version of the ac network voltages in equations (3.14) and (3.15) can be written as

$$\begin{bmatrix} e_r^d \\ e_r^q \end{bmatrix} = \begin{bmatrix} 0 \\ E_r \end{bmatrix} \quad (3.18)$$

$$\begin{bmatrix} e_i^d \\ e_i^q \end{bmatrix} = \begin{bmatrix} 0 \\ E_i \end{bmatrix} \quad (3.19)$$

The switching functions giving the state of an IGBT in the rectifier and inverter end converters, assuming a sinusoidal signal modulating the carrier input in the PWM based IGBT gating module [26], are given by

$$\begin{bmatrix} S_r^a \\ S_r^b \\ S_r^c \end{bmatrix} = \begin{bmatrix} \frac{1}{2} + \frac{M_r}{2} \cos(\omega_r t - \delta_r) \\ \frac{1}{2} + \frac{M_r}{2} \cos(\omega_r t - \delta_r - 120^\circ) \\ \frac{1}{2} + \frac{M_r}{2} \cos(\omega_r t - \delta_r + 120^\circ) \end{bmatrix}$$

$$\begin{bmatrix} S_i^a \\ S_i^b \\ S_i^c \end{bmatrix} = \begin{bmatrix} \frac{1}{2} + \frac{M_i}{2} \cos(\omega_i t - \delta_i) \\ \frac{1}{2} + \frac{M_i}{2} \cos(\omega_i t - \delta_i - 120^\circ) \\ \frac{1}{2} + \frac{M_i}{2} \cos(\omega_i t - \delta_i + 120^\circ) \end{bmatrix}$$

$$\begin{bmatrix} u_r^a \\ u_r^b \\ u_r^c \end{bmatrix} = \begin{bmatrix} S_r^a \\ S_r^b \\ S_r^c \end{bmatrix} V_{dcr} - \left(\frac{V_{dcr}}{3} \right) \sum_{k=a,b,c} S_r^k \quad (3.20)$$

$$\begin{bmatrix} u_i^a \\ u_i^b \\ u_i^c \end{bmatrix} = \begin{bmatrix} S_i^a \\ S_i^b \\ S_i^c \end{bmatrix} V_{dci} - \left(\frac{V_{dci}}{3} \right) \sum_{k=a,b,c} S_i^k \quad (3.21)$$

The relationship between the converter ac and dc side voltages on rectifier and inverter sides using equations (3.20) and (3.21) become as

$$\begin{bmatrix} u_r^a \\ u_r^b \\ u_r^c \end{bmatrix} = \frac{M_r V_{dcr}}{2} \begin{bmatrix} \cos(\omega_r t - \delta_r) \\ \cos(\omega_r t - \delta_r - 120^\circ) \\ \cos(\omega_r t - \delta_r + 120^\circ) \end{bmatrix} \quad (3.22)$$

$$\begin{bmatrix} u_i^a \\ u_i^b \\ u_i^c \end{bmatrix} = \frac{M_i V_{dci}}{2} \begin{bmatrix} \cos(\omega_i t - \delta_i) \\ \cos(\omega_i t - \delta_i - 120^\circ) \\ \cos(\omega_i t - \delta_i + 120^\circ) \end{bmatrix} \quad (3.23)$$

where M_r , M_i are the modulation index, δ_r , δ_i are the phase shift between the modulating signal and the carrier signal in the pulse width modulation (PWM) module and V_{dcr} , V_{dci} are the dc link voltages, on rectifier and inverter ends.

The converter ac side voltage on rectifier side in equation (3.22) can be written as

$$T_{dq0}^{-1} \begin{bmatrix} u_r^d \\ u_r^q \\ u_r^0 \end{bmatrix} = \frac{M_r V_{dcr}}{2} \begin{bmatrix} \cos(\omega_r t - \delta_r) \\ \cos(\omega_r t - \delta_r - 120^\circ) \\ \cos(\omega_r t - \delta_r + 120^\circ) \end{bmatrix}$$

Pre-multiplying both sides by T_{dq0}

$$T_{dq0} T_{dq0}^{-1} \begin{bmatrix} u_r^d \\ u_r^q \\ u_r^0 \end{bmatrix} = \frac{M_r V_{dcr}}{2} T_{dq0} \begin{bmatrix} \cos(\omega_r t - \delta_r) \\ \cos(\omega_r t - \delta_r - 120^\circ) \\ \cos(\omega_r t - \delta_r + 120^\circ) \end{bmatrix}$$

$$\begin{bmatrix} u_r^d \\ u_r^q \\ u_r^0 \end{bmatrix} = \frac{2 M_r V_{dcr}}{3} \begin{bmatrix} \sin \omega t & \sin(\omega t - 120^\circ) & \sin(\omega t + 120^\circ) \\ \cos \omega t & \cos(\omega t - 120^\circ) & \cos(\omega t + 120^\circ) \\ \frac{1}{2} & \frac{1}{2} & \frac{1}{2} \end{bmatrix} \begin{bmatrix} \cos(\omega_r t - \delta_r) \\ \cos(\omega_r t - \delta_r - 120^\circ) \\ \cos(\omega_r t - \delta_r + 120^\circ) \end{bmatrix}$$

$$\begin{bmatrix} u_r^d \\ u_r^q \\ u_r^0 \end{bmatrix} = \frac{M_r V_{dcr}}{2} \begin{bmatrix} \sin \delta_r \\ \cos \delta_r \\ 0 \end{bmatrix} \quad (3.24)$$

Similar equation for the inverter side is

$$\begin{bmatrix} u_i^d \\ u_i^q \\ u_i^0 \end{bmatrix} = \frac{M_i V_{dci}}{2} \begin{bmatrix} \sin \delta_i \\ \cos \delta_i \\ 0 \end{bmatrix} \quad (3.25)$$

Assuming balanced operation of interfacing ac network signifying, absence of zero axis components, the d-q transformed version of the converter ac voltages in equations (3.22) and (3.23) can be written as

$$\begin{bmatrix} u_r^d \\ u_r^q \end{bmatrix} = \frac{M_r V_{dcr}}{2} \begin{bmatrix} \sin \delta_r \\ \cos \delta_r \end{bmatrix} \quad (3.26)$$

$$\begin{bmatrix} u_i^d \\ u_i^q \end{bmatrix} = \frac{M_i V_{dci}}{2} \begin{bmatrix} \sin \delta_i \\ \cos \delta_i \end{bmatrix} \quad (3.27)$$

3.3 Decoupling the State Variables

To facilitate modal analysis of a composite power system incorporating VSC-HVDC link and also to obtain decoupled inner current loop model, using the transformation $x = Px_z$, the state matrix in equation (3.12), which is of the form, $\dot{x} = Ax + Bu$ can be written as

$$P \dot{x}_z = APx_z + Bu$$

$$\dot{x}_z = P^{-1}APx_z + P^{-1}Bu \quad (3.28)$$

Substituting modal matrix and its inverse for the state matrix from (A.6), (A.7) and also substituting equation (3.18) into the state equation (3.12)

$$\frac{d}{dt} \begin{bmatrix} i_{r\alpha}^d \\ i_{r\alpha}^q \end{bmatrix} = \frac{1}{2} \begin{bmatrix} 1 & -j1 \\ -j1 & 1 \end{bmatrix} \begin{bmatrix} -\frac{R_r}{L_r} & \omega_r \\ -\omega_r & -\frac{R_r}{L_r} \end{bmatrix} \begin{bmatrix} 1 & j1 \\ j1 & 1 \end{bmatrix} \begin{bmatrix} i_{r\alpha}^d \\ i_{r\alpha}^q \end{bmatrix} + \frac{1}{2} \begin{bmatrix} 1 & -j1 \\ -j1 & 1 \end{bmatrix} \left\{ \frac{1}{L_r} \begin{bmatrix} 0 \\ E_r \end{bmatrix} - \frac{1}{L_r} \begin{bmatrix} u_r^d \\ u_r^q \end{bmatrix} \right\}$$

The foregoing equation after using equation (A.8) reduces to,

$$\frac{d}{dt} \begin{bmatrix} i_{r\alpha}^d \\ i_{r\alpha}^q \end{bmatrix} = \begin{bmatrix} -\frac{R_r}{L_r} + j\omega_r & 0 \\ 0 & -\frac{R_r}{L_r} - j\omega_r \end{bmatrix} \begin{bmatrix} i_{r\alpha}^d \\ i_{r\alpha}^q \end{bmatrix} + \frac{1}{2L_r} \begin{bmatrix} -jE_r \\ E_r \end{bmatrix} - \frac{1}{2L_r} \begin{bmatrix} u_{r\alpha}^d - ju_{r\alpha}^q \\ u_{r\alpha}^q - ju_{r\alpha}^d \end{bmatrix} \quad (3.29)$$

jE_r , ju_r^q and ju_r^d in equation (3.29) are the projections of E_r , u_r^q , u_r^d on their respective orthogonal axes in an orthogonal system of coordinates and reduce to zero. Therefore, the state matrices in equations (3.12) and (3.13) subjected to similarity transformation [27], to obtain decoupled state space equations can be written as

$$\frac{d}{dt} \begin{bmatrix} i_{r\alpha}^d \\ i_{r\alpha}^q \end{bmatrix} = \begin{bmatrix} -\frac{R_r}{L_r} + j\omega_r & 0 \\ 0 & -\frac{R_r}{L_r} - j\omega_r \end{bmatrix} \begin{bmatrix} i_{r\alpha}^d \\ i_{r\alpha}^q \end{bmatrix} + \frac{1}{2L_r} \begin{bmatrix} -u_r^d \\ E_r - u_r^q \end{bmatrix} \quad (3.30)$$

$$\frac{d}{dt} \begin{bmatrix} i_{i\alpha}^d \\ i_{i\alpha}^q \end{bmatrix} = \begin{bmatrix} -\frac{R_i}{L_i} + j\omega_i & 0 \\ 0 & -\frac{R_i}{L_i} - j\omega_i \end{bmatrix} \begin{bmatrix} i_{i\alpha}^d \\ i_{i\alpha}^q \end{bmatrix} + \frac{1}{2L_i} \begin{bmatrix} -u_i^d \\ E_i - u_i^q \end{bmatrix} \quad (3.31)$$

whereas $i_{r\alpha}^d$, $i_{r\alpha}^q$, $i_{i\alpha}^d$, $i_{i\alpha}^q$ are the transformed state variables, the state variables related to the voltage i.e. u_r^d , u_r^q , u_i^d , u_i^q are the original state variables.

3.4 Fully Decoupled Controller Models

In this section two fully decoupled controller models are described, based on two different methods for estimating reference values of currents for the inner current loop controller.

3.4.1 d-q Controller

First controller comprises of a fast inner current loop controller controlling the ac current within the converter's current carrying capability limit, and a number of outer loop controllers providing reference values of currents to the inner current loop controller. The reference currents in d-q frame of reference are derived from the instantaneous measured values of real and reactive powers and using the d-q transformed values of the phase voltages in a-b-c frame measured at the interfacing bus. The measured values of the currents are obtained by d-q transforming the currents in a-b-c frame measured at the interfacing bus.

Inner Current Loop Controller

In HVDC transmission, V_{dc} needs to be kept sufficiently high. For different operational regimes requiring real and reactive powers to be controlled independently and e_q , hence u_d and u_q need to be controlled independently. Consequently, the modulation index and also the phase shift between the modulating signal and the carrier signal in PWM module need to be varied to achieve various operational requirements. With a view to achieve dead beat control leading to zero steady state error, using state equation (3.30) of the rectifier side and defining feedback loops and PI compensation, as

$$\begin{bmatrix} x_1 \\ x_2 \end{bmatrix} = \frac{1}{2L_r} \begin{bmatrix} -u_r^d \\ E_r - u_r^q \end{bmatrix}$$

where

$$x_1 = \left(k_p + \frac{k_i}{s} \right) (i_{ref}^d - i_r^d)$$

$$x_2 = \left(k_p + \frac{k_i}{s} \right) (i_{ref}^q - i_r^q)$$

implying $u_r^d = -2L_r x_1$ and $u_r^q = E_r - 2L_r x_2$, thus

$$\begin{aligned} u_r^d &= -2L_r \left(k_p + \frac{k_i}{s} \right) (i_{ref}^d - i_r^d) \\ u_r^q &= E_r - 2L_r \left(k_p + \frac{k_i}{s} \right) (i_{ref}^q - i_r^q) \end{aligned} \quad (3.32)$$

Similarly, from equation (3.31) for the inverter side,

$$\begin{aligned} u_i^d &= -2L_i \left(k_p + \frac{k_i}{s} \right) (i_{iref}^d - i_i^d) \\ u_i^q &= E_i - 2L_i \left(k_p + \frac{k_i}{s} \right) (i_{iref}^q - i_i^q) \end{aligned} \quad (3.33)$$

where, i_{ref}^d , i_{ref}^q and i_{iref}^d , i_{iref}^q are the reference values of the respective direct and quadrature axis currents on the rectifier and inverter ends computing from the outer loop controller. Equations (3.32) and (3.33) model the inner current loop controller. The control implementation involves the state variables i_r^d , i_r^q , u_r^d , u_r^q and i_i^d , i_i^q , u_i^d , u_i^q . However, to incorporate controller dynamics into the composite state matrix together with the VSC-HVDC power circuit dynamics and interfacing ac system dynamics for

carrying out modal analysis of the composite system, u_r^d , u_r^q and u_i^d , u_i^q may have to be transformed to u_{rz}^d , u_{rz}^q and u_{iz}^d , u_{iz}^q .

Once u_r^d , u_r^q and u_i^d , u_i^q are available, required modulation index and also the phase shift between the modulating signal and the carrier signal in PWM module on rectifier and inverter side can be determined using the relations

$$M_r = \frac{\sqrt{u_r^{d2} + u_r^{q2}}}{V_{dcr}/2} \quad \delta_r = \tan^{-1}\left(\frac{u_r^q}{u_r^d}\right) - \theta_r \quad (3.34)$$

$$M_i = \frac{\sqrt{u_i^{d2} + u_i^{q2}}}{V_{dci}/2} \quad \delta_i = \tan^{-1}\left(\frac{u_i^q}{u_i^d}\right) - \theta_i \quad (3.35)$$

Outer Loop Controller

The outer loop comprises of controllers such as the dc voltage controller, the active power controller and the reactive power controller. These controllers provide reference values of the respective direct and quadrature axis currents to the inner current control loop implemented in d-q frame.

(i) DC Voltage Controller

Inverter side is set to control the dc link voltage. A control equation for the direct axis current reference on the inverter side is implemented for the purpose. This outer loop controller is much slower than the inner current loop controller, to ensure stability. i_{iref}^d being in rotating d-q frame, yields dc component in steady state and is synonymous to the active current, assuming no power losses in the converter.

$$i_{iref}^d = (V_{dciref} - V_{dci}) \left(k_p + \frac{k_i}{S} \right) \quad (3.36)$$

where, V_{dciref} is the reference dc link voltage on the inverter side.

(ii) Active Power Controller

The reference value of the active part of the converter current is supplied from the outer active power loop. The reference value i_{rref}^d being in rotating d-q frame, yields dc component in steady state. The control of active power combines both open loop and the feedback loop as shown in equation (3.37). For implementation of the feedback loop, error between the desired dc power to be transferred and the active power measured on the interface bus is computed in the loop itself.

$$P_{rref} = P_{roed} + \Delta P_r \left(k_p + \frac{k_i}{S} \right) \quad (3.37)$$

where, $\Delta P_r = P_{roed} - P_r$

$$i_{rref}^d = \frac{P_{rref}}{e_r^q} \quad (3.38)$$

where, P_{rref} is the reference real power, P_{roed} is the required real power and P_r is the measured real power, on the rectifier end

(iii) Reactive Power Controller

The outer reactive power loop supplies reference value of the reactive part of the converter current. The reference values i_{rref}^q at the rectifier and i_{iref}^q at the inverter ends

being in rotating d-q frame, yield dc component in steady state. The control of reactive power combines both open loop and the feedback loop as shown in equations (3.39) and (3.41). For implementation of the feedback loop, error between the desired reactive power to be exchanged between the ac network and the dc link and the reactive power measured on the interface bus is computed in the loop itself.

$$Q_{rref} = Q_{rord} + \Delta Q_r \left(k_p + \frac{k_i}{S} \right) \quad (3.39)$$

where, $\Delta Q_r = Q_{rord} - Q_r$

$$i_{rref}^q = \frac{Q_{rref}}{e_r^q} \quad (3.40)$$

$$Q_{iref} = Q_{iond} + \Delta Q_i \left(k_p + \frac{k_i}{S} \right) \quad (3.41)$$

where, $\Delta Q_i = Q_{iond} - Q_i$

$$i_{iref}^q = \frac{Q_{iref}}{e_i^q} \quad (3.42)$$

where, Q_{rref} , Q_{iref} are the reference reactive power, Q_{rord} , Q_{iond} are the required reactive power and Q_r , Q_i is the measured reactive power, on the rectifier and inverter ends.

Processing of Measurements

Conventional complex power is valid only for a system in steady state with a fixed line frequency. While 3-phase instantaneous power is valid during steady as well as transient

states [28] and describes the total energy flow per second between two interfacing systems. Using instantaneous power theory, phase current and voltage measurements on the network can be transformed to Clarke variables.

$$\begin{aligned} i_\alpha &= \frac{2}{3} \left(i_a - \frac{1}{2} i_b - \frac{1}{2} i_c \right) \\ i_\beta &= \frac{2}{3} \left(\frac{\sqrt{3}}{2} i_b - \frac{\sqrt{3}}{2} i_c \right) \end{aligned} \quad (3.43)$$

$$\begin{aligned} e_\alpha &= \frac{2}{3} \left(e_a - \frac{1}{2} e_b - \frac{1}{2} e_c \right) \\ e_\beta &= \frac{2}{3} \left(\frac{\sqrt{3}}{2} e_b - \frac{\sqrt{3}}{2} e_c \right) \end{aligned} \quad (3.44)$$

Instantaneous real and reactive power measured on the rectifier side and the reactive power measured on the inverter side in terms of the respective Clarke's components are given as

$$P_r = e_r^\alpha i_r^\alpha + e_r^\beta i_r^\beta \quad (3.45)$$

$$Q_r = e_r^\beta i_r^\alpha - e_r^\alpha i_r^\beta \quad (3.46)$$

$$Q_i = e_i^\beta i_i^\alpha - e_i^\alpha i_i^\beta \quad (3.47)$$

The measured values of the active power and the both end reactive power are used to implement open and feedback control in the outer power loop. Figure 3.3 and Figure 3.4 show the respective d-q controller models on rectifier and inverter sides.

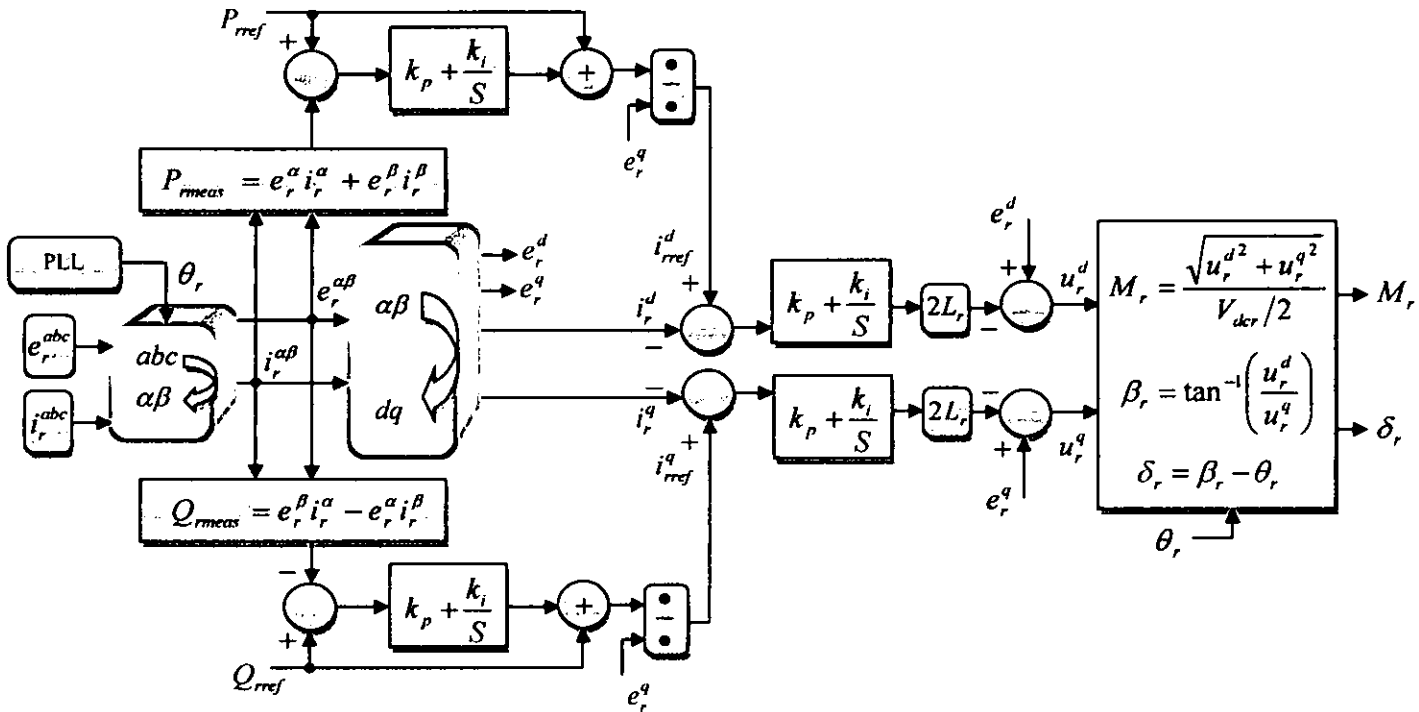


Figure 3-3: VSC-HVDC Rectifier d-q Controller

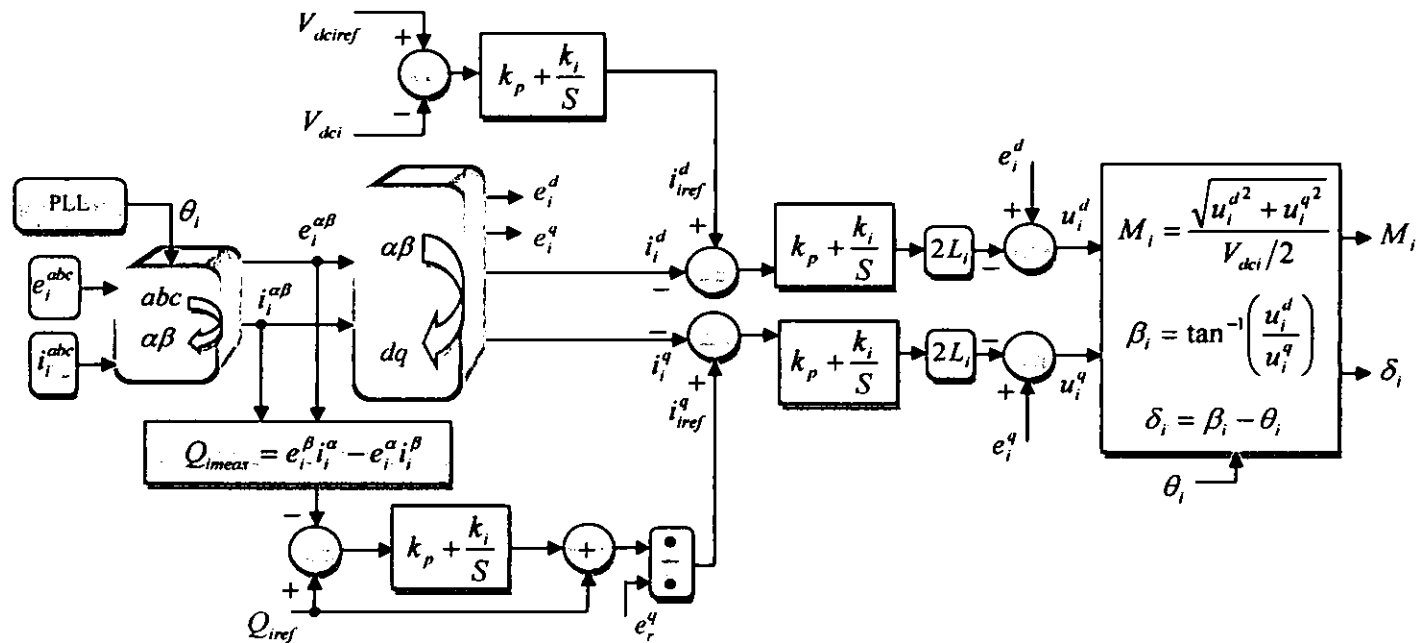


Figure 3-4: VSC-HVDC Inverter d-q Controller

3.4.2 Hybrid Controller

Second controller also comprises of a fast inner current loop similar to the d-q controller, controlling the ac current within the converter's current carrying capability limit. Real and reactive power outer loop controllers provide reference values of the instantaneous real and reactive powers for estimating reference values of the instantaneous Clarke's currents. These currents are then transformed to a d-q frame for the inner current loop controller, implemented in d-q reference frame. DC voltage controller used is similar to the first controller.

Estimating Reference Values of Currents for Inner Current Loop Controller

Usually rectifier side is set to control both real and reactive powers. Instantaneous active and reactive currents at the rectifier side are given as

$$i_r^{\alpha p} = \frac{e_r^\alpha}{(e_r^\alpha)^2 + (e_r^\beta)^2} P_{ref} \quad i_r^{\beta p} = \frac{e_r^\beta}{(e_r^\alpha)^2 + (e_r^\beta)^2} P_{ref} \quad (3.48)$$

$$i_r^{\alpha q} = \frac{e_r^\beta}{(e_r^\alpha)^2 + (e_r^\beta)^2} Q_{ref} \quad i_r^{\beta q} = \frac{-e_r^\alpha}{(e_r^\alpha)^2 + (e_r^\beta)^2} Q_{ref} \quad (3.49)$$

Instantaneous active and reactive reference currents in $\alpha\beta$ frame of reference for the rectifier side are now computed as

$$i_{ref}^\alpha = i_r^{\alpha p} + i_r^{\alpha q} \quad (3.50)$$

$$i_{ref}^\beta = i_r^{\beta p} + i_r^{\beta q} \quad (3.51)$$

Usually inverter side is set to control dc voltage and reactive power. The d-axis reference current is directly derived from the reference and measured values of dc voltages.

$$i_{iref}^d = (V_{dciref} - V_{dci}) \left(k_p + \frac{k_i}{s} \right) \quad (3.52)$$

Instantaneous active and reactive currents on the inverter side are given as

$$i_i^{\alpha p} = \frac{e_i^\alpha}{(e_i^\alpha)^2 + (e_i^\beta)^2} P_{iref} \quad i_i^{\beta p} = \frac{e_i^\beta}{(e_i^\alpha)^2 + (e_i^\beta)^2} P_{iref} \quad (3.53)$$

$$i_i^{\alpha q} = \frac{e_i^\beta}{(e_i^\alpha)^2 + (e_i^\beta)^2} Q_{iref} \quad i_i^{\beta q} = \frac{-e_i^\alpha}{(e_i^\alpha)^2 + (e_i^\beta)^2} Q_{iref} \quad (3.54)$$

Instantaneous reactive reference currents in $\alpha\beta$ frame of reference for the inverter side are given as

$$i_{iref}^\alpha = i_i^{\alpha p} + i_i^{\alpha q} \quad (3.55)$$

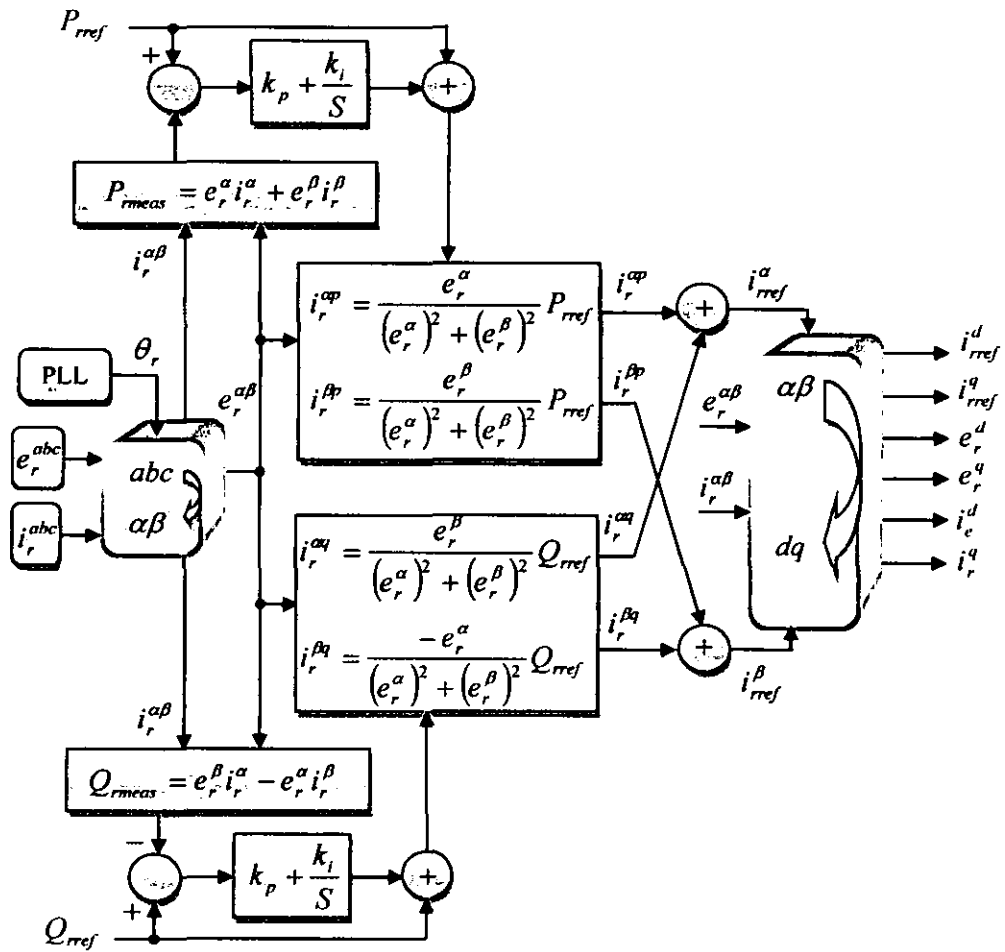
$$i_{iref}^\beta = i_i^{\beta p} + i_i^{\beta q} \quad (3.56)$$

The d-q variables can now be derived from the Clarks variables using equations (3.43), (3.44), (3.50), (3.51), (3.55) and (3.56), and also using the relationships as shown in equations (3.57) and (3.58). The transformation angle θ is available as the output of the phase locked loop (PLL).

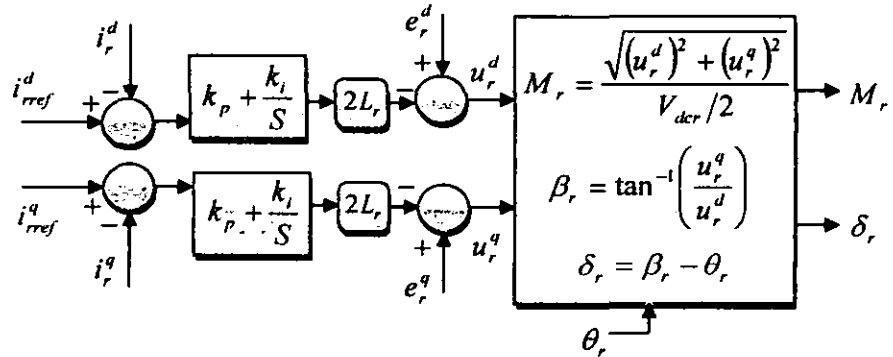
$$\begin{aligned} e^d &= e^\alpha \cos \theta + e^\beta \sin \theta \\ e^d &= -e^\alpha \sin \theta + e^\beta \cos \theta \end{aligned} \tag{3.57}$$

$$\begin{aligned} i^d &= i^\alpha \cos \theta + i^\beta \sin \theta \\ i^d &= -i^\alpha \sin \theta + i^\beta \cos \theta \end{aligned} \tag{3.58}$$

The complete hybrid controller models of the rectifier and the inverter side are shown in Figure 3.5 and Figure 3.6 respectively.

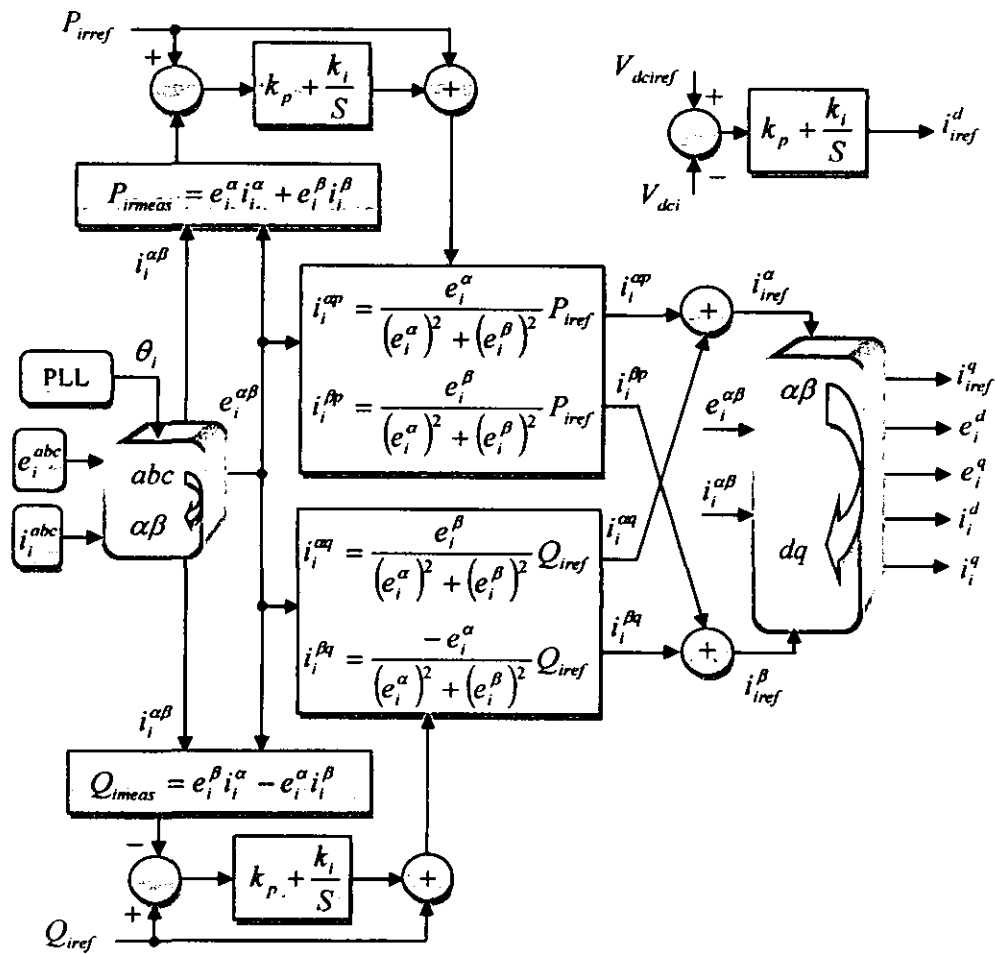


(a) Outer loop and reference value computation – Rectifier side

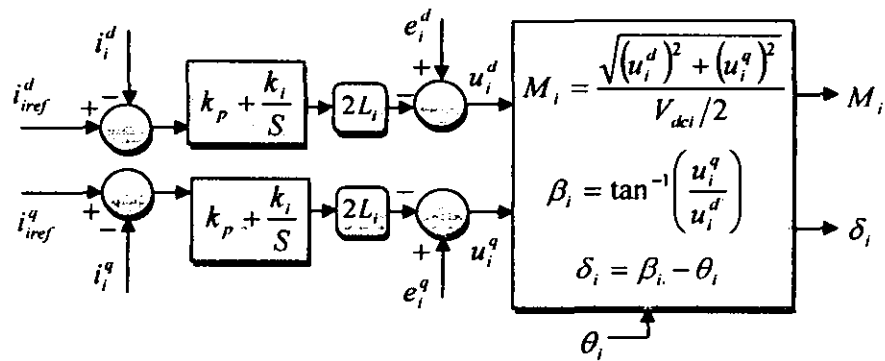


(b) Inner current loop – Rectifier side

Figure 3.5: VSC-HVDC Rectifier Hybrid Controller



(a) Outer loop and reference value computation – Inverter side



(b) Inner current loop – Inverter side

Figure 3.6: VSC-HVDC Inverter Hybrid Controller

3.5 Conclusion

This chapter develops the models of controllers for VSC-HVDC transmission system with a modified inner current loop wherein, not only the current errors in the d-q frame are decoupled, but the generation procedure of source side converter d-q voltages is also decoupled. The q component of the current error is not required to compute d component of the converter source side reference voltage and the d component of the current error is not required to compute q component of the converter source side reference voltage. This is expected to speed up reference voltage generation. The two controller models developed, implement two different methods for estimating reference values of currents for the inner current loop.

Conventional complex power is valid only for a system in steady state with a fixed line frequency. Whereas 3-phase instantaneous power is valid during steady as well as transient states and describes the total energy flow per second between two interfacing systems. Considering this, the computation of the measured Clarke's components of the real and reactive power in the outer power loop is proposed to be based on the instantaneous power theory.

The model performance is validated in chapter four, using SIMULINK Power System Blockset (PSB) based simulations on a composite power system, incorporating the developed controllers.

CHAPTER FOUR: MODEL VALIDATION

4.1. Introduction

The increasing rating and improved performance of self-commutated semiconductor devices has made possible High Voltage DC (HVDC) transmission based on Voltage-Sourced Converter (VSC). Performance of the VSC-HVDC controller models developed in the thesis are validated through SIMULINK power system block set (PSB) based simulations, carried on a composite power system incorporating the VSC-HVDC link and the developed controllers.

4.2. Power System Blockset

Power System Blockset operates in the SIMULINK environment to model electrical, mechanical and control systems. Electrical power systems are combinations of electrical circuits and electromechanical devices like motors and generators. These systems use power electronics and control systems to achieve their performance objectives. Power System Blockset has libraries containing models of typical power equipment such as transformers, lines, machines, and power electronics.

These models are proven ones coming from textbooks, and their validity is based on the experience of the Power Systems Testing and Simulation Laboratory of Hydro-Québec, a large North American utility located in Canada, and also on the experience of École de Technologie Supérieure and Université Laval. The Power System Blockset main library, powerlib, organizes its blocks into libraries according to their behavior. The main Power System Blockset powerlib library window also contains the Powergui block that opens a graphical user interface for the steady-state analysis of electrical circuits [29].

4.3 VSC-HVDC Transmission System Model

VSC-HVDC transmission system model is shown in Figure 4.1, 230 kv, 2000 MVA AC systems (AC system1 and AC system2 subsystems) are modeled by damped L-R equivalents with an angle of 80 degrees at fundamental frequency (50 Hz) as well as at third harmonic.

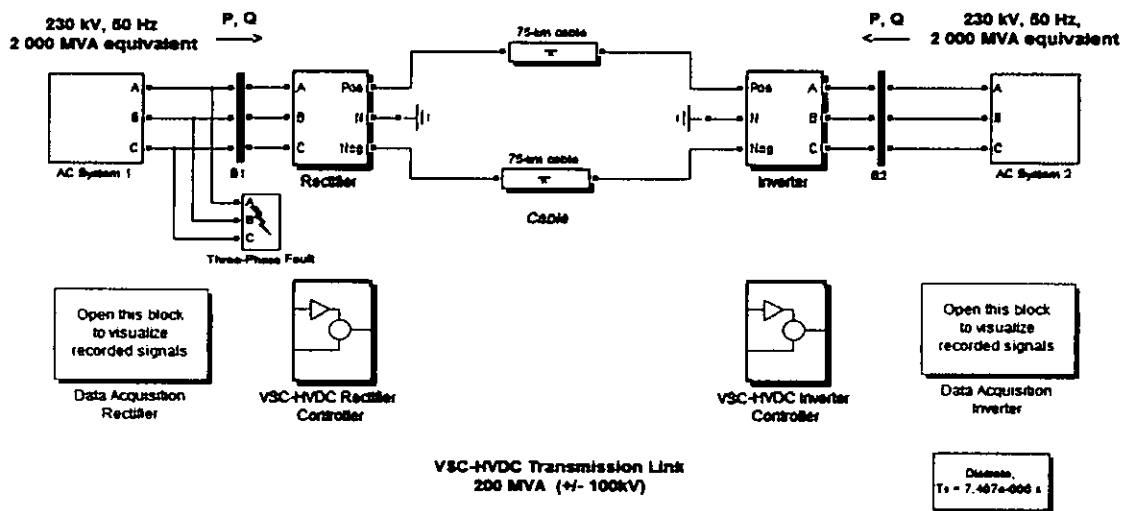


Figure 4.1: VSC-HVDC Transmission System Model

The VSC converters are three-level bridge blocks using close to ideal switching device model of IGBT. A converter transformer (Wye grounded /Delta) is used to permit the optimal voltage transformation. The winding arrangement blocks triplen harmonics produced by the converter. The tap position is at a fixed position determined by a multiplication factor applied to the primary nominal voltage of the converter transformers. The multiplication factors are chosen to have a modulation index around 0.85 (transformer ratios of 0.915 on the rectifier side and 1.015 on the inverter side). The converter reactor and the transformer leakage reactance permit the VSC output voltage to shift in phase and amplitude with respect to the AC system, and allow control of converter active and reactive power output.

AC filters are connected as shunt elements on the converter side of the converter transformer to meet AC system harmonic specifications. Since there are only high frequency harmonics, shunt filtering is relatively small compared to the converter rating. The shunt AC filters have 27th and 54th high pass filter legs totaling 40 Mvar.

The controllers of the VSC-HVDC link are modeled as described in chapter three. The rectifier side is set to control both real and reactive power and the inverter side is dedicated to control DC link voltage and reactive power.

The sampling time of the controller model ($T_{s_Control}$) is 74.07 μ sec, which is ten times the simulation sampling time. The power elements, the anti-aliasing filters and the PWM Generator block use the fundamental sampling time (T_{s_Power}) of 7.407 μ sec. The unsynchronized PWM mode of operation is chosen for our model. The normalized sampled voltages and currents (in pu) are provided to the controller.

The Clark Transformations block transforms the three phase reference frame to Clark's stationary frame. The d-q transformations block computes the "d" component and the "q" component from Clark's stationary frame. The Phase Locked Loop (PLL) block measures the system frequency and provides the phase synchronous angle for the d-q Transformations block. The Signal Calculations block calculates and filters quantities used by the controller i.e. active and reactive power, modulation index, phase shift between modulating signal and carrier signal, ac network voltage, and DC current and voltage.

4.3.1 Outer Loop Controller

The active and reactive power and voltage loop contains the outer loop regulators that calculate the reference value of the converter current (I_{ref_dq}) which is the input to the inner current loop controller. The control modes are: in the "d" axis, either the active

power flow at the AC network system or the pole-to-pole DC voltage; in the “q” axis, the reactive power flow at the AC network system. The main functions of the Active and reactive power and voltage loop are described below.

The Reactive Power Control regulator block combines a PI control with a feed forward control to increase the speed response. To avoid integrator wind-up, the following actions are taken: the error is reset to zero, when the measured AC network voltage is less than a constant value (i.e., during an AC perturbation); when the regulator output is limited, the limitation error is fed back with the right sign, to the integrator input.

The Active Power Control block is similar to the Reactive Power Control block. The extra Ramping block ramps the power order towards the desired value with an adjusted rate when the control is de-blocked. The ramped value is reset to zero when the converter is blocked.

The DC Voltage Control regulator block uses a PI regulator. The block is enabled when the Active Power Control block is disabled. The block output is a reference value, for the “d” component of converter current, for the Current Reference Limitation block.

The Current Reference Calculation block transforms the active and reactive power references, calculated by the P and Q controllers, to current references according to the measured voltage at the AC network bus. The current reference is estimated by two different methods as described in chapter three.

The current reference vector is limited to a maximum acceptable value (i.e., equipment dependent) by the Current Reference Limitation block. In power control mode, equal scaling is applied to the active and reactive power reference when a limit is imposed. In DC voltage control mode, higher priority is given to the active power when a limit is imposed for an efficient control of the voltage.

4.3.2 Inner Current Loop Controller

The main functions of Inner Current Loop block is to track the current reference value (“d” and “q” components) with a feed forward scheme, to achieve a fast control of the current at load changes and disturbances (e.g., short-circuit faults do not exceed the references) [30, 31]. In essence, it consist of knowing the U_{d-q} voltages and computing what the converter voltages have to be, by adding the voltage drops due to the currents across the impedance between the AC network and the converter AC voltages. The state equations representing the dynamics of the VSC currents are used (an approximation is made by neglecting the AC filters). The “d” and “q” components are decoupled to obtain two independent first-order plant models. A proportional integral (PI) feedback of the converter current is used to reduce the error to zero in steady state. The output of the AC Current Control block is the unlimited reference voltage vector $V_{ref_dq_tmp}$.

The Reference Voltage Conditioning block takes into account the actual DC voltage and the theoretical maximum peak value of the fundamental bridge phase voltage in relation to the DC voltage to generate the new optimized reference voltage vector. In our model (i.e., a three-level NPC with carrier based PWM), the ratio between the maximum fundamental peak phase voltage and the DC total voltage (i.e., for a modulation index of 1) is = 0.816. By choosing a nominal line voltage of 100 kV at the transformer secondary bus and a nominal total DC voltage of 200 kV the nominal modulation index would be 0.816. In theory, the converter should be able to generate up to $1/0.816$ or 1.23 pu when the modulation index is equal to 1. This voltage margin is important for generating significant capacitive converter current (i.e., a reactive power flow to the AC system). The Reference Voltage Limitation block limits the reference voltage vector amplitude to 1.0, since over modulation is not desired. The Inverse d-q and Inverse Clark transformation blocks are required to generate the three-phase voltage references to the PWM.

The system descriptions are presented in Table 4.1. Total simulation time is 3.0 sec, carrier frequency is 1350Hz and the integration time step is $7.407 \mu \text{ sec}$.

Table 4.1: System Description

Converter Transformer.	200 MVA, 0.15 p.u.	230kv/100kv
DC Link Rating	200 MW	$\pm 100\text{Kv}$
AC Side Harmonic Filters	40 MVAR	
27 th High Pass Damped	18 MVAR	Quality Factor = 15
54 th High Pass Damped	22 MVAR	Quality Factor = 15
Outer Loop Controllers		
P controller	$K_p=0.0$	$K_i=20.0$
Q controller	$K_p=0.0$	$K_i=20.0$
V_{dc} controller	$K_p=2.0$	$K_i=40.0$
Inner loop current controller	$K_p=4.0$	$K_i=40.0$

4.4 Comparative Performance Assessment of d-q Controller

Three scenarios are considered, to evaluate the performance of the developed model. In the first scenario, short circuit (SC) level at both rectifier and inverter end ac system buses is 2000 MVA i.e. the source impedance 26.45Ω is less than the converter transformer impedance 39.675Ω . The inverter end controls are activated at $t=0.1 \text{ sec}$ and the rectifier end controls are activated at $t=0.3 \text{ sec}$. In the second scenario, the short circuit level at both end ac system interfacing buses is 1000 MVA or a source impedance of 52.9Ω is more than the converter transformer impedance. Inverter end controls are initiated at $t=0.1 \text{ sec}$ and rectifier end controls are activated at $t=0.3 \text{ sec}$. In the third scenario, while the rectifier end source impedance is 52.9Ω , the inverter end source impedance is 26.45Ω . The activation time of respective end controls remain similar to the earlier two scenarios. The single line to ground fault occurs at the rectifier transformer primary side at $t=1.0 \text{ sec}$ and the fault is cleared at $t=1.2 \text{ sec}$.

Table 4.2: Scenario Description of d-q Controller

Case Study Description	Normal Fault Level	Lower fault Level	Single Line-Ground Fault
AC Network SC Level			
Rectifier Side	2000 MVA	1000 MVA	1000 MVA
Inverter Side	2000 MVA	1000 MVA	2000 MVA
Rectifier Side Controller	P, Q	P, Q	P, Q
Active controllers activated at	$t = 0.3$ sec	$t = 0.3$ sec	$t = 0.3$ sec
P_{ref}	1.0 p.u.	1.0 p.u.	1.0 p.u.
Q_{ref}	0.0 p.u.	0.0 p.u.	0.0 p.u.
Inverter Side Controller	V_{dc}, Q	V_{dc}, Q	V_{dc}, Q
Active controllers activated at	$t = 0.1$ sec	$t = 0.1$ sec	$t = 0.1$ sec
$V_{dc,ref}$	1.0 p.u.	1.0 p.u.	1.0 p.u.
Q_{ref}	-0.1 p.u.	-0.1 p.u.	-0.1 p.u.

Figure 4.2 shows the ac network voltage at the rectifier end in the three scenarios. The dynamic over voltage corresponding to higher source impedance is 6% as against 3% for the lower source impedance. With the real and reactive power controls activated at $t = 0.3$ sec on the rectifier end but without ac voltage control, ac network voltage is 4% lower than the rated one, under normal fault level condition. However, ac network voltage is 7% lower than the rated one, under lower fault level and single line to ground fault. The single line to ground fault occurs at the rectifier transformer primary side at $t = 1.0$ sec and the fault is cleared at $t = 1.2$ sec, ac network bus voltage is stable at $t = 1.3$ sec.

Figure 4.3 shows the ac network voltages at the inverter end in the three scenarios. Only dc link voltage and the reactive power flow control are activated at $t = 0.1$ sec on the inverter end and ac voltage remains inactive. The wave forms do not get influenced by the rectifier end asymmetrical fault at the transformer primary. Ac network voltage is 3% higher than the rated one, under all the three scenarios.

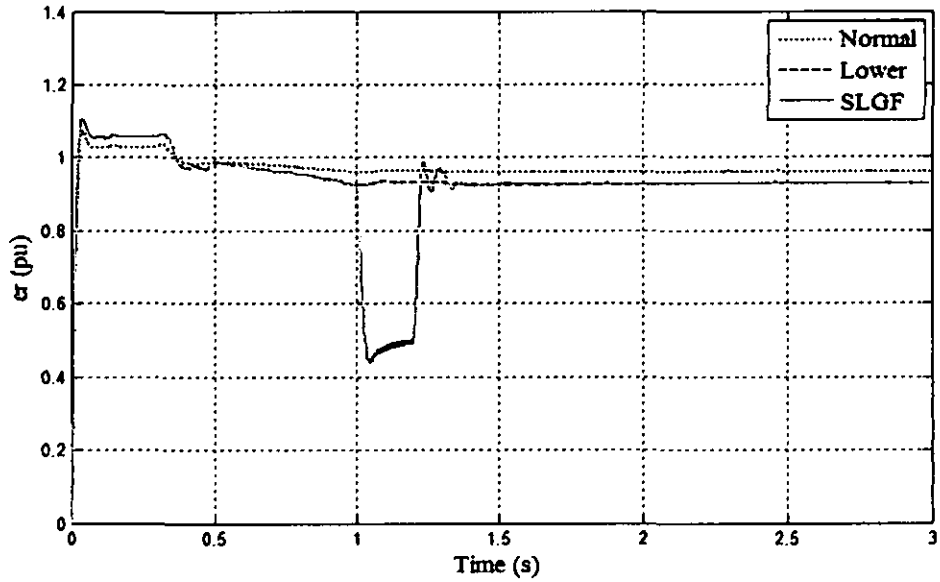


Figure 4.2: AC Network Bus Voltages - Rectifier Side d-q Controller

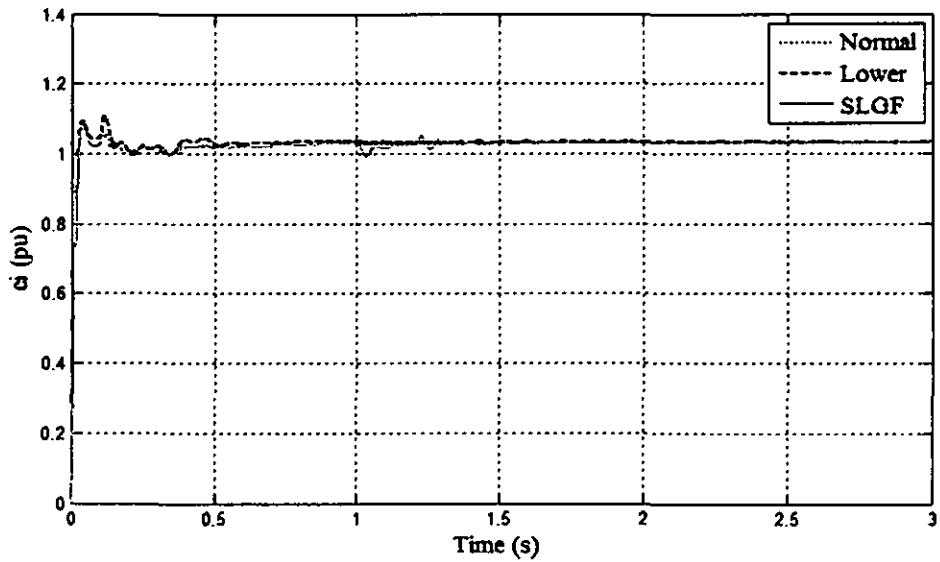


Figure 4.3: AC Network Bus Voltages - Inverter Side d-q Controller

Figure 4.4 shows the real power flow into dc link at rectifier side. Real power controller is activated at the rectifier side at $t=0.3$ sec and the real power reference is ramped up slowly to nominal rated power 1.0 p.u. Steady state is reached at $t=1.35$ sec on

normal and lower fault level. However, under single line to ground fault, real power drops to around 0.4 p.u. and the real power is controlled to a steady state by $t=1.6 \text{ sec}$ following the fault cleared at $t=1.2 \text{ sec}$.

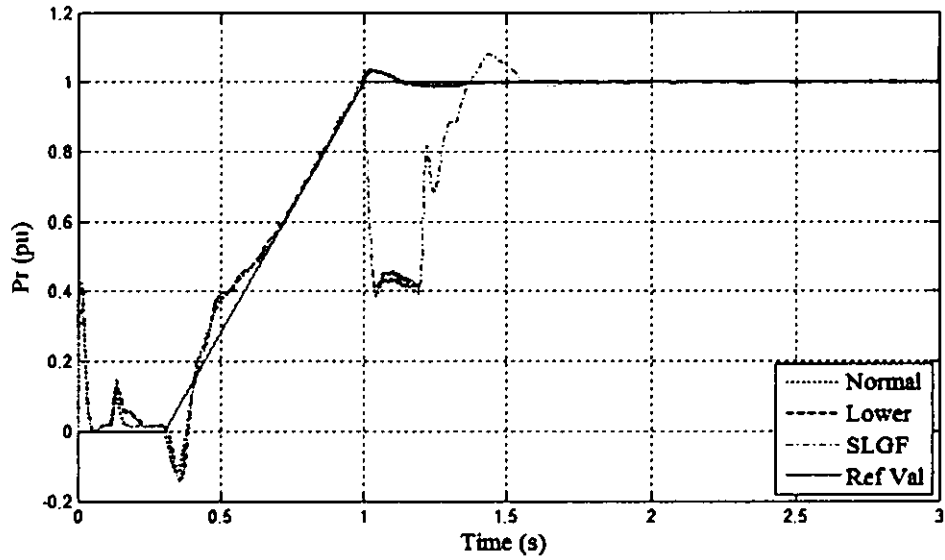


Figure 4-4: Real Power Flow into DC Link -Rectifier Side d-q Controller

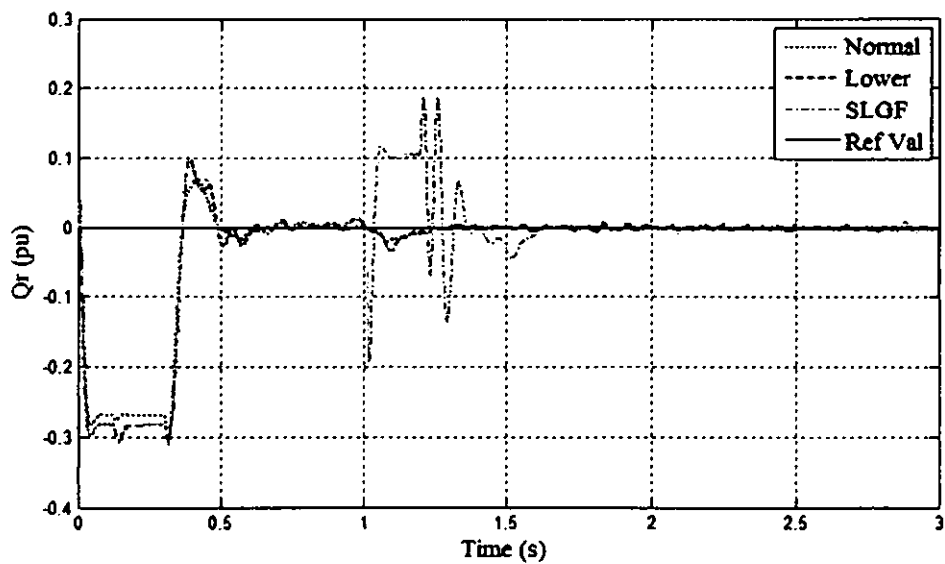


Figure 4.5: Reactive Power Flow into DC Link- Rectifier Side d-q Controller

Figure 4.5 shows the reactive power flow into the dc link at rectifier side. The rectifier end has the reactive power controller activated at $t=0.3$ sec. In all the scenarios reactive power reference import or export is set at zero. The reactive power flow is indeed controlled to its set value. However, oscillations are witnessed, when the rectifier side source impedance is higher than the converter transformer impedance. Under single line to ground fault, rectifier side changes operation from reactive power generation to consumption and reverse between -0.2 and 0.2 p.u. Furthermore, the reactive power is controlled to a steady state by $t=1.6$ sec following the fault cleared at $t=1.2$ sec.

Figure 4.6 shows the dc link voltage at the inverter side during all the three scenarios, the dc link voltage increases at the beginning cause dynamic overvoltage 25% and then goes back to the dc voltage reference 1.0 p.u wherein the dc voltage controller is activated at $t=0.1$ sec. Steady state is reached at $t=1.1$ sec on normal and lower fault level. Under single line to ground fault, dc voltage is oscillating around the reference value 1.0 p.u and the dc voltage is controlled to steady state by $t=1.5$ sec.

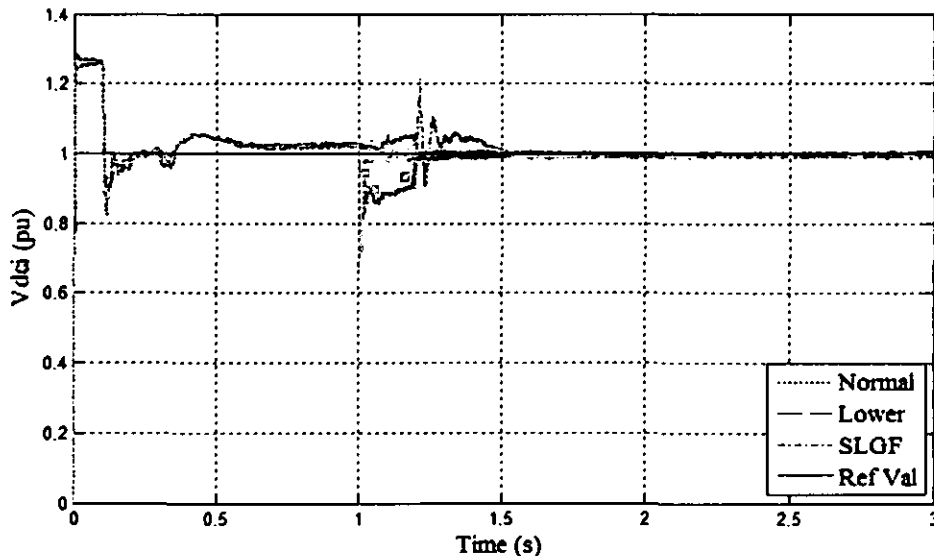


Figure 4.6: DC Link Voltage Measured on Inverter Side d-q Controller

Figure 4.7 presents' ac network phase voltages under single line to ground fault near rectifier transformer primary; the fault recovery time is 0.25 sec.

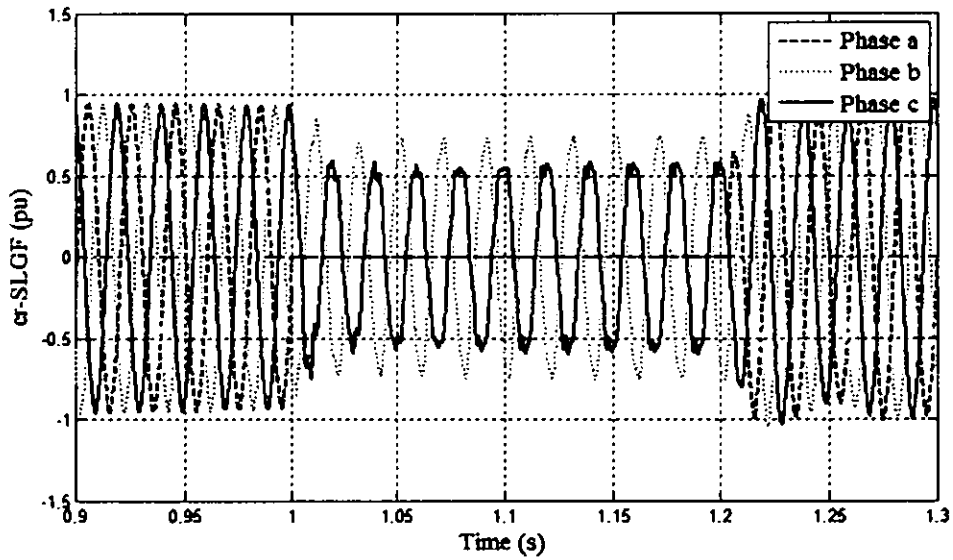


Figure 4.7: AC Network Phase Voltages – Single Line to Ground Fault near Rectifier Transformer Primary d-q Controller

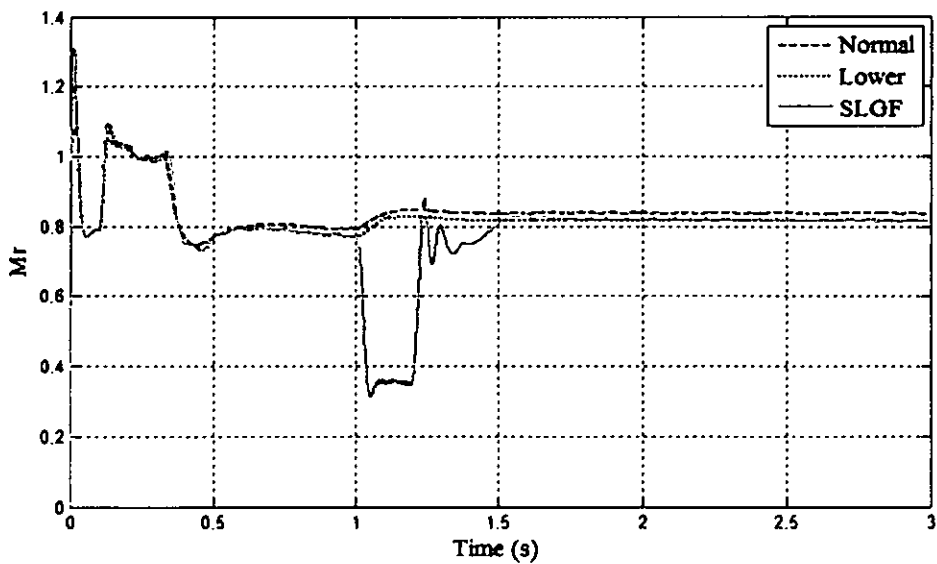


Figure 4.8: Modulation Index – Rectifier Side d-q Controller

Figure 4.8 shows the variation of the modulation index at the rectifier end. Over modulation is witnessed before the rectifier side controller is activated at $t=0.3 \text{ sec}$. Since over modulation is not desired, the rectifier side controller is controlled the modulation index close to its nominal value 0.816. The modulation index is become 0.84 under normal fault level, and 0.82 under lower fault level and single line to ground fault. Under single line to ground fault, modulation index drops to around 0.35 and the modulation index is controlled to a steady state by $t=1.8 \text{ sec}$ following the fault cleared at $t=1.2 \text{ sec}$.

4.5 Comparative Performance Assessment of the Hybrid Controller

In the scenario considered to evaluate the performance of the developed model, the short circuit level at both rectifier and inverter end ac system buses is 2000 MVA i.e. the source impedance 26.45Ω is less than the converter transformer impedance 39.675Ω . The inverter and the rectifier end controls are activated at $t=0.1 \text{ sec}$ and $t=0.3 \text{ sec}$.

Table 4.3: Scenario Description of Hybrid Controller

Case Study Description	Normal Fault Level
AC network Short Circuit Level	
Rectifier Side	2000 MVA
Inverter Side	2000 MVA
Rectifier Side Controller	
Active controllers activated at	P, Q $t = 0.3 \text{ sec}$
P_{ref}	1.0 p.u.
Q_{ref}	0.0 p.u.
Inverter Side Controller	
Active controllers activated at	V_{dc}, Q $t = 0.1 \text{ sec}$
P_{ref}	1.0 p.u.
$V_{dc\text{ref}}$	1.0 p.u.
Q_{ref}	-0.1 p.u.

Figure 4.9 shows the ac network voltage at the rectifier end bus. The dynamic over voltage is 3%. Since real and reactive power controls activated at $t=0.3$ sec on the rectifier end and ac voltage control remains inactive, the ac network voltage is 4% lower than the rated one.

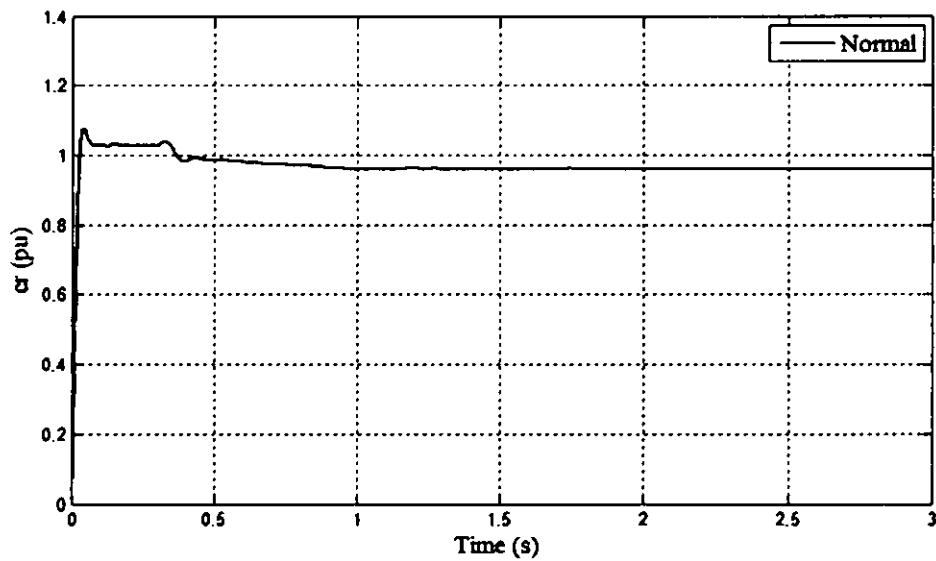


Figure 4.9: AC Network Bus Voltage - Rectifier Side Hybrid Controller

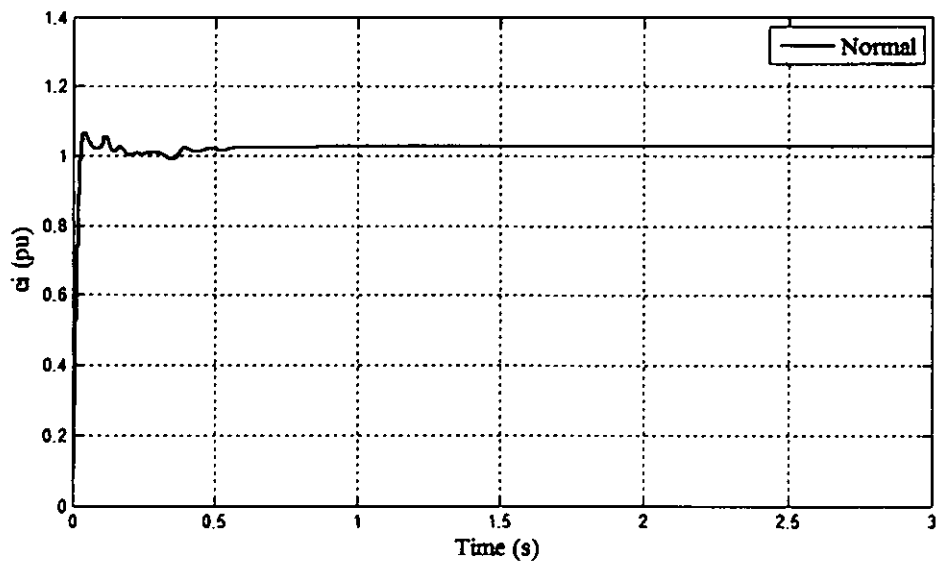


Figure 4.10: AC Network Bus Voltage - Inverter Side Hybrid Controller

Figure 4.10 shows the ac network voltages at the inverter end bus. Only dc link voltage and the reactive power flow control are activated at this end and ac voltage controller remains inactive.

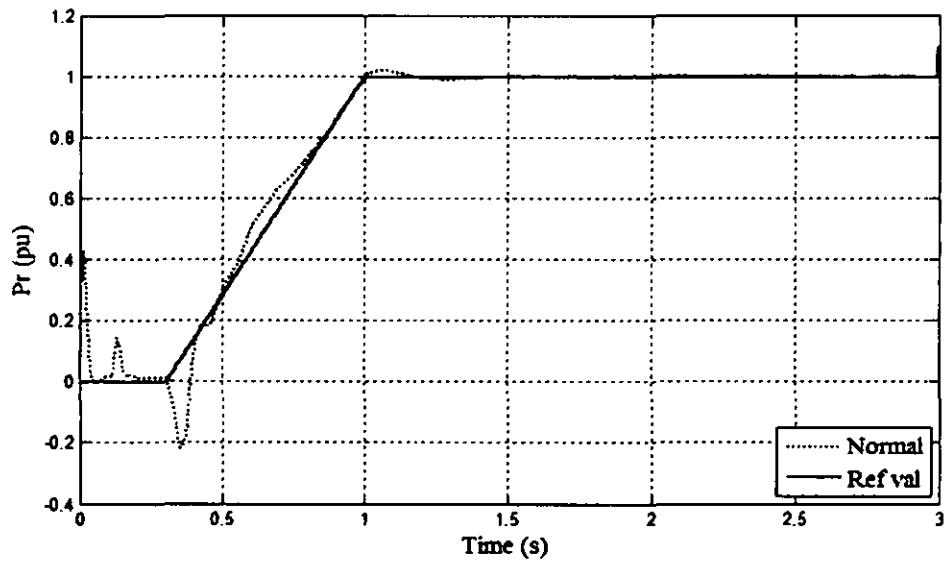


Figure 4.11: Real Power Flow into DC Link -Rectifier Side Hybrid Controller

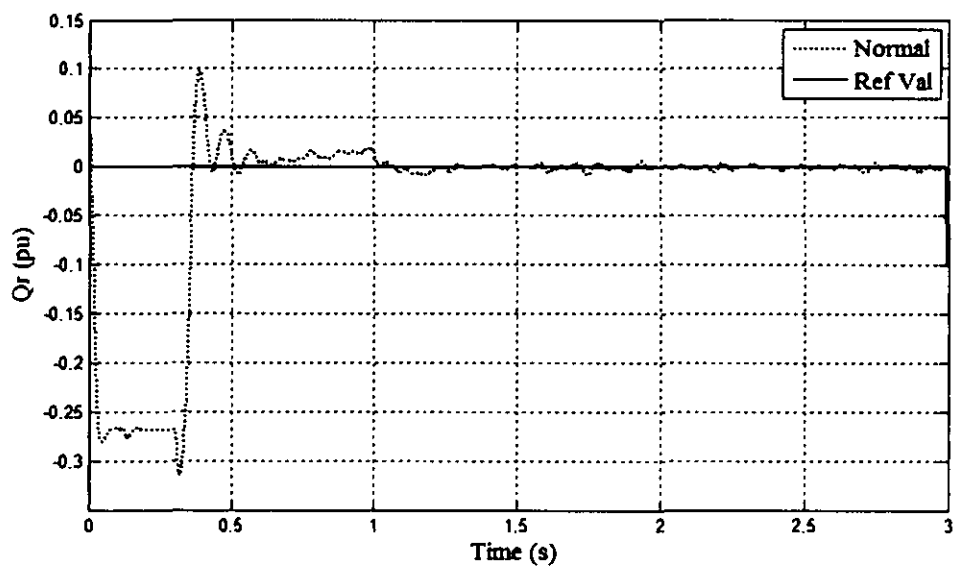


Figure 4.12: Reactive Power Flow into DC Link- Rectifier Side Hybrid Controller

Figure 4.11 shows the real power flow into dc link in rectifier side. Real power controller is activated at the rectifier side at $t=0.3 \text{ sec}$ and the real power reference is ramped up slowly to nominal rated power 1.0 p.u. Steady state is reached at $t=1.4 \text{ sec}$.

Figure 4.12 shows the reactive power flow into the dc link on rectifier side. The rectifier end has the reactive power controller activated at $t=0.3 \text{ sec}$. The reactive power import or export is set at zero. The reactive power flow is indeed controlled to its set value with some amount of oscillations within acceptable limits.

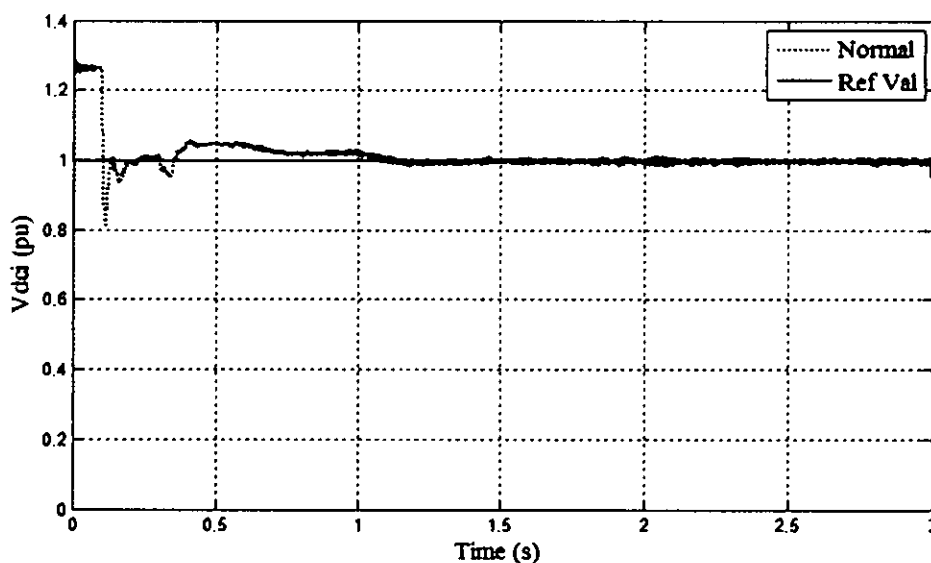


Figure 4.13: DC Link Voltage Measured on Inverter Side Hybrid Controller

Figure 4.13 shows the dc link voltage at the inverter side with the dc voltage controller activated at $t=0.1 \text{ sec}$. the dc link voltage increases at the beginning cause dynamic overvoltage 25% and then goes back to the dc voltage reference 1.0 p.u wherein the dc voltage controller is activated at $t=0.1 \text{ sec}$. Steady state is reached at $t=1.1 \text{ sec}$ on normal and lower fault level

Figure 4.14 presents the inverter side reactive power flow from the interfacing ac network into the inverter. The inverter end has the reactive power controller activated at

$t=0.1$ sec and the reactive power reference consumption is set at 0.1 p.u. The reactive power flow is indeed controlled to its set value. However, oscillations are witnessed and the reactive power is controlled to a steady state by $t=1.1$ sec.

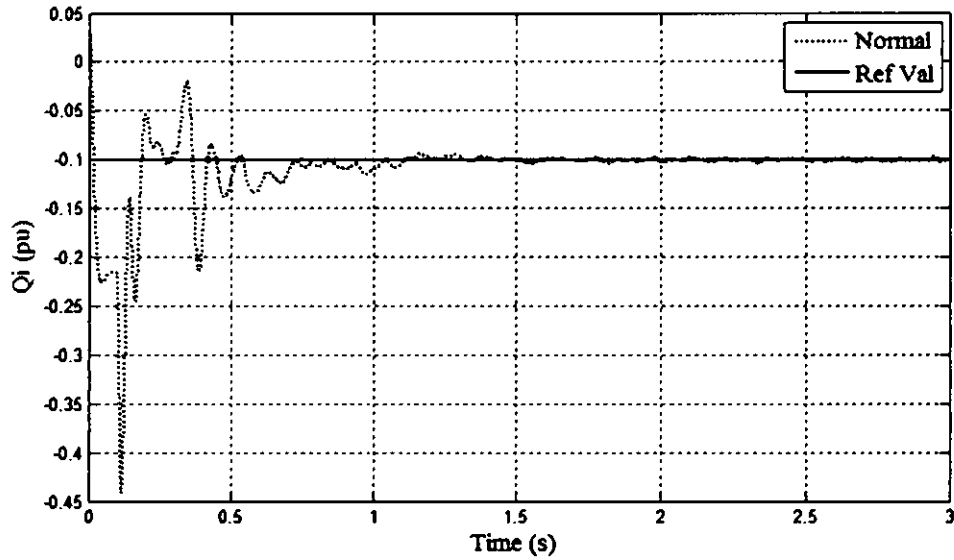


Figure 4.14: Reactive Power Flow into DC Link- Inverter Side Hybrid Controller

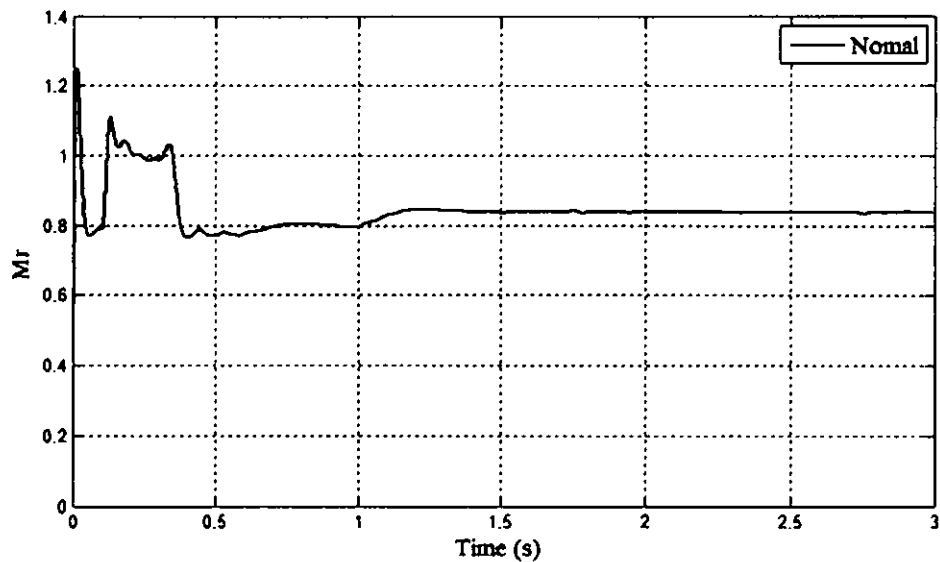


Figure 4.15: Modulation Index – Rectifier Side Hybrid Controller

Figure 4.15 shows the variation of the modulation index at the rectifier end. Over modulation is witnessed before the rectifier side controller is activated at $t=0.3 \text{ sec}$. Since over modulation is not desired, the rectifier side controller is controlled the modulation index close to its nominal value 0.816 which is 0.84. The modulation index is controlled to a steady state by $t=1.2 \text{ sec}$.

4.6 Conclusion

The performance of the developed controller models is assessed through SIMULINK Power System Blockset (PSB) simulations on a VSC-HVDC link interfacing an ac system. The simulation results show that the two controller models under normal fault level perform in the similar way and have fast response.

CHAPTER FIVE: CONCLUSION AND FUTURE WORK

5.1 Conclusion

Instantaneous power theory is advantageous for measuring real and reactive power, as it is suitable for steady and transient states as well as for non sinusoidal waveforms, a distinct possibility in presence of harmonics during system operation. Similarity transformation can be used to obtain a fully decoupled model for the inner current control loop control circuit implementation involves original current and voltage state variables.

The results discussed from system disturbances imposed on the AC grid and the HVDC link controller's ability to restore the values of the key variables is demonstrated on the time and event labeled response curves. conclusion on the appropriate behaviour of the performance of the developed controller is demonstrated through the behaviour of the variables such an active power, reactive power and the Vdc, which converge to the set point values for the given disturbances in the AC network. A lower fault level ac system interfacing with the VSC-HVDC link may lead to longer settling time, higher dynamic over voltages and relatively a longer fault recovery time.

However, to facilitate small signal stability assessment of a composite system comprising of VSC-HVDC link as well as interfacing ac system, the variables need to be transformed while framing the state matrix.

5.2 Contributions of the Research

The main contributions of the research are as follows:

- A fully decoupled controller model exploiting similarity transformation is developed.
- Instantaneous power theory is used for obtaining the measured values of the real and reactive powers, and also for deriving reference values of the currents used in the inner current control loop.

5.3 Future Work

The future direction may be towards improving the simulation procedure. The simulation carried out through SIMULINK Block set involves fixed integration time steps. This poses problems while simulating a model involving transfer functions having derivative terms. Such a model has also been developed during the course of this research and is available in the paper presented at PECON2008, and provided in the appendix of this thesis. To handle this model, integration with variable time step is required to introduce shorter time steps during steep changes, a common feature with semiconductor devices responding to fast network changes.

REFERENCES

- [1] M. P. Bahrman, "Overview of HVDC transmission," in Proc. of the IEEE Power Systems Conference and Exposition (PSCE), pp.18–23, 2006.
- [2] M. P. Bahrman, J. G. Johansson and B. A. Nilsson, "Voltage source converter transmission technologies-the right fit for the application," presented at 2003 IEEE PES General Meeting, Toronto, Canada, pp. 13–18, July 2003.
- [3] R. Rudervall, J.P. Chrpentier, and R. Sharma, "High Voltage Direct Current (HVDC) Transmission Systems Technology Review Paper," in Energy Week 2000, Washington, D.C, USA, March 2000.
- [4] V. k. Sood, *HVDC and FACTS Controllers: Applications of Static Converters in Power Systems*, Springer, 2004.
- [5] <http://www.abb.com/hvdc>, accessed at 2008.
- [6] G. Asplund, "Application of HVDC Light to power system enhancement," in Proc. of the IEEE PES 2000 winter meeting, vol. 4, pp. 2498–2503, February 2000.
- [7] K. Eriksson, "HVDC Light and development of Voltage Source Converters," presented at IEEE/PES T & D 2002 Latin American Conference, Sao Paulo, Brazil, pp. 1-5, 2002.
- [8] A.K. Skytt, P. Holmberg, and L.E. Juhlin, "HVDC Light for connection of wind farms," in Proc. Second International Workshop on Transmission Networks for off shore Wind Farms Royal Institute of Technology Stockholm, Sweden, March 2001.
- [9] B.R. Andersen, "VSC transmission," CIGRE B4, HVDC and Power Electronics HVDC Colloquium, Oslo, 2006.

- [10] F. Schettler, H. Huang, and N. Christl, "HVDC Transmission Systems using Voltage Sourced Converters- Design and Application," in Proc. of the IEEE PES 2000 summer meeting, vol. 2, pp. 715–720, July 2000.
- [11] S. N. Singh, *Electric Power Generation, Transmission and Distribution*, PHI Learning Pvt. Ltd., 2004,
- [12] M. H. Rashid, *Power Electronics Handbook*, Academic Press, Second Edition, 2006.
- [13] J. Arrillaga, *High Voltage Direct Current Transmission*, IET, Second Edition, 1998.
- [14] J. Arrillaga, Y. H. Liu and N. R. Watson, *Flexible Power Transmission: The HVDC Options*, John Wiley and Sons, 2007.
- [15] B.R. Andersen, L. Xu, P. J. Horton, and P. Cartwright, "Topologies for VSC transmission," *Power Engineering Journal*, vol. 16, no. 3, pp. 142–150, June 2002.
- [16] N. Stretch, M. Kazerani, and R. El Shatshat, "A Current-Sourced Converter-based HVDC Light Transmission System," in Proc. 2006 IEEE International Symposium on Industrial Electronics (ISIE), Canada, pp. 2001–2006, July 2006.
- [17] Y. Ye, M. kazerani, and V.H. Quintana, "Current-Source Converter Based STATCOM: Modeling and Control," *IEEE Trans. Power Delivery*, vol. 20, no. 2, pp. 795–800, April 2005.
- [18] M. Bahrman, A.A. Edris, and R. Haley, "Asynchronous back-to-back HVDC link with the voltage source converters," presented at Minnesota Power Systems Conference, USA, pp. 1–7, November 1999.
- [19] J.L. Thomas, S. Poullain and A. Benchaib, "Analysis of a Robust DC–Bus Voltage Control System for a VSC Transmission Scheme," in Proc. 2001 Seventh International Conference on AC–DC Power Transmission IEE, pp. 119–124, 2001.

- [20] H. Akagi, E. H. Watanabe and M. Aredes, *Instantaneous Power Theory and Applications to Power Conditioning*, Wiley-IEEE Press, 1998.
- [21] C. Schauder, and H. Mehta, "Vector analysis and control of advanced static VAR compensators," *IEE Proc. Gen., Transm. and Distrib.*, vol. 140, no. 4, pp. 299–306, July 1993.
- [22] C. Du, A. Sannino, and M. Bollen, "Analysis of the Control Algorithms of Voltage-Source Converter HVDC," in *Proc. 2005 IEEE Russia Power Tech*, pp. 1–7, June 2005.
- [23] H. Nikkhajoei, and R. Iravani, "Dynamic Model and Control of AC–DC–AC Voltage-Sourced Converter System for Distributed Resources," *IEEE Trans. Power Delivery*, vol. 22, no. 2, pp. 1169–1178, April 2007.
- [24] A Lindberg, and L Lindberg, "Inner current loop for large voltage source converters operating at low switching frequency," in *Proc. Fifth International Conference on Power Electronics and Variable-Speed Drives IEE*, pp. 217–222, October 1994.
- [25] A Lindberg, and T Larsson, "PWM and control of three level voltage source converters in an HVDC back-to-back station," in *Proc. Sixth International Conference on AC–DC Power Transmission IEE*, pp. 297–302, April/May 1996.
- [26] A. Nabavi-Niaki, and M. R. Iravani, "Steady-state and dynamic models of unified power flow controller (UPFC) for power system studies," *IEEE Transactions on power systems*, vol. 11, no. 4, pp. 1937–1943, November 1996.
- [27] A. Mahjoub, and R. Mukerjee, "Modeling of Controller for Voltage Sourced Converter based HVDC Transmission System," in *Proc. of IEEE 2nd International Power and Energy Conference (PECon 08)*, Johor Baharu, Malaysia, pp. 849–854, December 2008.

[28] H. Akagi, Y. Kanazawa, and A Nabae, "Instantaneous reactive power compensators comprising switching devices without energy storage components," IEEE Trans. Industry Applications, vol. IA-20, no. 3, pp. 625–630, May/June 1984.

[29] <http://www.mathworks.com>, accessed at 2008.

[30] W. Lu and B-T. ooi, "Optimal Acquisition and Aggregation of Offshore Wind Power by Multiterminal Voltage-Source HVDC," IEEE Transactions on Power Delivery, vol. 18, no. 1, pp. 201–206, January 2003.

[31] C. K. Sao, P. W. Lehn, M. R. Iravani, and J. A. Martinez, "A Benchmark System for Digital Time-Domin Simulation of a pulse-Width-Modulated D-STATCOM," IEEE Transactions on Power Delivery, vol. 17, no. 4, pp. 1113–1120, October 2002.

APPENDIX

Appendix A

Eigen values of the state matrix for rectifier side in equation (3.12) can be determined by solving the characteristic equation given by $A - \lambda_r I = 0$

$$\begin{bmatrix} -\frac{R_r}{L_r} & \omega_r \\ -\omega_r & -\frac{R_r}{L_r} \end{bmatrix} - \lambda_r \begin{bmatrix} 1 & 0 \\ 0 & 1 \end{bmatrix} = 0 \quad (\text{A.1})$$

Equation (A.1) yields two Eigen values

$$\lambda_{r1} = -\frac{R_r}{L_r} - j\omega_r$$
$$\lambda_{r2} = -\frac{R_r}{L_r} + j\omega_r$$

Eigen vector corresponding to λ_{r1} can be determined from $(A - \lambda_{r1}I)V_1 = 0$

$$\left\{ \begin{bmatrix} -\frac{R_r}{L_r} & \omega_r \\ -\omega_r & -\frac{R_r}{L_r} \end{bmatrix} - \lambda_{r1} \begin{bmatrix} 1 & 0 \\ 0 & 1 \end{bmatrix} \right\} \begin{bmatrix} v_{11} \\ v_{21} \end{bmatrix} = 0 \quad (\text{A.2})$$

Substituting $\lambda_{r1} = -\frac{R_r}{L_r} - j\omega_r$ in equation (A.2) yields

$$\begin{aligned}
-\left[\frac{R_r}{L_r} - \frac{R_r}{L_r} + j\omega_r\right]v_{11} + \omega_r v_{21} &= 0 \\
-\omega_r v_{11} - \left[\frac{R_r}{L_r} - \frac{R_r}{L_r} + j\omega_r\right]v_{21} &= 0 \\
-j\omega_r v_{11} + \omega_r v_{21} &= 0 \\
-\omega_r v_{11} - j\omega_r v_{21} &= 0
\end{aligned} \tag{A.3}$$

Treating v_{11} as the free variable in equation (A.3) and assigning an arbitrary value of 1 yields

$$V_1 = \begin{bmatrix} v_{11} = 1 \\ v_{21} = j1 \end{bmatrix}$$

Likewise, eigenvector corresponding to λ_{r2} , can be determined from $|A - \lambda_{r2}I|V_2 = 0$

$$\left\{ \begin{bmatrix} -\frac{R_r}{L_r} & \omega_r \\ -\omega_r & -\frac{R_r}{L_r} \end{bmatrix} - \lambda_{r2} \begin{bmatrix} 1 & 0 \\ 0 & 1 \end{bmatrix} \right\} \begin{bmatrix} v_{12} \\ v_{22} \end{bmatrix} = 0 \tag{A.4}$$

Substituting $\lambda_{r2} = -\frac{R_r}{L_r} - j\omega_r$ into equation (A.4) yields

$$\begin{aligned}
-\left[\frac{R_r}{L_r} - \frac{R_r}{L_r} - j\omega_r\right]v_{12} + \omega_r v_{22} &= 0 \\
-\omega_r v_{12} - \left[\frac{R_r}{L_r} - \frac{R_r}{L_r} - j\omega_r\right]v_{22} &= 0 \\
j\omega_r v_{12} + \omega_r v_{22} &= 0 \\
-\omega_r v_{12} + j\omega_r v_{22} &= 0
\end{aligned} \tag{A.5}$$

Treating v_{22} as the free variable in equation (A.5) and assigning an arbitrary value of 1 yields

$$V_2 = \begin{bmatrix} v_{12} = j1 \\ v_{22} = 1 \end{bmatrix}$$

Modal matrix and its inverse of the state matrix in equation (3.12) are

$$P = [V_1 \ V_2] = \begin{bmatrix} 1 & j1 \\ j1 & 1 \end{bmatrix} \quad (\text{A.6})$$

$$P^{-1} = \frac{1}{2} \begin{bmatrix} 1 & -j1 \\ -j1 & 1 \end{bmatrix} \quad (\text{A.7})$$

Similarity transformation $P^{-1}AP$ of state matrix in equation (3.12), which is of the form,

$\dot{x} = Ax + Bu$ is given by

$$P^{-1}AP = \frac{1}{2} \begin{bmatrix} 1 & -j1 \\ -j1 & 1 \end{bmatrix} \begin{bmatrix} -\frac{R_r}{L_r} & \omega_r \\ -\omega_r & -\frac{R_r}{L_r} \end{bmatrix} \begin{bmatrix} 1 & j1 \\ j1 & 1 \end{bmatrix}$$

$$P^{-1}AP = \begin{bmatrix} -\frac{R_r}{L_r} + j\omega_r & 0 \\ 0 & -\frac{R_r}{L_r} - j\omega_r \end{bmatrix} \quad (\text{A.8})$$

Appendix B

Ahmed Mahjoub and Ravindra Mukerjee, "Modeling of Controller for Voltage Sourced Converter based HVDC Transmission System," 2nd IEEE International Conference on Power and Energy (PECon 08), Johor Baharu, Malaysia, pp. 849–854, December 2008.

Modeling of Controller for Voltage Sourced Converter based HVDC Transmission System

Ahmed Mahjoub* and Ravindra Mukerjee**

* Universiti Teknologi PETRONAS, Perak, Malaysia, E-mail: mahjoub_ahmed@yahoo.com

** Universiti Teknologi PETRONAS, Perak, Malaysia, E-mail: mukerjee@petronas.com.my

Abstract: This paper develops the dynamic mathematical model of the rectifier and inverter side controllers for a Voltage Sourced Converter (VSC) based high voltage DC (VSC-HVDC) link employing Insulated Gate Bipolar Transistor (IGBT) with PWM control. The controller derived using instantaneous power theory, parks transformation, and similarity transformation is expected to maintain the dc link voltage and reactive power at the sending end and control both active and reactive power at the receiving end under changing operating conditions. The model also facilitates systems oscillatory performance assessment.

Keywords: VSC-HVDC, PWM Controller Modeling, HVDC Dynamic Performance

1. INTRODUCTION

High Voltage Direct Current (HVDC) technology has characteristics which make it especially attractive for long distance bulk power transmission or asynchronous interconnection applications. Most of the HVDC links currently in operation use line commutated converter (LCC) technology. However, HVDC transmission system based on line commutated thyristor have few shortcomings: converters absorb reactive power to the extent of 50% of the real power being transferred, injection of low order harmonic currents into the interfacing AC system, risk of inverter commutation failures in presence of Faults and switching operations in AC network, and its dependence on reasonably strong AC systems having active sources to provide commutating voltages [1]. With the emergence of offshore renewable energy sources resulting in increased distance between offshore generation and onshore distribution grid, developments in the high voltage and high current self commutated GTO and IGBT based voltage sourced converters together with Pulse Width Modulation (PWM) control, feasible use of polymeric cables having light weight and requiring smaller bending radius, absence of charging current endangering marine life, VSC-HVDC provides a preferred alternative for

power evacuation from the off-shore renewable energy installations.

VSC-HVDC transmission system has the following advantages compared with conventional LCC-HVDC transmission system: capability to rapidly control both active and reactive power independently of each other, PWM control moves characteristic harmonics to higher order, no communication required between the sending and receiving end converter stations, possible operation with weak AC systems and lower dynamic over voltages. Voltage sourced converters in VSC-HVDC not only control the power flow but also, provide dynamic voltage regulation to the interfacing ac network [1, 2, 3].

HVDC converter station can comprise of either voltage-sourced converters or current-sourced converters. Whereas the CSCs' are robust, the VSCs' have higher efficiency, low initial cost, and smaller physical size. Voltage-sourced converter is preferred over current-sourced converter since current-sourced converter has series diode with each switch, resulting in increased cost and losses. CSC also requires smoothing DC inductors across the three-phase bridge terminals, which are generally larger and more expensive than capacitors used in voltage-sourced converters [2, 6]. IGBT module commercially available is more suitable for voltage-source PWM converter, since a free-wheeling diode is connected in anti-parallel with each IGBT. Thus the IGBT does not need to be provided with the built-in reverse voltage blocking capability, thus bringing more flexibility to device design, a compromise between switching losses and short-circuit capability.

The operational requirements imposed on an HVDC link keep on varying, depending on the changes in interfacing ac network operating conditions at its sending and receiving ends. Normal power transfer in forward direction, reverse power transfer, sending end and/or receiving end ac network short circuit capacity low due to

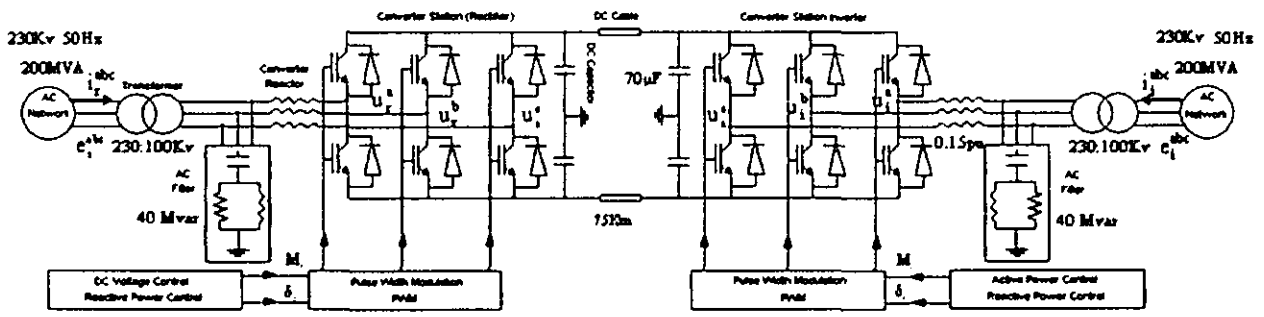


Fig. 1: schematic of VSC-HVDC

network fault, DC line witnessing fault, are some of the operating conditions, the VSC may have to encounter. Through control of modulation index and the phase shift between network voltage and converter input voltage on the sending end side and /or between converter output voltage and the network voltage on the receiving end side, the operational requirements are met by modifying the instant and duration of conduction of the IGBT switches of the VSC converters. The change in PWM pattern enables this. The change in PWM pattern realized through the controller provided with decision logics, enables change in fundamental frequency voltage phase angle and the fundamental frequency voltage magnitudes of the converters and hence the required change in active and reactive power flows [3]. However, for ensuring appropriate design, extensive simulation tests on the composite system incorporating its controllers, need to be carried out.

This paper develops the model of the controller, to facilitate dynamic performance assessment of the composite system through digital simulation. The model takes into account the complete dynamics of a VSC-HVDC link. The model performance is validated through SIMULINK power system blockset (PSB) based simulations on the composite power system incorporating the developed controllers.

II. VSC-HVDC OPERATION

The converter phase angle can be used for the active power control. A VSC operates as a rectifier when AC voltage of the converter u_{ac} phase lags the AC network voltage e_{ac} i.e. $\delta_{ac} > 0$. The active power flows into VSC from AC system in this case.

$$P_{ac} = \frac{e_{ac} u_{ac}}{x_{ac}} \sin \delta_{ac} \quad (1)$$

The voltage magnitude can be used to control reactive power. The converter provides reactive power support to the AC network, when the converter AC voltage $|u_{ac}|$ is higher than the AC network voltage $|e_{ac}|$.

$$Q_{ac} = \frac{e_{ac}^2}{x_{ac}} - \frac{e_{ac} u_{ac}}{x_{ac}} \cos \delta_{ac} \quad (2)$$

Fig. 2 illustrates the characteristic variation in active power, P, and reactive power, Q, capability of a VSC-HVDC link as a function of AC system voltage, measured at the network interfacing point. The reactive power delivery to the network increases with decreasing network voltage [3, 4]. Similarly, the converter reactive power absorption increases with increasing network voltage. For a given ac system voltage, the converter can be operated at any point within the P-Q circle, as required.

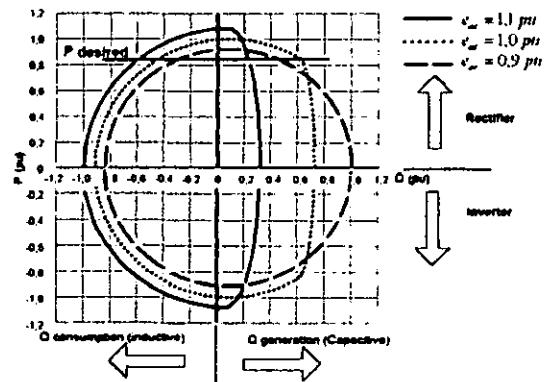


Fig. 2: P-Q diagram for VSC-HVDC

III. VSC-HVDC DECOUPLED CONTROLLER MODEL

Assuming flows from the network to the converters at both rectifier and the inverter ends to be positive as shown in Fig. 1, the voltage and current relationships at

the network side of the respective coupling transformers are given by (3) and (4):

$$e_r^{abc} = R_r i_r^{abc} + L_r \frac{di_r^{abc}}{dt} + u_r^{abc} \quad (3)$$

$$e_i^{abc} = R_i i_i^{abc} + L_i \frac{di_i^{abc}}{dt} + u_i^{abc} \quad (4)$$

Assuming balanced interfacing ac network operation signifying absence of zero axis components, the d-q transformed versions of (3) & (4) after rearranging can be written as [7, 8]

$$e_r^d = \left(\frac{di_r^d}{dt} + \frac{R_r}{L_r} i_r^d \right) L_r - \omega_r L_r i_r^q + u_r^d \quad (5)$$

$$e_r^q = \left(\frac{di_r^q}{dt} + \frac{R_r}{L_r} i_r^q \right) L_r + \omega_r L_r i_r^d + u_r^q$$

$$e_i^d = \left(\frac{di_i^d}{dt} + \frac{R_i}{L_i} i_i^d \right) L_i - \omega_i L_i i_i^q + u_i^d \quad (6)$$

$$e_i^q = \left(\frac{di_i^q}{dt} + \frac{R_i}{L_i} i_i^q \right) L_i + \omega_i L_i i_i^d + u_i^q$$

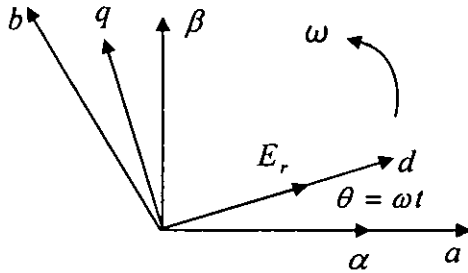


Fig. 3: Inter-relationship between frames of references for VSC-HVDC

With reference to Fig. 3, network voltage on the rectifier side is given by

$$\begin{bmatrix} e_r^a \\ e_r^b \\ e_r^c \end{bmatrix} = E_r \begin{bmatrix} \cos \omega_r t \\ \cos(\omega_r t - 120^\circ) \\ \cos(\omega_r t + 120^\circ) \end{bmatrix} \quad (7)$$

Similar equation exists for inverter side as well with suffix r replaced by i. Equation (7) when d-q transformed with reference to Fig.3 yields:

$$e_r^d = E_r, e_r^q = 0, e_i^d = E_i, e_i^q = 0 \quad (8)$$

Assuming a sinusoidal signal modulating the carrier input in the pulse width modulator based IGBT gating module, the switching function giving the state of a IGBT in the converter, is given by

$$\begin{bmatrix} S_r^a \\ S_r^b \\ S_r^c \end{bmatrix} = \begin{bmatrix} \frac{1}{2} + \frac{M_r}{2} \cos(\omega_r t - \delta_r) \\ \frac{1}{2} + \frac{M_r}{2} \cos(\omega_r t - \delta_r - 120^\circ) \\ \frac{1}{2} + \frac{M_r}{2} \cos(\omega_r t - \delta_r + 120^\circ) \end{bmatrix} \quad (9)$$

The relationship between the converter as side and dc side voltages is given by

$$\begin{bmatrix} u_r^a \\ u_r^b \\ u_r^c \end{bmatrix} = \frac{M_r V_{dcr}}{2} \begin{bmatrix} \cos(\omega_r t - \delta_r) \\ \cos(\omega_r t - \delta_r - 120^\circ) \\ \cos(\omega_r t - \delta_r + 120^\circ) \end{bmatrix} \quad (10)$$

The d-q transformation of (10) with reference to Fig. 3 for both converters yields

$$\begin{aligned} u_r^d &= \frac{M_r}{2} V_{dcr} \cos \delta_r, u_r^q = -\frac{M_r}{2} V_{dcr} \sin \delta_r \\ u_i^d &= \frac{M_i}{2} V_{dci} \cos \delta_i, u_i^q = -\frac{M_i}{2} V_{dci} \sin \delta_i \end{aligned} \quad (11)$$

Defining $T_r = \frac{L_r}{R_r}$ and $T_i = \frac{L_i}{R_i}$, then linearizing (5)

& (6) results in, [8]

$$\Delta u_r^d = -L_r \left(S + \frac{1}{T_r} \right) \Delta i_r^d + \omega_r L_r \Delta i_r^q \quad (12)$$

$$\Delta u_r^q = -L_r \left(S + \frac{1}{T_r} \right) \Delta i_r^q - \omega_r L_r \Delta i_r^d$$

$$\Delta u_i^d = -L_i \left(S + \frac{1}{T_i} \right) \Delta i_i^d + \omega_i L_i \Delta i_i^q \quad (13)$$

$$\Delta u_i^q = -L_i \left(S + \frac{1}{T_i} \right) \Delta i_i^q - \omega_i L_i \Delta i_i^d$$

Linearization of (11) yields,

$$\begin{bmatrix} \Delta u_r^d \\ \Delta u_r^q \end{bmatrix} = \begin{bmatrix} -\frac{V_{dcr}}{2} M_r \sin \delta & \frac{V_{dcr}}{2} \cos \delta_r \\ -\frac{V_{dcr}}{2} M_r \cos \delta_r & -\frac{V_{dcr}}{2} \sin \delta_r \end{bmatrix} \begin{bmatrix} \Delta \delta_r \\ \Delta M_r \end{bmatrix} \quad (14)$$

$$\begin{bmatrix} \Delta u_i^d \\ \Delta u_i^q \end{bmatrix} = \begin{bmatrix} -\frac{V_{dci}}{2} M_i \sin \delta & \frac{V_{dci}}{2} \cos \delta_i \\ -\frac{V_{dci}}{2} M_i \cos \delta_i & -\frac{V_{dci}}{2} \sin \delta_i \end{bmatrix} \begin{bmatrix} \Delta \delta_i \\ \Delta M_i \end{bmatrix}$$

Since (14) are a set of coupled equations, to achieve decoupled control, Subjecting (14) to similarity transformation yields:

$$\begin{bmatrix} \Delta u_r^d \\ \Delta u_r^q \end{bmatrix} = \begin{bmatrix} \lambda_{r1} & 0 \\ 0 & \lambda_{r2} \end{bmatrix} \begin{bmatrix} \Delta \delta_r \\ \Delta M_r \end{bmatrix}$$

$$\begin{bmatrix} \Delta u_i^d \\ \Delta u_i^q \end{bmatrix} = \begin{bmatrix} \lambda_{i1} & 0 \\ 0 & \lambda_{i2} \end{bmatrix} \begin{bmatrix} \Delta \delta_i \\ \Delta M_i \end{bmatrix} \quad (15)$$

Where,

$$\lambda_{r1} = \frac{-(M_r + 1) \sin \delta_r + \sqrt{(M_r + 1)^2 \sin^2 \delta_r - 4M_r}}{2} * \frac{V_{dcr}}{2}$$

$$\lambda_{r2} = \frac{-(M_r + 1) \sin \delta_r - \sqrt{(M_r + 1)^2 \sin^2 \delta_r - 4M_r}}{2} * \frac{V_{dcr}}{2}$$

$$\lambda_{i1} = \frac{-(M_i + 1) \sin \delta_i + \sqrt{(M_i + 1)^2 \sin^2 \delta_i - 4M_i}}{2} * \frac{V_{dci}}{2}$$

$$\lambda_{i2} = \frac{-(M_i + 1) \sin \delta_i - \sqrt{(M_i + 1)^2 \sin^2 \delta_i - 4M_i}}{2} * \frac{V_{dci}}{2}$$

From (15),

$$\Delta \delta_r = \frac{1}{\lambda_{r1}} \Delta u_r^d \quad \Delta M_r = \frac{1}{\lambda_{r2}} \Delta u_r^q$$

$$\Delta \delta_i = \frac{1}{\lambda_{i1}} \Delta u_i^d \quad \Delta M_i = \frac{1}{\lambda_{i2}} \Delta u_i^q \quad (16)$$

Processing of Measurements:

Conventional complex power is valid only for a system in steady state with a fixed line frequency. Whereas 3-phase instantaneous power is valid during steady as well as transient states [5] and describes the total energy flow

per second between two interfacing systems. Using instantaneous power theory, phase current and voltage measurements on the network can be transformed to Clarke variables.

$$e^a = \frac{2}{3} \left[e^a - \frac{1}{2} e^b - \frac{1}{2} e^c \right]$$

$$e^\beta = \frac{2}{3} \left[\frac{\sqrt{3}}{2} e^b - \frac{\sqrt{3}}{2} e^c \right]$$

$$i^a = \frac{2}{3} \left[i^a - \frac{1}{2} i^b - \frac{1}{2} i^c \right]$$

$$i^\beta = \frac{2}{3} \left[\frac{\sqrt{3}}{2} i^b - \frac{\sqrt{3}}{2} i^c \right] \quad (17)$$

Instantaneous reactive power on the rectifier and both real & reactive powers on the inverter sides can be now derived as

$$Q_r = e_r^\beta i_r^\alpha - e_r^\alpha i_r^\beta$$

$$P_i = e_i^\alpha i_i^\alpha + e_i^\beta i_i^\beta$$

$$Q_i = e_i^\beta i_i^\alpha - e_i^\alpha i_i^\beta \quad (18)$$

Deriving Q_{rref} , P_{iref} and Q_{iref}

$$\Delta Q_r = Q_{rord} - Q_i, Q_{rref} = Q_{rord} + \Delta Q_r$$

$$\Delta P_i = P_{iord} - P_i, P_{iref} = P_{iord} + \Delta P_i$$

$$\Delta Q_i = Q_{iord} - Q_i, Q_{iref} = Q_{iord} + \Delta Q_i \quad (19)$$

Deriving d-q variables from Clarks variables

$$e^d = e^\alpha \cos \theta + e^\beta \sin \theta$$

$$e^q = -e^\alpha \sin \theta + e^\beta \cos \theta$$

$$i^d = i^\alpha \cos \theta + i^\beta \sin \theta$$

$$i^q = -i^\alpha \sin \theta + i^\beta \cos \theta \quad (20)$$

Estimating current values of modulation and the phase angle

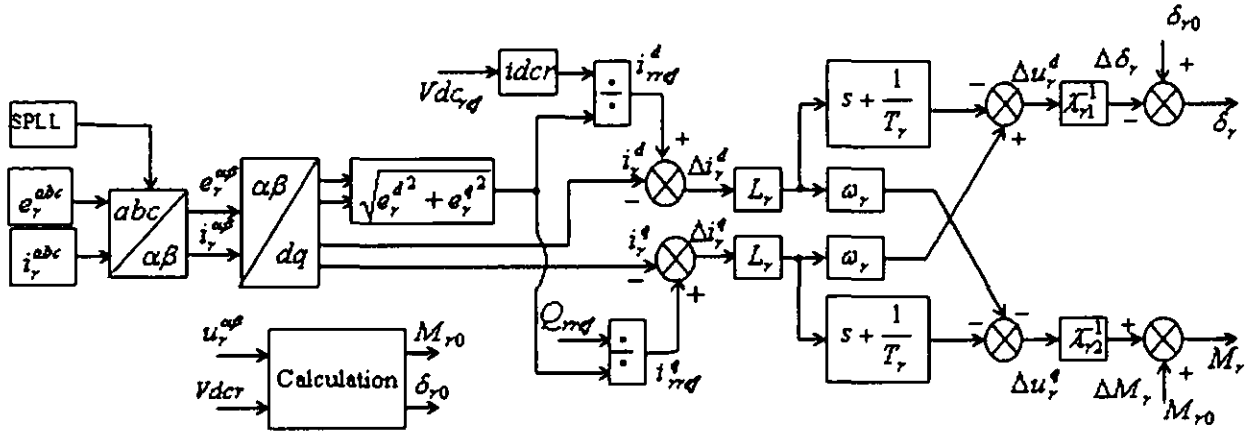


Fig.4 Controller scheme for Voltage-Sourced Rectifier

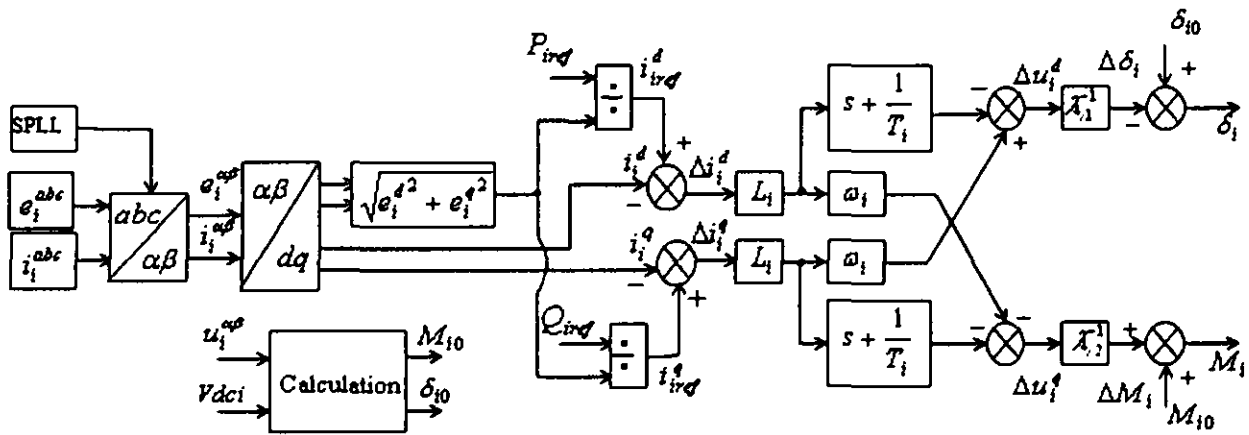


Fig.5: Controller scheme for Voltage-Sourced Inverter

$$M_r = \frac{\sqrt{u_r^{\alpha^2} + u_r^{\beta^2}}}{V_{dcr}/2}$$

$$M_i = \frac{\sqrt{u_i^{\alpha^2} + u_i^{\beta^2}}}{V_{dci}/2}$$

$$\delta_r = \cos^{-1} \left(\frac{u_r^\alpha e_r^\alpha + u_r^\beta e_r^\beta}{\sqrt{u_r^{\alpha^2} + u_r^{\beta^2}} * \sqrt{e_r^{\alpha^2} + e_r^{\beta^2}}} \right)$$

$$\delta_i = \cos^{-1} \left(\frac{u_i^\alpha e_i^\alpha + u_i^\beta e_i^\beta}{\sqrt{u_i^{\alpha^2} + u_i^{\beta^2}} * \sqrt{e_i^{\alpha^2} + e_i^{\beta^2}}} \right) \quad (21)$$

Equations (12) through (21) model the proposed controllers on rectifier and the inverter sides of a VSC-HVDC.

The controllers determine the incremental corrections required in the current values of both modulation index and the phase angles, at both the ends, to achieve a specified operating condition.

IV. MODEL PERFORMANCE

The operating scenario related to the system shown in Fig. 1, is generated on SIMULINK. The control initiation takes place at $T=0.1$ sec on rectifier side and at $T=0.3$ sec on inverter side. As result of this, ramping up/down continues until $T=1.0$ sec. At $T=2.0$ sec on rectifier side V_{dc} is reduced by 5%, additional Q supply becomes available to network.

On the inverter side real power outflow to the network is reduced by 10% and Q supply to the network is maintained at 0.1 pu. Figures 6-10, depict the changes in the controlled variables during this operating regime.

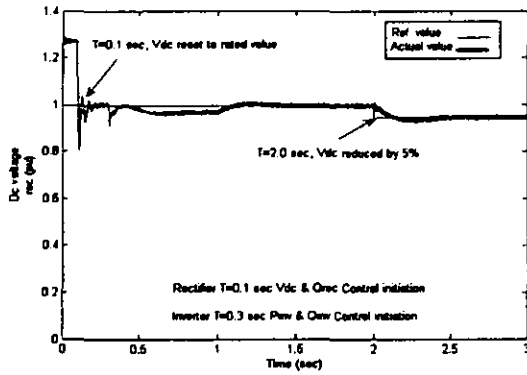


Fig. 6: Dc voltage variation of rectifier

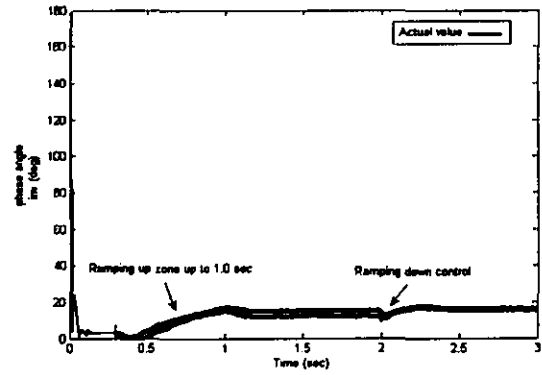


Fig. 10: Phase angle variation between modulating signal and carrier wave input of inverter

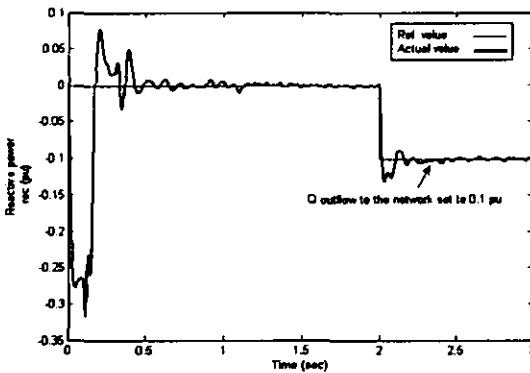


Fig. 7: Reactive power variation of rectifier

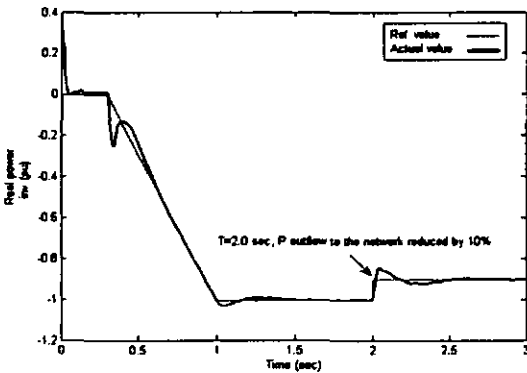


Fig. 8: Real power variation of inverter

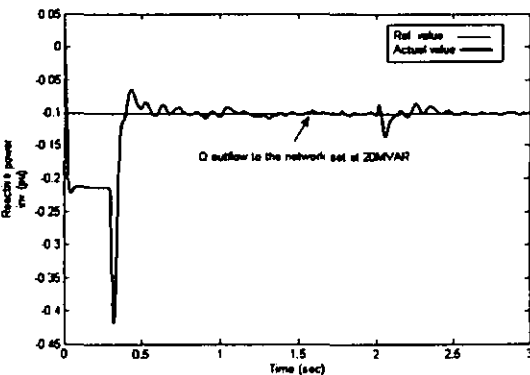


Fig. 9: Reactive power variation of inverter

V. CONCLUSION

The instantaneous power theory based network real and reactive power measurement estimation is appropriate for VSC-HVDC. The proposed model realizes incremental correction in both modulation index and phase shift angle between modulating signal and carrier input to PWM module.

The controller models can be put into state space form to facilitate small disturbance oscillatory performance analysis of a composite power system with VSC-HVDC link.

REFERENCES

- [1] Michael P. Bahrman, Jan G. Johansson and Bo A. Nilsson, "Voltage source converter transmission technologies-the right fit for the application", 2003.
- [2] F. Schettler, H. Huang and N. Christl, "HVDC Transmission Systems using Voltage Sourced Converters- Design and Application", p 715 – 720, 2000.
- [3] Michael Bahrman, Abdel-Aty Edris and Rich Haley, "Asynchronous back-to-back HVDC link with the voltage source converters", presented at Minnesota power systems conference, USA, Nov 1999.
- [4] B. R. Andersen, "VSC transmission", CIGRE B4, HVDC and Power Electronics HVDC Colloquium, Oslo, April 2006.
- [5] Hirofumi Akagi, Yoshihira Kanazawa and Akira Nabae, "Instantaneous reactive power compensators comprising switching devices without energy storage components", IEEE transactions on industry applications, vol. IA-20, No.3, May/June 1984.
- [6] B. R. Andersen, L. Xu, P. J. Horton and P. Cartwright, "Topologies for VSC transmission", POWER ENGINEERING JOURNAL, JUNE 2002.
- [7] JL Thomas, S. Poullain and A. Benchaib, "Analysis of a Robust DC – Bus Voltage Control System for a VSC Transmission Scheme", Conference publication No. 485, IEE 2001.
- [8] C. Schauder and H. Mehta, "Vector analysis and control of advanced static VAR compensators", IEE PROCEEDINGS-C, Vol. 140, No. 4, JULY 1993.

Appendix C

Ravindra N. Mukerjee and **Ahmed Mahjoub**, "A Fully Decoupled Controller Model for VSC-HVDC Transmission System," Elsevier Electric Power Systems Research. Manuscript # EPSR-D-09-00189.

A Fully Decoupled Controller Model for VSC-HVDC Transmission System

Ravindra N. Mukerjee*, Ahmed Mahjoub

Department of Electrical & Electronic Engineering

Universiti Teknologi PETRONAS, Bandar Seri Iskandar, 31750 Tronoh, Perak, Malaysia.

mmukerjee@gmail.com, mahjoub_ahmed@yahoo.com

ABSTRACT

VSC-HVDC has two distinct advantages over its earlier generation thyristor based High Voltage DC transmission. Synchronous voltage source is not required to commute against, for its operation and it does not suffer from commutation failures under adverse conditions in interfacing ac system. These two properties make it amenable to wider application areas. To make it adapt to operational conditions imposed on it in various applications, its controller parameters need to be assessed and tuned through extensive simulation studies. To facilitate this, a fully decoupled controller model exploiting similarity transformation and using instantaneous power theory based measurements suitable for steady as well as transient states is developed in the paper. The performance of the model is assessed through simulations on a VSC-HVDC link interfacing an ac system having normal fault level, low fault level and witnessing a single line to ground fault on rectifier transformer primary side.

Keywords: VSC-HVDC, Instantaneous Power Theory, Modal Transformation, Distributed Generation, Park's Transformation.

1. Introduction

VSC-High-voltage direct current transmission a high power electronics based technology provides economical alternatives to ac transmission for long-distance bulk power delivery from remote sources, provides immunity against network congestion or loop flow on parallel paths facilitating power trading, is useful as asynchronous link to provide a firewall against propagation of cascading outages in one network crossing over to another network. It also facilitates interconnection of AC systems in the lower and middle power range. VSC-HVDC has two distinct advantages over its earlier generation thyristor based High Voltage DC transmission. Synchronous voltage source is not required to commute against, for its operation and voltage source converters (VSC) do not suffer from commutation failures under adverse conditions in interfacing ac system, allowing fast recoveries from nearby ac faults. These two properties make it amenable to wider application

areas. VSC-HVDC reverses power through reversal of current direction rather than voltage polarity, facilitating power reversal at an intermediate tap point independent of the main power flow direction in Multi-terminal HVDC systems [1].

VSC-HVDC transmission using self commutated IGBT and Pulse Width Modulation (PWM) with switching frequencies considerably higher than the AC system power frequency, permits simple converter topology, achieves high speed control of both active & reactive power, generates ac output voltage with any desired phase angle or amplitude instantly with a close to sinusoidal wave shape, reducing harmonic generation and eliminating low order harmonics, and causing a rather small harmonic interference compared to the line commutated converters in thyristor based HVDC. Up to a certain limit, any phase angle or amplitude can be created by changing the PWM pattern [2,3]. IGBT being a MOS-device, power need for the control of the component is very low. To achieve a high HVDC link voltage, series connection of many semiconductors with good voltage distribution even at switching frequencies in kHz range is possible [4-6].

VSC-HVDC converter station can comprise of either VSC or current-sourced converters (CSC). Whereas the CSCs' are robust, the VSCs' have higher efficiency, low initial cost, and smaller physical size. VSC is preferred over CSC, since both power and control circuits in CSC are more complex. Filter capacitors are required at the ac terminals of a CSC to improve output ac current waveform quality, adding to cost. CSC requires switches of sufficient reverse voltage withstand capability such as Gate-Turn-off thyristors, capable of blocking voltages of both polarities in off-state. Alternatively, series diode is required with each switch, resulting in increased cost and conduction losses. CSC also requires smoothing DC inductors across the three-phase bridge terminals, which are generally larger and more expensive than capacitors used in VSCs [7,8]. IGBT module commercially available is more suitable for voltage-source PWM converter, since a free-wheeling diode is connected in anti-parallel with each IGBT. Thus IGBTs do not need the built-in reverse voltage blocking capability, bringing in more flexibility to device design.

The operational requirements imposed on an HVDC link keep on varying, depending on the changes in interfacing ac network operating conditions at its sending and receiving ends. Normal power transfer in forward direction, reverse power transfer, sending end and/or receiving end ac network short circuit capacity low due to network fault, DC line witnessing fault, are some of the operating conditions, the VSC may have to encounter. Through control of modulation index and the phase shift between network voltage and converter input voltage at the sending end and /or between converter output voltage and the network voltage at the receiving end, the

operational requirements are met by modifying the instant and duration of conduction of the IGBT switches of the VSC converters. The change in PWM pattern enables this. The change in PWM pattern realized through the controller provided with decision logics, enables change in fundamental frequency voltage phase angle and the fundamental frequency voltage magnitudes of the converters and hence the required change in active and reactive power flows [9].

VSC with PWM can operate in all four quadrants of PQ-plane, i.e. it can operate as rectifier or inverter at variable frequency and absorb or supply reactive power to the interfacing AC network. Reactive power can also be controlled at each terminal independent of the dc transmission voltage level. This control capability gives total flexibility to place converters anywhere in the ac network as there is no restriction on minimum network short circuit capacity. HVDC transmission and reactive power compensation with VSC technology has attributes beneficial to overall system performance. It can be used for the dynamic compensation of power transmission systems, providing increased transient stability and improved damping. The STATCOM functionality enables it to adjust reactive power support to an AC system to control AC bus voltage and improve system stability [6]. The dynamic support of the ac voltage at each converter terminal improves the voltage stability and increases the transfer capability of the sending and receiving end ac systems.

Controllability of VSC-HVDC facilitates it to operate under constant power; ac voltage control and frequency control modes, enabling it to be radially interconnected to an electric distribution system having feed from synchronous generation. A VSC-HVDC link supplying power to (i) an electric distribution network with or without embedded generation and interfacing directly with the loads having varying characteristics, (ii) an industrial electric distribution system having feed from the onsite generation or (iii) serving as asynchronous link between two ac systems, has to adjust itself to avoid oscillations under changing operating conditions. To suppress these oscillations, design and operational strategy of controllers in a VSC-HVDC arrived at through dynamic simulations, plays a significant role.

To facilitate dynamic simulation of a composite power system incorporating a VSC-HVDC link and assess performance of a controller supervising PWM module for ultimate firing control of the IGBT valves, models for the VSC-HVDC controllers were developed by several authors [10–14]. The control system in a VSC-HVDC comprises a fast inner current controller controlling the ac current within the converter's current carrying capability limit and a number of outer loop controllers providing reference values of current to the inner current controller, for the control strategy chosen at the rectifier or the inverter end. The outer controllers could be dc

voltage controller, active power controller, reactive power controller and the frequency controller. Not all the outer controllers are used at the same time. However, one of the two converters must control the link dc voltage to achieve active power balance between the power entering the rectifier end and leaving the inverter end [11].

In [10], state model $\dot{x} = Ax + Bu$ is developed with currents in direct and quadrature axes of a synchronously rotating reference frame as state variables and using d-q transformed equivalent of the source side circuit of the VSC converter, originally framed in a-b-c frame of reference. Synchronously rotating d-axis is assumed to be leading the phase 'a' by a transformation angle θ , derived through a phase locked loop. Decoupled control rule for the current state variables or the inner current controller is obtained by defining the feedback loop and the PI compensation. The inner current controller loop is implemented in d-q frame. However, control law for determining the converter source side reference voltage variables u_d and u_q still need cross-coupled terms. These voltages and the dc link voltage V_{dc} , determine the amplitude and angle modulation indices. The measured real and reactive power on the network side is assessed using the Clarke's variables viz. instantaneous voltage and current vectors.

In [11], strategy is similar as in [10], except that a one-sample delay is implemented in the inner current controller for slow current control and a smith predictor is used in the current controller to compensate for the time delay for fast current control. The inner current control loop is implemented in d-q frame. The dead beat current control is achieved through proportional control of the current error. However, to wipe-off the steady state current error, integral part can also be added. The measured values of the d-q transformed currents are derived from the real and reactive power computed after transforming the voltages and the currents acquired in a-b-c reference frame to rotating d-q frame. The computation of converter source side reference voltage variables u_d and u_q need i_q and i_d respectively, and in that sense use coupled expressions. These reference voltages are transformed to the a-b-c frame via Clarke's transformation.

[12] also follows somewhat similar strategy as in [10] and [11]. Fundamental frequency model in terms of d-q variables is formed through transformation from a-b-c frame to switching reference frame and then to dq0 frame. The inner current loop is once again implemented in d-q frame. The current components are decoupled. However, computation of d component of converter source side terminal voltage needs q component of current and similarly, computation of q component of converter source side voltage needs d component of current and hence the model is like the earlier two models in this respect. Like in [10] converter source side voltages and the dc link voltage V_{dc} , determine the amplitude and angle modulation indices.

In [13] and [14] converter source side phase voltages in a-b-c frame are transformed into Clarke's components. The components are then identified and separated into positive and negative sequence voltages. While positive sequence voltage is subjected to a counter clockwise d-q transformation, the negative sequence voltage is transformed to a clockwise d-q transformation. This transforms both of them into dc components during filtering, and avoids any phase shift. The two filtered components are then used to compute the mean value of the source voltage during the sample period, specifically witnessing AC system disturbances. Reference values of the active and reactive parts of the converter currents in rotating d-q frame are supplied from the outer power loop. The outer loop on the rectifier side includes a PI-control of the dc link voltage and a forward feed of the d-component of the reference value derived from the outer power loop of the inverter side, thus facilitating change of the ordered active current without influencing the dc link voltage. The inner current loop is implemented in d-q frame, wherein the current errors are computed using the measured d-q currents and two sample delayed reference currents. This avoids failure of the dead-beat current control during normal ac network conditions. Dead-beat current control works satisfactorily with strong ac network interfacing the VSC-HVDC. Converter source side reference voltages are transformed to a-b-c frame, before feeding the PWM block with amplitude and angle modulation indices as inputs.

This paper develops the model of the controller with a modified inner current loop wherein, not only the current errors in the d-q frame are decoupled, but the generation procedure of source side converter d-q voltages is also decoupled. The q component of the current error is not required to compute d component of the converter source side reference voltage and the d component of the current error is not required to compute q component of the converter source side reference voltage. This is expected to speed up reference voltage generation.

Conventional complex power is valid only for a system in steady state with a fixed line frequency. Whereas 3-phase instantaneous power is valid during steady as well as transient states [15] and describes the total energy flow per second between two interfacing systems. Considering this, the computation of the measured Clarke's components of the real and reactive power in the outer power loop is proposed to be based on the instantaneous power theory. The model performance is validated through SIMULINK Power System Blockset (PSB) based simulations on the composite power system incorporating the developed controllers.

2. VSC-HVDC OPERATION

The converter phase angle can be used for the active power control. A VSC operates as a rectifier when AC voltage of the converter u_{ac} phase lags the AC network voltage e_{ac} i.e. $\delta_{ac} > 0$. The active power flows into VSC from AC system in this case as shown in Fig. 1.

$$p_{ac} = \frac{e_{ac} u_{ac}}{x_{ac}} \sin \delta_{ac} \quad (1)$$

The voltage magnitude can be used to control reactive power. The converter provides reactive power support to the AC network, when the converter AC voltage $|u_{ac}|$ is higher than the AC network voltage $|e_{ac}|$.

$$Q_{ac} = \frac{e_{ac}^2}{x_{ac}} - \frac{e_{ac} u_{ac}}{x_{ac}} \cos \delta_{ac} \quad (2)$$

3. State Space Model

Assuming flows from the network to the converters at both rectifier and the inverter is positive as shown in Fig. 2, the voltage and current relationships at the network side of the respective coupling transformers are given by:

$$e_r^{abc} = R_r i_r^{abc} + L_r \frac{di_r^{abc}}{dt} + u_r^{abc}, \quad e_i^{abc} = R_i i_i^{abc} + L_i \frac{di_i^{abc}}{dt} + u_i^{abc} \quad (3)$$

Transforming the equations in a-b-c frame of reference to a synchronously rotating reference frame shown in Fig. 3, Eq. (3) can be written as

$$T_{dq0}^{-1} e_r^{dq0} = R_r T_{dq0}^{-1} i_r^{dq0} + L_r \frac{d(T_{dq0}^{-1} i_r^{dq0})}{dt} + T_{dq0}^{-1} u_r^{dq0}, \quad T_{dq0}^{-1} e_i^{dq0} = R_i T_{dq0}^{-1} i_i^{dq0} + L_i \frac{d(T_{dq0}^{-1} i_i^{dq0})}{dt} + T_{dq0}^{-1} u_i^{dq0} \quad (4)$$

Where, the transformation and its inverse transformation with reference to Fig. 3 are given as

$$T_{dq0} = \frac{2}{3} \begin{bmatrix} \sin \theta & \sin(\theta - 120^\circ) & \sin(\theta + 120^\circ) \\ \cos \theta & \cos(\theta - 120^\circ) & \cos(\theta + 120^\circ) \\ \frac{1}{2} & \frac{1}{2} & \frac{1}{2} \end{bmatrix}, \quad T_{dq0}^{-1} = \begin{bmatrix} \sin \theta & \cos \theta & 1 \\ \sin(\theta - 120^\circ) & \cos(\theta - 120^\circ) & 1 \\ \sin(\theta + 120^\circ) & \cos(\theta + 120^\circ) & 1 \end{bmatrix}$$

Pre multiplying both sides by T_{dq0} , and expanding the 2nd term on the right hand side, Eq. (4) yields

$$e_r^{dq0} = R_r i_r^{dq0} + L_r \left(\frac{di_r^{dq0}}{dt} + T_{dq0} \frac{dT_{dq0}^{-1}}{dt} i_r^{dq0} \right) + u_r^{dq0}, \quad e_i^{dq0} = R_i i_i^{dq0} + L_i \left(\frac{di_i^{dq0}}{dt} + T_{dq0} \frac{dT_{dq0}^{-1}}{dt} i_i^{dq0} \right) + u_i^{dq0} \quad (5)$$

Eq. (5) after simplification [appendix A, Eq. (A.1) & (A.2)] and assuming balanced operation of interfacing ac network signifying, absence of zero axis components, the d-q transformed versions of Eq. (3) is

$$\frac{1}{L_r} \begin{bmatrix} e_r^d \\ e_r^q \end{bmatrix} = \begin{bmatrix} \frac{R_r}{L_r} & 0 \\ 0 & \frac{R_r}{L_r} \end{bmatrix} \begin{bmatrix} i_r^d \\ i_r^q \end{bmatrix} + \begin{bmatrix} 0 & -\omega_r \\ \omega_r & 0 \end{bmatrix} \begin{bmatrix} i_r^d \\ i_r^q \end{bmatrix} + \frac{d}{dt} \begin{bmatrix} i_r^d \\ i_r^q \end{bmatrix} + \frac{1}{L_r} \begin{bmatrix} u_r^d \\ u_r^q \end{bmatrix} \quad (6)$$

$$\frac{1}{L_i} \begin{bmatrix} e_i^d \\ e_i^q \end{bmatrix} = \begin{bmatrix} \frac{R_i}{L_i} & 0 \\ 0 & \frac{R_i}{L_i} \end{bmatrix} \begin{bmatrix} i_i^d \\ i_i^q \end{bmatrix} + \begin{bmatrix} 0 & -\omega_i \\ \omega_i & 0 \end{bmatrix} \begin{bmatrix} i_i^d \\ i_i^q \end{bmatrix} + \frac{d}{dt} \begin{bmatrix} i_i^d \\ i_i^q \end{bmatrix} + \frac{1}{L_i} \begin{bmatrix} u_i^d \\ u_i^q \end{bmatrix} \quad (7)$$

Eq. (6) and (7), with currents along d-q axes i_r^d , i_i^d and i_r^q , i_i^q as state variables, can be written in state space

form $\dot{x} = Ax + Bu$ as

$$\frac{d}{dt} \begin{bmatrix} i_r^d \\ i_r^q \end{bmatrix} = \begin{bmatrix} -\frac{R_r}{L_r} & \omega_r \\ -\omega_r & -\frac{R_r}{L_r} \end{bmatrix} \begin{bmatrix} i_r^d \\ i_r^q \end{bmatrix} + \frac{1}{L_r} \begin{bmatrix} e_r^d - u_r^d \\ e_r^q - u_r^q \end{bmatrix}, \quad \frac{d}{dt} \begin{bmatrix} i_i^d \\ i_i^q \end{bmatrix} = \begin{bmatrix} -\frac{R_i}{L_i} & \omega_i \\ -\omega_i & -\frac{R_i}{L_i} \end{bmatrix} \begin{bmatrix} i_i^d \\ i_i^q \end{bmatrix} + \frac{1}{L_i} \begin{bmatrix} e_i^d - u_i^d \\ e_i^q - u_i^q \end{bmatrix} \quad (8)$$

Ac network voltages on rectifier and inverter sides of the dc link are assumed to be

$$\begin{bmatrix} e_r^a \\ e_r^b \\ e_r^c \end{bmatrix} = E_r \begin{bmatrix} \cos \omega_r t \\ \cos(\omega_r t - 120^\circ) \\ \cos(\omega_r t + 120^\circ) \end{bmatrix}, \quad \begin{bmatrix} e_i^a \\ e_i^b \\ e_i^c \end{bmatrix} = E_i \begin{bmatrix} \cos \omega_i t \\ \cos(\omega_i t - 120^\circ) \\ \cos(\omega_i t + 120^\circ) \end{bmatrix} \quad (9)$$

Assuming balanced operation of interfacing ac network signifying, absence of zero axis components, the d-q transformed version of Eq. (9) can be written as [appendix A, Eq. (A.3)]

$$\begin{bmatrix} e_r^d \\ e_r^q \end{bmatrix} = \begin{bmatrix} 0 \\ E_r \end{bmatrix}, \quad \begin{bmatrix} e_i^d \\ e_i^q \end{bmatrix} = \begin{bmatrix} 0 \\ E_i \end{bmatrix} \quad (10)$$

The relationship between the converter ac side and dc side voltages on rectifier and inverter sides is given by [appendix A, Eq. (A.5)]

$$\begin{bmatrix} u_r^a \\ u_r^b \\ u_r^c \end{bmatrix} = \frac{M_r V_{dcr}}{2} \begin{bmatrix} \cos(\omega_r t - \delta_r) \\ \cos(\omega_r t - \delta_r - 120^\circ) \\ \cos(\omega_r t - \delta_r + 120^\circ) \end{bmatrix}, \quad \begin{bmatrix} u_i^a \\ u_i^b \\ u_i^c \end{bmatrix} = \frac{M_i V_{dci}}{2} \begin{bmatrix} \cos(\omega_i t - \delta_i) \\ \cos(\omega_i t - \delta_i - 120^\circ) \\ \cos(\omega_i t - \delta_i + 120^\circ) \end{bmatrix} \quad (11)$$

Assuming balanced operation of interfacing ac network signifying, absence of zero axis components, the d-q transformed version of Eq. (11), [appendix A, Eq. (A.6)] can be written as

$$\begin{bmatrix} u_r^d \\ u_r^q \end{bmatrix} = \frac{M_r V_{dcr}}{2} \begin{bmatrix} \sin \delta_r \\ \cos \delta_r \end{bmatrix}, \quad \begin{bmatrix} u_i^d \\ u_i^q \end{bmatrix} = \frac{M_i V_{dci}}{2} \begin{bmatrix} \sin \delta_i \\ \cos \delta_i \end{bmatrix} \quad (12)$$

The state matrices in Eq. (8) can be subjected to similarity transformation [16], to obtain decoupled state space equations [appendix A, Eq. (C.3) & (C.4)]

$$\frac{d}{dt} \begin{bmatrix} i_{rz}^d \\ i_{rz}^q \end{bmatrix} = \begin{bmatrix} -\frac{R_r}{L_r} + j\omega_r & 0 \\ 0 & -\frac{R_r}{L_r} - j\omega_r \end{bmatrix} \begin{bmatrix} i_{rz}^d \\ i_{rz}^q \end{bmatrix} + \frac{1}{2L_r} \begin{bmatrix} -u_r^d \\ E_r - u_r^q \end{bmatrix} \quad (13)$$

$$\frac{d}{dt} \begin{bmatrix} i_{iz}^d \\ i_{iz}^q \end{bmatrix} = \begin{bmatrix} -\frac{R_i}{L_i} + j\omega_i & 0 \\ 0 & -\frac{R_i}{L_i} - j\omega_i \end{bmatrix} \begin{bmatrix} i_{iz}^d \\ i_{iz}^q \end{bmatrix} + \frac{1}{2L_i} \begin{bmatrix} -u_i^d \\ E_i - u_i^q \end{bmatrix} \quad (14)$$

4. Fully Decoupled Controller Model

4.1. Inner current loop

In HVDC transmission, V_{dc} needs to be kept sufficiently high. For different operational regimes requiring real and reactive powers to be controlled independently, e_q and hence u_d & u_q need to be controlled independently. Consequently, the modulation index and also the phase shift between the modulating signal and the carrier signal in PWM module need to be varied to achieve various operational requirements. With a view to achieve dead beat control leading to zero steady state error, using state Eq. (13) and defining feedback loops and PI compensation, as

$$\begin{bmatrix} x_1 \\ x_2 \end{bmatrix} = \frac{1}{2L_r} \begin{bmatrix} -u_r^d \\ E_r - u_r^q \end{bmatrix}$$

$$\text{Where, } x_1 = \left(k_p + \frac{k_i}{s} \right) (i_{rref}^d - i_r^d), \quad x_2 = \left(k_p + \frac{k_i}{s} \right) (i_{rref}^q - i_r^q)$$

Implies, $u_r^d = -2L_r x_1$ & $u_r^q = E_r - 2L_r x_2$ thus,

$$u_r^d = -2L_r \left(k_p + \frac{k_i}{s} \right) (i_{rref}^d - i_r^d), \quad u_r^q = E_r - 2L_r \left(k_p + \frac{k_i}{s} \right) (i_{rref}^q - i_r^q) \quad (15)$$

Similarly, from state Eq. (14)

$$u_i^d = -2L_i \left(k_p + \frac{k_i}{s} \right) (i_{iref}^d - i_i^d), \quad u_i^q = E_i - 2L_i \left(k_p + \frac{k_i}{s} \right) (i_{iref}^q - i_i^q) \quad (16)$$

Eq. (15) and (16) model the inner current control loop. The control implementation involves the state variables $i_r^d, i_r^q, u_r^d, u_r^q$. However, to incorporate controller dynamics into the composite state matrix together with the VSC-HVDC power circuit dynamics and the interfacing ac system dynamics for carrying out modal analysis of the composite system u_r^d, u_r^q may have to be transformed to u_{rz}^d, u_{rz}^q . Once u_r^d, u_r^q and u_i^d, u_i^q are available, required modulation index and also the phase shift between the modulating signal and the carrier signal in PWM module can be determined using the relations

$$M_r = \frac{\sqrt{u_r^{d2} + u_r^{q2}}}{V_{dcr}/2}, \quad \delta_r = \tan^{-1} \left(\frac{u_r^q}{u_r^d} \right) - \theta_r, \quad M_i = \frac{\sqrt{u_i^{d2} + u_i^{q2}}}{V_{dci}/2}, \quad \delta_i = \tan^{-1} \left(\frac{u_i^q}{u_i^d} \right) - \theta_i \quad (17)$$

4.2. Outer loop

The outer loop comprises of the DC voltage controller, the active power controller and the reactive power controller. These controllers provide reference values of the respective direct and quadrature axis currents to the inner current control loop, implemented in d-q frame.

4.2.1. DC voltage controller

Inverter side is set to control the DC link voltage. A control equation for the direct axis current reference on the inverter side is implemented for the purpose. This outer controller is much slower than the inner loop current controller, to ensure stability. i_{iref}^d being in rotating d-q frame, yields dc component in steady state and is synonymous to the active current, assuming no power losses in the converter.

$$i_{iref}^d = (V_{dcref} - V_{dcl}) \left(k_p + \frac{k_i}{S} \right) \quad (18)$$

4.2.2. Active power controller

The reference value of the active part of the converter current is supplied from the outer active power loop. The reference value i_{rref}^d being in rotating d-q frame, yields dc component in steady state. The control of active power combines both open loop and the feedback loop as shown in Eq. (19). For implementation of the feedback loop, error between the desired dc power to be transferred and the active power measured on the interface bus is computed in the loop itself.

$$P_{rref} = P_{rord} + (P_{rord} - P_r) \left(k_p + \frac{k_i}{S} \right), \quad i_{rref}^d = \frac{P_{rref}}{e_r^q} \quad (19)$$

4.2.3. Reactive power controller

The outer reactive power loop supplies reference value of reactive part of the converter current. The reference values i_{rref}^q at the rectifier and i_{iref}^q at the inverter ends being in rotating d-q frame, yield dc component in steady state. The control of reactive power combines both open loop and the feedback loop as shown in Eq. (20) & (21). For implementing the feedback loop, error between the desired reactive power to be exchanged between the ac network and dc link and the reactive power measured on the interface bus is computed in the loop itself.

$$Q_{rref} = Q_{rord} + (Q_{rord} - Q_r) \left(k_p + \frac{k_i}{S} \right), \quad i_{rref}^q = \frac{Q_{rref}}{e_r^q} \quad (20)$$

$$Q_{iref} = Q_{iord} + (Q_{iord} - Q_i) \left(k_p + \frac{k_i}{S} \right), \quad i_{iref}^q = \frac{Q_{iref}}{e_i^q} \quad (21)$$

4.3. Processing of Measurements

Transforming network phase currents & voltages to Clarke variables using instantaneous power theory,

$$e_a = \frac{2}{3} \left(e_a - \frac{1}{2} e_b - \frac{1}{2} e_c \right), \quad e_\beta = \frac{2}{3} \left(\frac{\sqrt{3}}{2} e_b - \frac{\sqrt{3}}{2} e_c \right) \quad (22)$$

Instantaneous real and reactive power measured at the rectifier side and the reactive power measured at the inverter side in terms of the respective Clarke's components are given as [15]

$$P_r = e_r^\alpha i_r^\alpha + e_r^\beta i_r^\beta, \quad Q_r = e_r^\beta i_r^\alpha - e_r^\alpha i_r^\beta, \quad Q_i = e_i^\beta i_i^\alpha - e_i^\alpha i_i^\beta \quad (23)$$

The measured values of the active power and the both end reactive power are used to implement open and feedback control in the outer power loop. Fig. 4 and Fig. 5 show the respective converter controller models on rectifier and inverter sides.

5. Controller Model Performance Assessment

The system and the scenario descriptions are presented in Tables 1 & 2 respectively. Total simulation time is 3.0 sec, carrier frequency is 1350 Hz and the integration time step is 7.407 μ sec

5.1 Comparative Performance Assessment

Three scenarios are considered, to evaluate the performance of the developed model. In the first scenario, short circuit level at both rectifier and inverter end AC system buses is 2000MVA i.e. the source impedance 26.45 Ω is less than the converter transformer impedance 39.675 Ω . The inverter end controls are activated at $t = 0.1$ second and the rectifier end controls are activated at $t = 0.3$ sec. In the second scenario, the short circuit level at both end ac system interfacing buses is 1000MVA or a source impedance of 52.9 Ω is more than the converter transformer impedance. Inverter end controls are initiated at $t = 0.1$ sec and rectifier end controls are activated at $t = 0.3$ sec. In the third scenario, while the rectifier end source impedance is 52.9 Ω , the inverter end source impedance is 26.45 Ω . The activation time of respective end controls remain similar to the earlier two scenarios. The single line to ground fault occurs at the rectifier transformer primary side at $t=1.0$ sec and the fault is cleared at $t=1.2$ sec.

Fig. 6 shows the ac network voltages at the rectifier end in the three scenarios. The dynamic over voltage corresponding to higher source impedance is 6% as against 3% for the lower source impedance. With the real and reactive power controls activated at the rectifier end but without ac voltage control, ac voltage is 4% lower than the rated one, under normal fault level condition. Fig. 7 shows the ac network voltages at the inverter end in the three scenarios. Only dc link voltage and the reactive power flow control are activated at this end and ac voltage control remains inactive. The wave forms do not get influenced by the rectifier end asymmetrical fault at the transformer primary. Fig. 8 shows the real power flow into DC link on rectifier side. Real power controller is activated at the rectifier side at $t=0.3$ sec. Fig. 9 shows the reactive power flow into the DC link on rectifier side. The rectifier end has the reactive power controller activated at $t= 0.3$ sec. In all the scenarios Q import or

export is set at zero. Taking reactive power flow from network to the converter at both the ends as positive, Fig. 9 shows that the Q flow is indeed controlled to its set value. However, oscillations are witnessed, when the rectifier side source impedance is higher than the converter transformer impedance. Fig. 10 shows the DC link voltage at the inverter side during all the three scenarios, wherein the DC voltage controller is activated at 0.1 sec. Fig. 11 shows the variation of the modulation index at the rectifier end.

6. Conclusion

Instantaneous power theory is advantageous for measuring real and reactive power, as it is suitable for steady and transient states as well as for non sinusoidal waveforms, a distinct possibility in presence of harmonics during system operation. Similarity transformation can be used to obtain a fully decoupled model for the inner current control loop control circuit implementation involves original current and voltage state variables.

However, to facilitate small signal stability assessment of a composite system comprising of VSC-HVDC link as well as interfacing ac system, the variables need to be transformed while framing the state matrix. A lower fault level ac system interfacing with the VSC-HVDC link may lead to longer settling time, higher dynamic over voltages and relatively a longer fault recovery time.

Appendix A

Noting that in Eq. (5),

$$T_{dq0} \frac{d}{dt} T_{dq0}^{-1} = \frac{2}{3} \begin{bmatrix} \sin \omega t & \sin(\omega t - 120^\circ) & \sin(\omega t + 120^\circ) \\ \cos \omega t & \cos(\omega t - 120^\circ) & \cos(\omega t + 120^\circ) \\ \frac{1}{2} & \frac{1}{2} & \frac{1}{2} \end{bmatrix} \begin{bmatrix} \omega \cos \omega t & -\omega \sin \omega t & 0 \\ \omega \cos(\omega t - 120^\circ) & -\omega \sin(\omega t - 120^\circ) & 0 \\ \omega \cos(\omega t + 120^\circ) & -\omega \sin(\omega t + 120^\circ) & 0 \end{bmatrix}$$

$$T_{dq0} \frac{d}{dt} T_{dq0}^{-1} = \omega \begin{bmatrix} 0 & -1 & 0 \\ 1 & 0 & 0 \\ 0 & 0 & 0 \end{bmatrix}$$

Eq. (5) reduces to

$$\begin{bmatrix} e_r^d \\ e_r^q \\ e_r^0 \end{bmatrix} = R_r \begin{bmatrix} i_r^d \\ i_r^q \\ i_r^0 \end{bmatrix} + L_r \frac{d}{dt} \begin{bmatrix} i_r^d \\ i_r^q \\ i_r^0 \end{bmatrix} + \omega_r L_r \begin{bmatrix} 0 & -1 & 0 \\ 1 & 0 & 0 \\ 0 & 0 & 0 \end{bmatrix} \begin{bmatrix} i_r^d \\ i_r^q \\ i_r^0 \end{bmatrix} + \begin{bmatrix} u_r^d \\ u_r^q \\ u_r^0 \end{bmatrix} \quad (\text{A.1})$$

$$\begin{bmatrix} e_i^d \\ e_i^q \\ e_i^0 \end{bmatrix} = R_i \begin{bmatrix} i_i^d \\ i_i^q \\ i_i^0 \end{bmatrix} + L_i \frac{d}{dt} \begin{bmatrix} i_i^d \\ i_i^q \\ i_i^0 \end{bmatrix} + \omega_i L_i \begin{bmatrix} 0 & -1 & 0 \\ 1 & 0 & 0 \\ 0 & 0 & 0 \end{bmatrix} \begin{bmatrix} i_i^d \\ i_i^q \\ i_i^0 \end{bmatrix} + \begin{bmatrix} u_i^d \\ u_i^q \\ u_i^0 \end{bmatrix} \quad (\text{A.2})$$

Ac network voltage on rectifier side in Eq. (9) can be written as

$$T_{dq0}^{-1} \begin{bmatrix} e_r^d \\ e_r^q \\ e_r^0 \end{bmatrix} = E_r \begin{bmatrix} \cos \omega_r t \\ \cos(\omega_r t - 120^\circ) \\ \cos(\omega_r t + 120^\circ) \end{bmatrix}$$

Pre-multiplying both sides by T_{dq0}

$$T_{dq0} T_{dq0}^{-1} \begin{bmatrix} e_r^d \\ e_r^q \\ e_r^0 \end{bmatrix} = E_r T_{dq0} \begin{bmatrix} \cos \omega_r t \\ \cos(\omega_r t - 120^\circ) \\ \cos(\omega_r t + 120^\circ) \end{bmatrix}$$

$$\begin{bmatrix} e_r^d \\ e_r^q \\ e_r^0 \end{bmatrix} = \frac{2}{3} E_r \begin{bmatrix} \sin \omega t & \sin(\omega t - 120^\circ) & \sin(\omega t + 120^\circ) \\ \cos \omega t & \cos(\omega t - 120^\circ) & \cos(\omega t + 120^\circ) \\ \frac{1}{2} & \frac{1}{2} & \frac{1}{2} \end{bmatrix} \begin{bmatrix} \cos \omega_r t \\ \cos(\omega_r t - 120^\circ) \\ \cos(\omega_r t + 120^\circ) \end{bmatrix}$$

$$\begin{bmatrix} e_r^d \\ e_r^q \\ e_r^0 \end{bmatrix} = \begin{bmatrix} 0 \\ E_r \\ 0 \end{bmatrix}, \text{ similar equation for the inverter side is } \begin{bmatrix} e_i^d \\ e_i^q \\ e_i^0 \end{bmatrix} = \begin{bmatrix} 0 \\ E_i \\ 0 \end{bmatrix} \quad (\text{A.3})$$

The switching functions giving the state of an IGBT in the rectifier and inverter end converters, assuming a sinusoidal signal modulating the carrier input in the PWM based IGBT gating module, are given by

$$\begin{bmatrix} S_r^a \\ S_r^b \\ S_r^c \end{bmatrix} = \begin{bmatrix} \frac{1}{2} + \frac{M_r}{2} \cos(\omega_r t - \delta_r) \\ \frac{1}{2} + \frac{M_r}{2} \cos(\omega_r t - \delta_r - 120^\circ) \\ \frac{1}{2} + \frac{M_r}{2} \cos(\omega_r t - \delta_r + 120^\circ) \end{bmatrix}, \quad \begin{bmatrix} S_i^a \\ S_i^b \\ S_i^c \end{bmatrix} = \begin{bmatrix} \frac{1}{2} + \frac{M_i}{2} \cos(\omega_i t - \delta_i) \\ \frac{1}{2} + \frac{M_i}{2} \cos(\omega_i t - \delta_i - 120^\circ) \\ \frac{1}{2} + \frac{M_i}{2} \cos(\omega_i t - \delta_i + 120^\circ) \end{bmatrix}$$

$$\begin{bmatrix} u_r^a \\ u_r^b \\ u_r^c \end{bmatrix} = \begin{bmatrix} S_r^a \\ S_r^b \\ S_r^c \end{bmatrix} V_{dcr} - \left(\frac{V_{dcr}}{3} \right) \sum_{k=a,b,c} S_r^k, \quad \begin{bmatrix} u_i^a \\ u_i^b \\ u_i^c \end{bmatrix} = \begin{bmatrix} S_i^a \\ S_i^b \\ S_i^c \end{bmatrix} V_{dci} - \left(\frac{V_{dci}}{3} \right) \sum_{k=a,b,c} S_i^k \quad (\text{A.4})$$

Using Eq. (A.4), the relationship between the converter ac side and dc side voltages on rectifier and inverter sides is given by

$$\begin{bmatrix} u_r^a \\ u_r^b \\ u_r^c \end{bmatrix} = \frac{M_r V_{dcr}}{2} \begin{bmatrix} \cos(\omega_r t - \delta_r) \\ \cos(\omega_r t - \delta_r - 120^\circ) \\ \cos(\omega_r t - \delta_r + 120^\circ) \end{bmatrix}, \quad \begin{bmatrix} u_i^a \\ u_i^b \\ u_i^c \end{bmatrix} = \frac{M_i V_{dci}}{2} \begin{bmatrix} \cos(\omega_i t - \delta_i) \\ \cos(\omega_i t - \delta_i - 120^\circ) \\ \cos(\omega_i t - \delta_i + 120^\circ) \end{bmatrix} \quad (\text{A.5})$$

The converter ac side voltage on rectifier side in Equation (A.5) can be written as

$$T_{dq0}^{-1} \begin{bmatrix} u_r^d \\ u_r^q \\ u_r^0 \end{bmatrix} = \frac{M_r V_{dcr}}{2} \begin{bmatrix} \cos(\omega_r t - \delta_r) \\ \cos(\omega_r t - \delta_r - 120^\circ) \\ \cos(\omega_r t - \delta_r + 120^\circ) \end{bmatrix}$$

Pre-multiplying both sides by T_{dq0}

$$T_{dq0} T_{dq0}^{-1} \begin{bmatrix} u_r^d \\ u_r^q \\ u_r^0 \end{bmatrix} = \frac{M_r V_{dcr}}{2} T_{dq0} \begin{bmatrix} \cos(\omega_r t - \delta_r) \\ \cos(\omega_r t - \delta_r - 120^\circ) \\ \cos(\omega_r t - \delta_r + 120^\circ) \end{bmatrix}$$

$$\begin{bmatrix} u_r^d \\ u_r^q \\ u_r^0 \end{bmatrix} = \frac{2 M_r V_{dcr}}{3} \begin{bmatrix} \sin \omega t & \sin(\omega t - 120^\circ) & \sin(\omega t + 120^\circ) \\ \cos \omega t & \cos(\omega t - 120^\circ) & \cos(\omega t + 120^\circ) \\ \frac{1}{2} & \frac{1}{2} & \frac{1}{2} \end{bmatrix} \begin{bmatrix} \cos(\omega_r t - \delta_r) \\ \cos(\omega_r t - \delta_r - 120^\circ) \\ \cos(\omega_r t - \delta_r + 120^\circ) \end{bmatrix}$$

$$\begin{bmatrix} u_r^d \\ u_r^q \\ u_r^0 \end{bmatrix} = \frac{M_r V_{dcr}}{2} \begin{bmatrix} \sin \delta_r \\ \cos \delta_r \\ 0 \end{bmatrix}, \text{ similar equation for the inverter side is } \begin{bmatrix} u_i^d \\ u_i^q \\ u_i^0 \end{bmatrix} = \frac{M_i V_{dci}}{2} \begin{bmatrix} \sin \delta_i \\ \cos \delta_i \\ 0 \end{bmatrix} \quad (\text{A.6})$$

Appendix B

Eigen values of the state matrix for rectifier in Eq. (8) can be determined by solving the characteristic equation

$$\text{given by } A - \lambda_r I = 0 \quad \text{or} \quad \begin{bmatrix} -\frac{R_r}{L_r} & \omega_r \\ -\omega_r & -\frac{R_r}{L_r} \end{bmatrix} - \lambda_r \begin{bmatrix} 1 & 0 \\ 0 & 1 \end{bmatrix} = 0 \quad (\text{B.1})$$

Eq. (B.1) yields two Eigen values $\lambda_{r1} = -\frac{R_r}{L_r} - j\omega_r$ & $\lambda_{r2} = -\frac{R_r}{L_r} + j\omega_r$

Eigen vector corresponding to λ_{r1} , $V_1 = \begin{bmatrix} v_{11} \\ v_{21} \end{bmatrix}$, can be determined from $|A - \lambda_{r1} I| V_1 = 0$

$$\left\{ \begin{bmatrix} -\frac{R_r}{L_r} & \omega_r \\ -\omega_r & -\frac{R_r}{L_r} \end{bmatrix} - \lambda_{r1} \begin{bmatrix} 1 & 0 \\ 0 & 1 \end{bmatrix} \right\} \begin{bmatrix} v_{11} \\ v_{21} \end{bmatrix} = 0 \quad (\text{B.2})$$

Substituting $\lambda_{r1} = -\frac{R_r}{L_r} + j\omega_r$ in Eq. (B.2) yields

$$-\left[\frac{R_r}{L_r} - \frac{R_r}{L_r} + j\omega_r \right] v_{11} + \omega_r v_{21} = 0 \quad \& \quad -\omega_r v_{11} - \left[\frac{R_r}{L_r} - \frac{R_r}{L_r} + j\omega_r \right] v_{21} = 0$$

$$\text{Or } -j\omega_r v_{11} + \omega_r v_{21} = 0 \quad \& \quad -\omega_r v_{11} - j\omega_r v_{21} = 0 \quad (\text{B.3})$$

Treating v_{11} as the free variable in Eq. (B.3) and assigning an arbitrary value of 1 yields $V_1 = \begin{bmatrix} v_{11} = 1 \\ v_{21} = j1 \end{bmatrix}$

Eigenvector corresponding to λ_{r2} , $V_2 = \begin{bmatrix} v_{12} \\ v_{22} \end{bmatrix}$ can be determined from $|A - \lambda_{r2} I| V_2 = 0$

$$\left\{ \begin{bmatrix} -\frac{R_r}{L_r} & \omega_r \\ -\omega_r & -\frac{R_r}{L_r} \end{bmatrix} - \lambda_{r2} \begin{bmatrix} 1 & 0 \\ 0 & 1 \end{bmatrix} \right\} \begin{bmatrix} v_{12} \\ v_{22} \end{bmatrix} = 0 \quad (\text{B.4})$$

Substituting $\lambda_{r2} = -\frac{R_r}{L_r} - j\omega_r$ in (B.4) yields

$$-\left[\frac{R_r}{L_r} - \frac{R_r}{L_r} - j\omega_r \right] v_{12} + \omega_r v_{22} = 0 \quad \& \quad -\omega_r v_{12} - \left[\frac{R_r}{L_r} - \frac{R_r}{L_r} - j\omega_r \right] v_{22} = 0$$

Or $j\omega_r v_{12} + \omega_r v_{22} = 0$ & $-\omega_r v_{12} + j\omega_r v_{22} = 0$ (B.5)

Treating v_{22} as the free variable in Eq. (B.5) and assigning an arbitrary value of 1 yields $V_2 = \begin{bmatrix} v_{12} = j1 \\ v_{22} = 1 \end{bmatrix}$

Modal matrix of the state matrix in Eq. (8) is $P = [V_1 \ V_2] = \begin{bmatrix} 1 & j1 \\ j1 & 1 \end{bmatrix}$, its inverse is $P^{-1} = \frac{1}{2} \begin{bmatrix} 1 & -j1 \\ -j1 & 1 \end{bmatrix}$

Similarity transformation $P^{-1}AP$ of state matrix in Eq. (8), which is of the form, $\dot{x} = Ax + Bu$ is given by

$$P^{-1}AP = \frac{1}{2} \begin{bmatrix} 1 & -j1 \\ -j1 & 1 \end{bmatrix} \begin{bmatrix} -\frac{R_r}{L_r} & \omega_r \\ -\omega_r & -\frac{R_r}{L_r} \end{bmatrix} \begin{bmatrix} 1 & j1 \\ j1 & 1 \end{bmatrix} \quad \text{or} \quad P^{-1}AP = \begin{bmatrix} -\frac{R_r}{L_r} + j\omega_r & 0 \\ 0 & -\frac{R_r}{L_r} - j\omega_r \end{bmatrix} \quad (\text{B.6})$$

Appendix C

To facilitate modal analysis of a composite power system incorporating VSC-HVDC link, using the

transformation $x = Px_z$, the state matrix in Eq. (8), which is of the form, $\dot{x} = Ax + Bu$ can be written as

$$P \dot{x}_z = APx_z + Bu \quad \text{Or} \quad \dot{x}_z = P^{-1}APx_z + P^{-1}Bu \quad (\text{C.1})$$

Modal matrix and its inverse for the state matrix are given as $P = \begin{bmatrix} 1 & j1 \\ j1 & 1 \end{bmatrix}$ and $P^{-1} = \frac{1}{2} \begin{bmatrix} 1 & -j1 \\ -j1 & 1 \end{bmatrix}$

Substituting these into the state equation and also substituting Eq. (10),

$$\frac{d}{dt} \begin{bmatrix} i_{rz}^d \\ i_{rz}^q \end{bmatrix} = \frac{1}{2} \begin{bmatrix} 1 & -j1 \\ -j1 & 1 \end{bmatrix} \begin{bmatrix} -\frac{R_r}{L_r} & \omega_r \\ -\omega_r & -\frac{R_r}{L_r} \end{bmatrix} \begin{bmatrix} 1 & j1 \\ j1 & 1 \end{bmatrix} \begin{bmatrix} i_{rz}^d \\ i_{rz}^q \end{bmatrix} + \frac{1}{2} \begin{bmatrix} 1 & -j1 \\ -j1 & 1 \end{bmatrix} \left\{ \frac{1}{L_r} \begin{bmatrix} 0 \\ E_r \end{bmatrix} - \frac{1}{L_r} \begin{bmatrix} u_r^d \\ u_r^q \end{bmatrix} \right\}$$

The foregoing equation after using Eq. (B.6) reduces to,

$$\frac{d}{dt} \begin{bmatrix} i_{rz}^d \\ i_{rz}^q \end{bmatrix} = \begin{bmatrix} -\frac{R_r}{L_r} + j\omega_r & 0 \\ 0 & -\frac{R_r}{L_r} - j\omega_r \end{bmatrix} \begin{bmatrix} i_{rz}^d \\ i_{rz}^q \end{bmatrix} + \frac{1}{2L_r} \begin{bmatrix} -jE_r \\ E_r \end{bmatrix} - \frac{1}{2L_r} \begin{bmatrix} u_{rz}^d - ju_{rz}^q \\ u_{rz}^q - ju_{rz}^d \end{bmatrix} \quad (C.2)$$

jE_r , ju_r^q and ju_r^d in Eq. (C.2) are the projections of E_r , u_r^q , u_r^d on their respective orthogonal axes in an orthogonal system of coordinates and reduce to zero. Eq. (C.2) can be written as

$$\frac{d}{dt} \begin{bmatrix} i_{rz}^d \\ i_{rz}^q \end{bmatrix} = \begin{bmatrix} -\frac{R_r}{L_r} + j\omega_r & 0 \\ 0 & -\frac{R_r}{L_r} - j\omega_r \end{bmatrix} \begin{bmatrix} i_{rz}^d \\ i_{rz}^q \end{bmatrix} + \frac{1}{2L_r} \begin{bmatrix} -u_r^d \\ E_r - u_r^q \end{bmatrix} \quad (C.3)$$

Similarly the state equation for inverter in Eq. (8) reduces to,

$$\frac{d}{dt} \begin{bmatrix} i_{iz}^d \\ i_{iz}^q \end{bmatrix} = \begin{bmatrix} -\frac{R_i}{L_i} + j\omega_i & 0 \\ 0 & -\frac{R_i}{L_i} - j\omega_i \end{bmatrix} \begin{bmatrix} i_{iz}^d \\ i_{iz}^q \end{bmatrix} + \frac{1}{2L_i} \begin{bmatrix} -u_i^d \\ E_i - u_i^q \end{bmatrix} \quad (C.4)$$

Whereas i_{rz}^d , i_{rz}^q , i_{iz}^d , i_{iz}^q are not the original state variables, the state variables related to the voltage i.e. u_r^d and u_r^q are the original state variables.

References

- [1] M.P. Bahrman, Overview of HVDC transmission, in: Proc. 2006 IEEE Power Systems Conference and Exposition (PSCE), 2006, pp.18-23.
- [2] G. Asplund, Application of HVDC Light to power system enhancement, in: Proc. of the IEEE PES 2000 winter meeting, 2000, pp. 2498-2503.
- [3] K. Eriksson, HVDC Light and development of Voltage Source Converters, in: presented at IEEE/PES T & D 2002 Latin American Conference, Sao Paulo, Brazil, 2002, pp. 1-5.
- [4] A.K. Skytt, P. Holmberg, L.E. Juhlin, HVDC Light for connection of wind farms, in: Second International Workshop on Transmission Networks for off shore Wind Farms Royal Institute of Technology Stockholm, Sweden, 2001.
- [5] B.R. Andersen, VSC transmission, in: CIGRE B4, HVDC and Power Electronics HVDC Colloquium, Oslo, 2006.
- [6] F. Schettler, H. Huang, N. Christl, HVDC Transmission Systems using Voltage Sourced Converters- Design and Application, in: Proc. of the IEEE PES 2000 summer meeting, 2000, pp. 715-720.
- [7] N.Stretch, M. Kazerani, R. El Shatshat, A Current-Sourced Converter-based HVDC Light Transmission System, in: Proc. 2006 IEEE International Symposium on Industrial Electronics (ISIE), Canada, 2006, pp. 2001-2006.
- [8] Y. Ye, M. kazerani, V.H. Quintana, Current-Source Converter Based STATCOM: Modeling and Control, IEEE Trans. Power Delivery, 20 (2005) 795-800.

- [9] M. Bahrman, A.A. Edris, R. Haley, Asynchronous back-to-back HVDC link with the voltage source converters, in: presented at Minnesota Power Systems Conference, USA, 1999, 1-7.
- [10] C. Schauder, H. Mehta, Vector analysis and control of advanced static VAR compensators, IEE Proc. Generation, Transmission and Distribution, 140 (1993) 299-306.
- [11] C. Du, A. Sannino, M. Bollen, Analysis of the Control Algorithms of Voltage-Source Converter HVDC, in: Proc. 2005 IEEE Russia Power Tech, 2005, pp. 1-7.
- [12] H. Nikkhajoei, R. Iravani, Dynamic Model and Control of AC–DC–AC Voltage-Sourced Converter System for Distributed Resources, IEEE Trans. Power Delivery, 22 (2007) 1169-1178.
- [13] A. Lindberg, L. Lindberg, Inner current loop for large voltage source converters operating at low switching frequency, in: Fifth International Conference on Power Electronics and Variable-Speed Drives IEE, 1994, pp. 217-222.
- [14] A. Lindberg, T. Larsson, PWM and control of three level voltage source converters in an HVDC back-to-back station, in: Sixth International Conference on AC–DC Power Transmission IEE, 1996, pp. 297-302.
- [15] H. Akagi, Y. Kanazawa, A Nabae, Instantaneous reactive power compensators comprising switching devices without energy storage components, IEEE Trans. Industry Applications, IA-20 (1984) 625-630.
- [16] A. Mahjoub, R. Mukerjee, Modeling of Controller for Voltage Sourced Converter based HVDC Transmission System, in: IEEE 2nd International Power and Energy Conference (PECon 08), Johor Baharu, Malaysia, 2008, pp. 849-854.

R.N Mukerjee completed his BE in electrical engineering from MMM Engineering College, Gorakhpur, India in 1972, M.Sc (Engg) in control systems from Birla Institute of Technology, Mesra, Ranchi, India in 1983 and had his PhD in electrical engineering (power systems) from Indian Institute of Technology Kharagpur in 1987.

He is currently with the department of electrical & electronics engineering, Universiti Teknologi PETRONAS, Malaysia. Earlier he taught at the Birla Institute of Technology, Ranchi, Institute of Technology, Benaras Hindu University, Varanasi, India and Universiti Tenaga Nasional, Malaysia. He also worked with Metallurgical & Engineering Consultants India Ltd. from 1975 to 1991 and Calcutta Electricity Company from 1993 to 1995, where he was involved in engineering and design of power plants, transmission systems, utility and industrial power distribution networks. He was also with the Analytical Methods and Specialized Studies Section of System Planning Division, Ontario Hydro Toronto, Canada, where he worked on small signal stability and coherency identification problems. His fields of interest include power system dynamics, nonlinear theory, power quality, and application of AI techniques to power system problems.

Ahmed Mahjoub completed his BSc in electrical engineering from Sudan University of Science & Technology, Khartoum, Sudan in 2006. Currently he is carrying out his master's study in electrical & Electronics engineering, at Universiti Teknologi PETRONAS, Malaysia. His fields of interest include power system operation & control and High Voltage DC Transmission.

Figure captions

Fig.1. P-Q diagram for VSC-HVDC

Fig.2. VSC-HVDC Power Circuit and Measurement Scheme

Fig.3. Inter-relationship between frames of references for VSC-HVDC

Fig.4. VSC-HVDC RECTIFIER CONTROLLER

Fig.5. VSC-HVDC INVERTER CONTROLLER

Fig6. AC Network Bus voltages - Rectifier side

Fig7. AC Network Bus voltages - Inverter side

Fig8. Real Power Flow into DC Link -Rectifier side

Fig9. Reactive Power Flow into DC Link- Rectifier side

Fig10. DC Link Voltage Measured on Rectifier side

Fig11. Modulation Index – Rectifier side

Tables

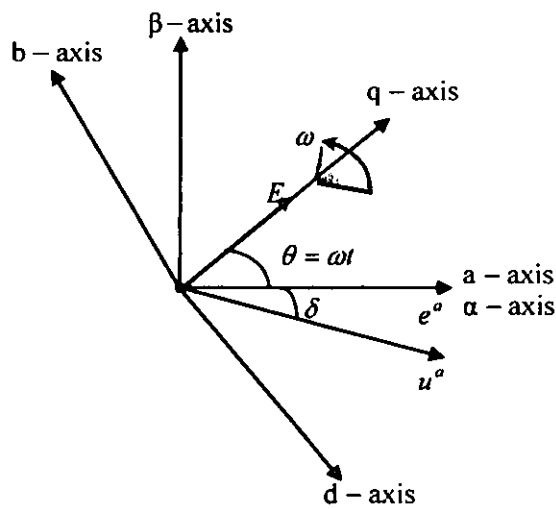
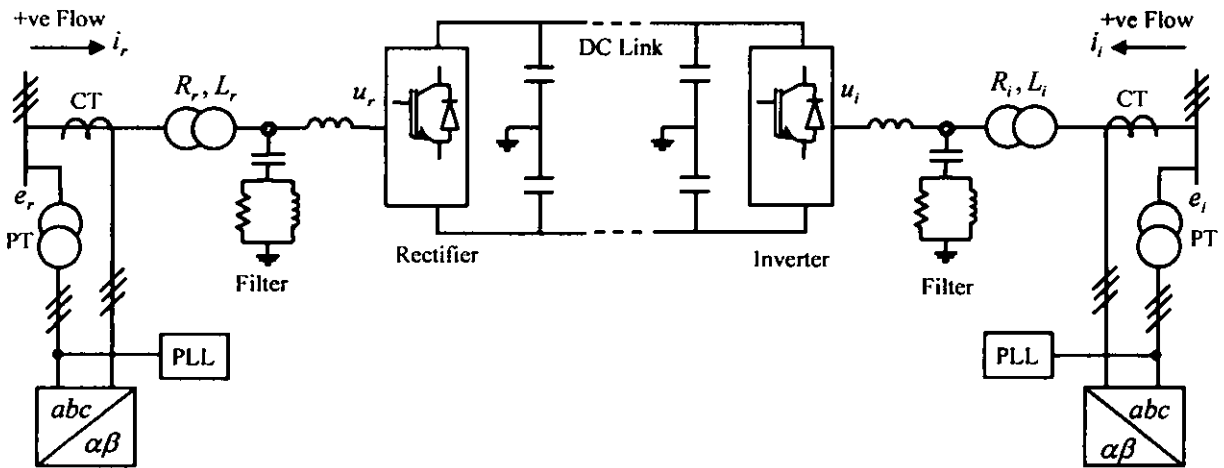
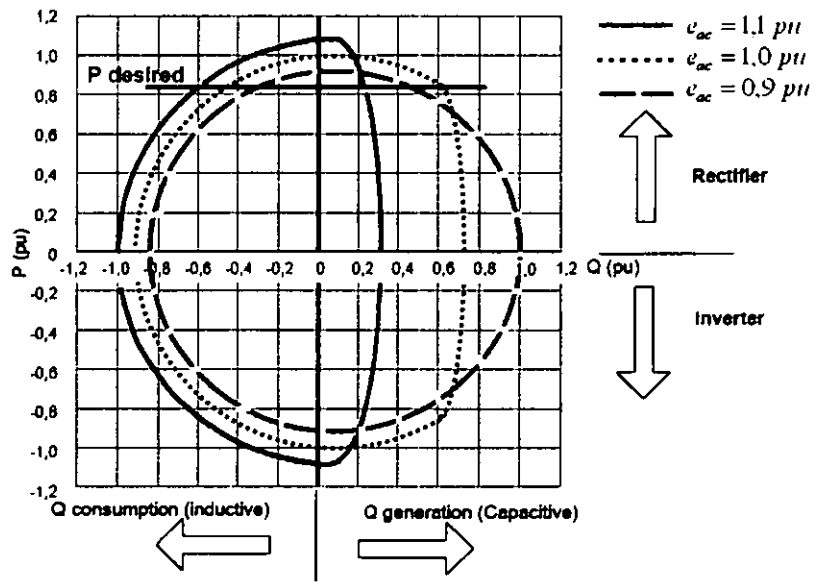
Table 1
System Description

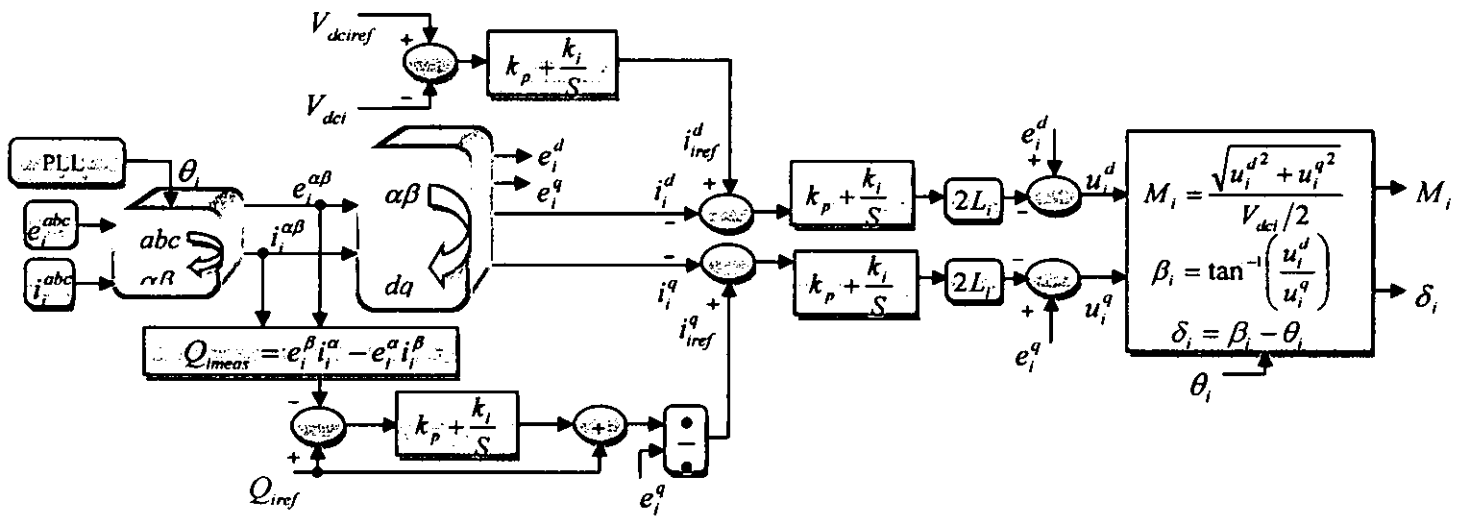
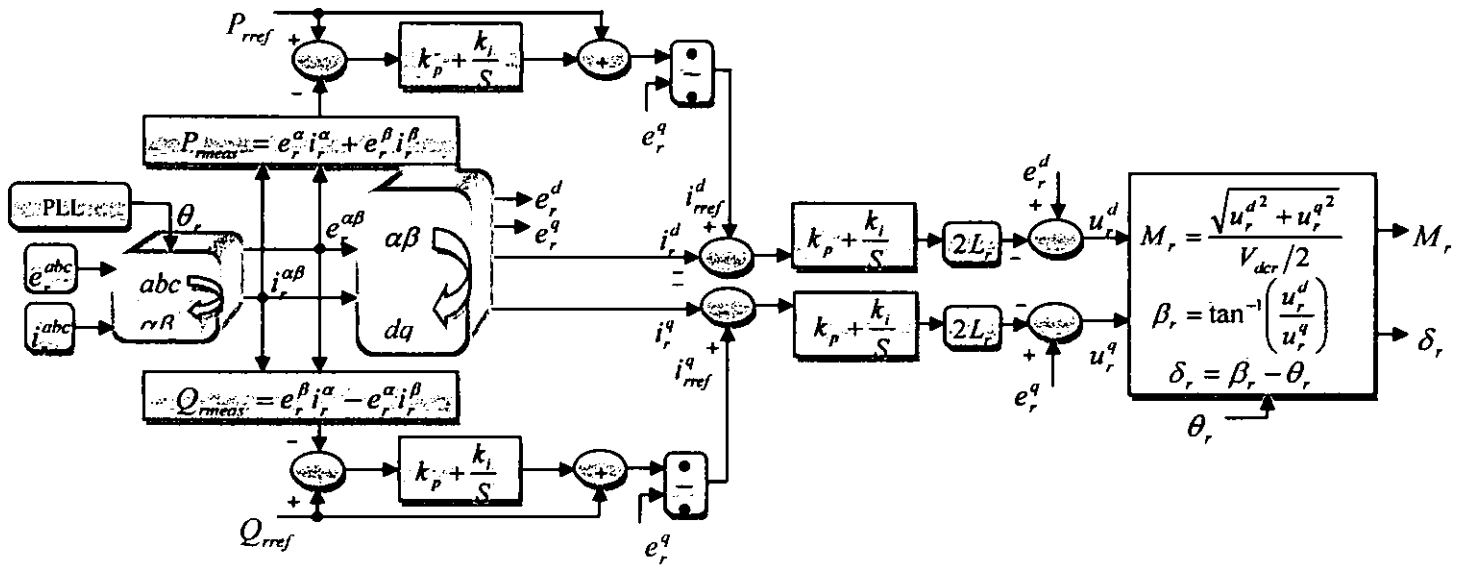
Converter Transformer	200 MVA, 0.15 p.u.	230kV/100kV
DC Link Rating	200 MW	$\pm 100\text{Kv}$
AC Side Harmonic Filters	40 MVAR	Quality Factor = 15
27 th High Pass Damped	18 MVAR	
54 th High Pass Damped	22 MVAR	
Outer Loop Controllers		
P controller	$K_p=0.0$	$K_i=20.0$
Q controller	$K_p=0.0$	$K_i=20.0$
V _{dc} controller	$K_p=2.0$	$K_i=40.0$
Inner loop current controller	$K_p=4.0$	$K_i=40.0$

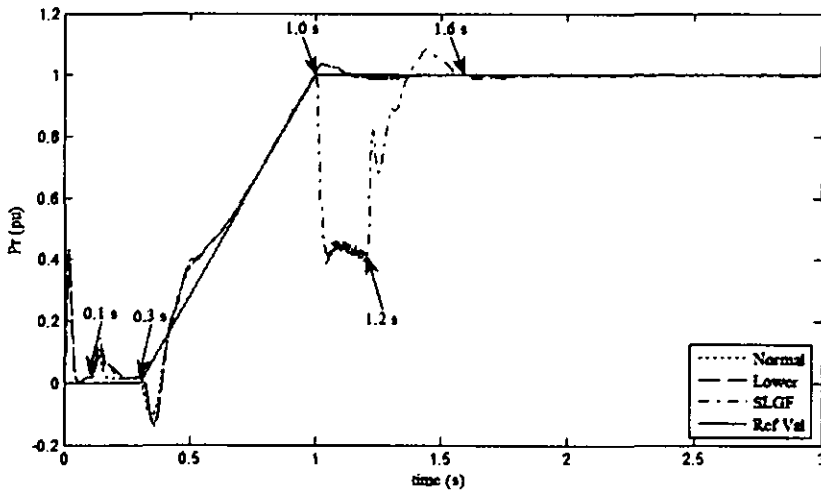
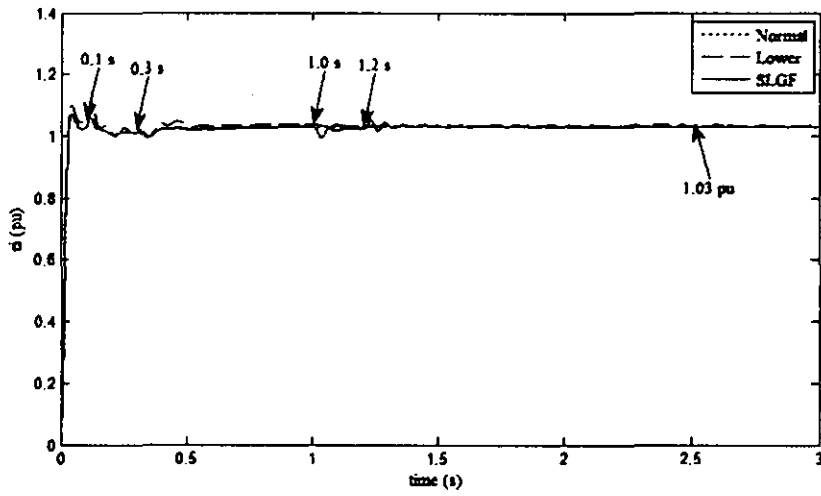
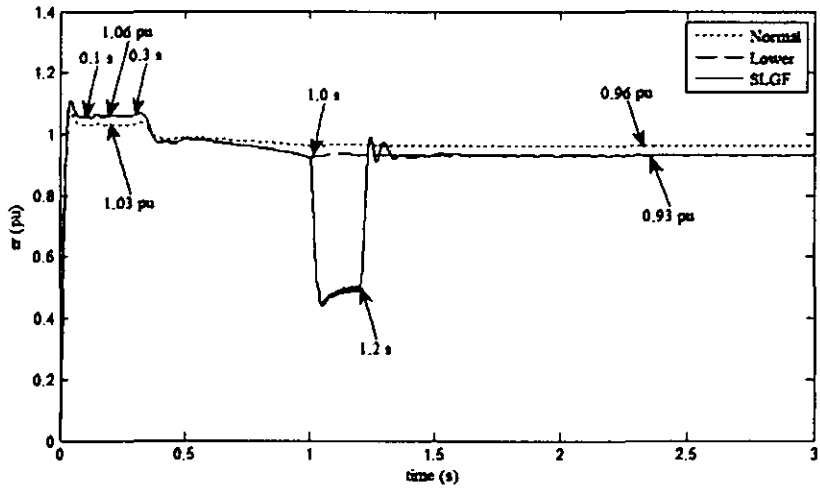
Table 2
Scenario Description

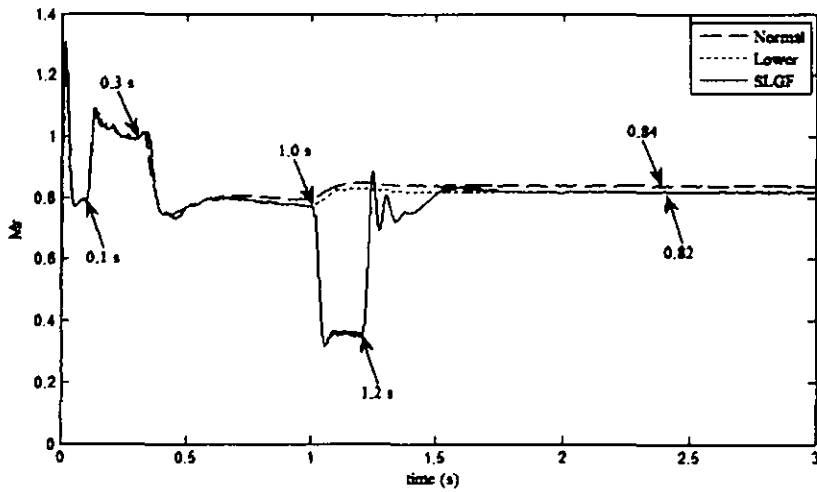
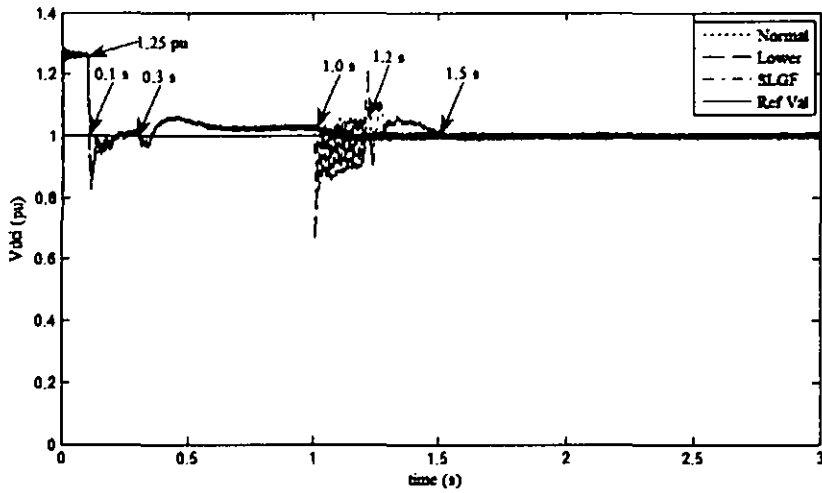
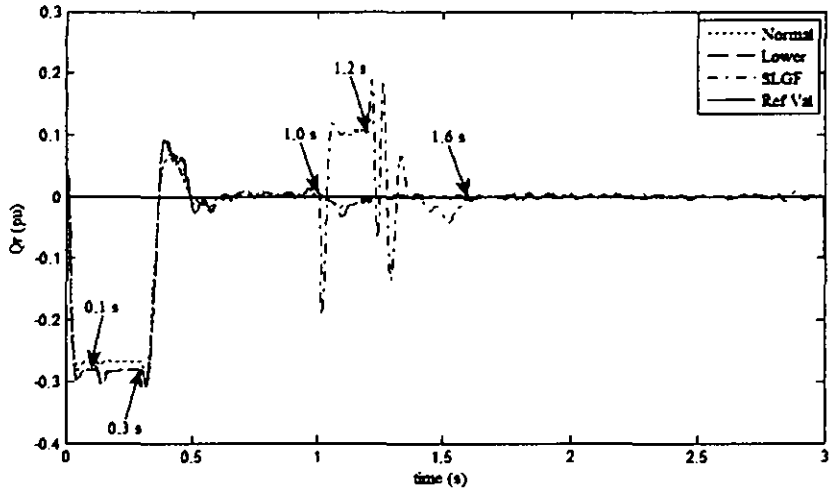
Case Study Description	Normal Fault Level	Lower fault Level	Single Line-Ground Fault
AC network Short Circuit Level			
Rectifier Side	2000 MVA	1000 MVA	1000 MVA
Inverter Side	2000 MVA	1000 MVA	2000 MVA
Rectifier Side Controller	P, Q	P, Q	P, Q
Active controllers activated at	$t = 0.3 \text{ sec}$	$t = 0.3 \text{ sec}$	$t = 0.3 \text{ sec}$
P_{ref}	1.0 p.u.	1.0 p.u.	1.0 p.u.
Q_{ref}	0.0 p.u.	0.0 p.u.	0.0 p.u.
Inverter Side Controller	V_{dc}, Q	V_{dc}, Q	V_{dc}, Q
Active controllers activated a	$t = 0.1 \text{ sec}$	$t = 0.1 \text{ sec}$	$t = 0.1 \text{ sec}$
$V_{\text{dc} \text{ref}}$	1.0 p.u.	1.0 p.u.	1.0 p.u.
Q_{ref}	-0.1 p.u.	-0.1 p.u.	-0.1 p.u.

Figures









Appendix D

Ravindra N. Mukerjee and **Ahmed Mahjoub**, "A Instantaneous Power Theory Based Fully Decoupled Controller Model for VSC-HVDC Transmission System," European Transactions on Electrical Power. Manuscript# ETEP-09-0125.

A Instantaneous Power Theory Based Hybrid Controller for VSC-HVDC Transmission System

Ravindra N. Mukerjee*, Ahmed Mahjoub

Department of Electrical & Electronic Engineering

Universiti Teknologi PETRONAS, Bandar Seri Iskandar, 31750 Tronoh, Perak, Malaysia.

rmukerjee@gmail.com, Mahjoub_ahmed@yahoo.com

SUMMARY

An AC system interfacing electronics based power transmission or distribution network experiences non-sinusoidal voltage and current waveforms. Events in an ac power network may prompt variation in fault level at the interface point or some amount of system unbalance or even initiation of transients. Since VSC-HVDC controller performance depends on the accuracy in the measured values of currents and voltages and the reference values of the currents derived there from, it is important to use a measurement processing technique appropriate for the non-sinusoidal waveforms and transients. Instantaneous power theory is used in this paper for not only obtaining the measured values of the real and reactive powers, but also for deriving reference values of currents used in the inner current control loop. A fully decoupled controller model exploiting similarity transformation is also developed. The performance of the model is assessed through simulations on a VSC-HVDC link interfacing an ac system.

Keywords: VSC-HVDC, Instantaneous Power Theory, Modal Transformation, Distributed Generation, Park's Transformation.

1. Introduction

VSC-High-voltage direct current transmission a high power electronics based technology provides economical alternatives to ac transmission for long-distance bulk power delivery from remote sources, immunity against network congestion or loop flow on parallel paths facilitating power trading and is useful as asynchronous link to provide a firewall against propagation of cascading outages in one network crossing over to another network. It also facilitates interconnection of AC systems in the lower and middle power range. VSC-HVDC has two distinct advantages over its earlier generation thyristor based HVDC transmission. Synchronous voltage source is not required to commute against, for its operation and voltage source converters (VSC) do not suffer from commutation failures under adverse conditions in interfacing ac system, allowing fast recoveries from nearby ac faults. These two properties make it amenable to wider application areas. Thyristor based HVDC requires switching for polarity reversal. VSC-HVDC transmission reverses power through reversal of current direction rather than voltage polarity, facilitating power reversal at an intermediate tap point independent of the main power flow direction in Multi-terminal HVDC systems [1].

VSC-HVDC transmission using self commutated IGBT based VSC and Pulse Width Modulation (PWM) with a switching frequency considerably higher than the AC system power frequency, permits simple converter topology and reduced filter size, achieves high speed control of both active and reactive power, generates ac output voltage having desired

phase angle or amplitude instantly with a close to sinusoidal wave shape, reducing harmonic generation and eliminating low order harmonics and causing a rather small harmonic interference compared to a line commutated converter in thyristor based HVDC. The desired fundamental frequency voltage is created through low pass filtering of the high frequency pulse modulated voltage. Up to a certain limit, any phase angle or amplitude can be created by changing the PWM pattern [2, 3]. IGBT being a MOS-device, power need for the control of the component is very low. Series connection of many semiconductors with good voltage distribution even at switching frequencies in kHz range is possible, to achieve a high HVDC link voltage [4–6].

VSC-HVDC converter station can comprise of either VSC or current-sourced converters (CSC). Whereas the CSCs' are robust, the VSCs' have higher efficiency, low initial cost, and smaller physical size. VSC is preferred over CSC, since both power and control circuits in CSC are more complex. Filter capacitors are required at the ac terminals of a CSC to improve output ac current waveform quality, adding to cost. CSC requires switches of sufficient reverse voltage withstand capability such as Gate-Turn-off thyristors, capable of blocking voltages of both polarities in off-state. Alternatively, series diode is required with each switch, resulting in increased cost and conduction losses. CSC also requires smoothing DC inductors across the three-phase bridge terminals, which are generally larger and more expensive than capacitors used in VSCs [7, 8]. IGBT module commercially available is more suitable for voltage-source PWM converter, since a free-wheeling diode is connected in anti-parallel with each IGBT. Thus IGBTs do not need the built-in reverse voltage blocking capability, bringing in more flexibility to device design.

VSC with PWM can operate in all four quadrants of PQ-plane. It can operate as rectifier or inverter at variable frequency and absorb or supply reactive power to the interfacing AC network. Reactive power can also be controlled at each terminal independent of the dc transmission voltage level. This control capability gives total flexibility to place converters anywhere in the ac network as there is no restriction on minimum network short circuit capacity. HVDC transmission and reactive power compensation with VSC technology has attributes beneficial to overall system performance. It can be used for the dynamic compensation of power transmission systems, providing increased transient stability and improved damping. The STATCOM functionality enables it to adjust reactive power support to control AC bus voltage and improve system stability. The dynamic support of the ac voltage at each converter terminal improves the voltage stability and increases the transfer capability of sending and receiving end ac systems.

VSC can be used as virtual synchronous generator supplying passive networks or areas which either have no local power generation or lack enough power in the rotating machines implying low short circuit power, thus improving power quality of the weak system. Controllability of VSC-HVDC facilitates a remote wind generation in-feed using a VSC-HVDC link to be radially interconnected to an electric distribution system having feed from upstream synchronous generation and operate in parallel under constant power, ac voltage control and frequency control modes. Absence of minimum power or current restrictions facilitates reverse power flow and permits economic power schedules. It can be used in Back-to-back schemes [1].

Forced commutation, dynamic voltage control and black start capability allow VSC-HVDC to serve isolated loads on islands over long distance submarine cables without any need for running expensive local generation. VSC converters can operate at variable frequency to feed large drives such as compressors or pumps on offshore oil or gas platforms from shore, eliminating expensive, less efficient higher emission offshore power production. Large remote wind generation arrays require (i) a collector system, (ii) reactive power support for doubly fed induction generators and (iii) power evacuation facility. VSC-HVDC underground transmission circuits can be placed on dual-use right-of-way to bring in power as well as provide voltage support. VSC-HVDC being an asynchronous link and connecting a wind farm in-feed to an electric distribution system as distributed generation can isolate the power system from the wind power fluctuations.

The operational requirements imposed on an HVDC link keep on varying, depending on the changes in interfacing ac network operating conditions at its sending and receiving ends. Normal power transfer in forward direction, reverse power transfer, sending end and/or receiving end ac network short circuit capacity low due to network fault, DC line witnessing fault, are some of the operating conditions, the VSC may have to encounter. Through control of modulation index and the phase shift between network voltage and converter input voltage on the sending end and /or between converter output voltage and the network voltage on the receiving end, the operational requirements are met by modifying the instant and duration of conduction of the IGBT switches in VSC. The change in PWM pattern enables this. The change in PWM pattern realized through the controller provided with decision logics, enables change in fundamental frequency voltage phase angle and the fundamental frequency voltage magnitudes of the converters and hence the required change in active and reactive power flows [9]. A VSC-HVDC link often has to adjust itself to avoid oscillations under changing operating conditions. To suppress these oscillations, design and operational strategy of controllers in a VSC-HVDC arrived at through dynamic simulations, plays a significant role.

To facilitate dynamic simulation of a composite power system incorporating a VSC-HVDC link and assess performance of a controller supervising PWM module for ultimate firing control of the IGBT valves, VSC-HVDC controller models were developed by several authors [10–14]. The control system in a VSC-HVDC comprises a fast inner current loop controlling the ac current within the converter's current carrying capability limit and a number of outer loops providing reference values of current to the inner current controller, for the control strategy chosen at the rectifier or the inverter end. The outer controllers could be dc voltage controller, active power controller, reactive power controller and the frequency controller. Not all the outer controllers are used at the same time. However, one of the two converters must control dc link voltage for active power balance between the power entering the rectifier and leaving the inverter [11].

In [10], state model $\dot{x} = Ax + Bu$ is developed with currents in direct and quadrature axes of a synchronously rotating reference frame as state variables and using d-q transformed equivalent of the source side circuit of the VSC converter, originally framed in a-b-c frame of reference. Synchronously rotating d-axis is assumed to be leading the phase 'a' by a transformation angle θ , derived through a phase locked loop. Decoupled control rule for the current state variables or the inner current controller is obtained by defining the feedback

loop and the PI compensation. The inner current controller loop is implemented in d-q frame. However, control law for determining the converter source side reference voltage variables u_d and u_q still need cross-coupled terms. These voltages and the dc link voltage V_{dc} , determine the amplitude and angle modulation indices. The measured real and reactive power on the network side is assessed using the Clarke's variables viz. instantaneous voltage and current vectors.

[11], is similar to [10], except that a one-sample delay is implemented in the inner current controller for slow current control and a smith predictor is used in the current controller to compensate for the time delay for fast current control. The inner current control loop is implemented in d-q frame. The dead beat current control is achieved through proportional control of the current error. However, to wipe-off the steady state current error, integral part can also be added. The measured values of the d-q transformed currents are derived from the real and reactive power computed after transforming the voltages and the currents acquired in a-b-c reference frame to rotating d-q frame. The computation of converter source side reference voltage variables u_d and u_q need i_q and i_d respectively, and in that sense use coupled expressions. These reference voltages are transformed to the a-b-c frame via Clarke's transformation.

[12] also follows similar strategy as in [10] and [11]. Fundamental frequency model in terms of d-q variables is formed through transformation from a-b-c frame to switching reference frame and then to dq0 frame. The inner current loop is once again implemented in d-q frame. The current components are decoupled. However, computation of d component of voltage needs q component of current and computation of q component of converter source side voltage needs d component of current like the earlier two models. Like in [10] converter source side voltages and the dc link voltage V_{dc} , determine the amplitude and angle modulation indices.

In [13] and [14] converter source side phase voltages in a-b-c frame are transformed into Clarke's components. The components are then identified and separated into positive and negative sequence voltages. While positive sequence voltage is subjected to a counter clockwise d-q transformation, the negative sequence voltage is transformed to a clockwise d-q transformation. This transforms both of them into dc components during filtering and avoids any phase shift. The two filtered components are then used to compute the mean value of the source side converter voltage during the sample period, specifically witnessing AC system disturbances. Reference values of the active and reactive parts of the converter currents in rotating d-q frame are supplied from the outer power loop. The outer loop on the rectifier side includes a PI-control of the dc link voltage and a forward feed of the d-component of the reference value derived from the outer power loop of the inverter side, thus facilitating change of the ordered active current without influencing the dc link voltage. The inner current loop is implemented in d-q frame, wherein the current errors are computed using the measured d-q currents and two sample delayed reference currents. This avoids failure of the dead-beat current control during normal ac network conditions. Dead-beat current control works satisfactorily with strong ac network interfacing the VSC-HVDC. The reference value of the converter source side voltages are transformed to a-b-c frame, before feeding the PWM block with amplitude and angle modulation indices as inputs.

This paper develops the model of the controller with a modified inner current loop wherein, not only the current errors in the d-q frame are decoupled, but the procedure of generation of source side converter d-q voltages is also decoupled. The q component of the current error is not required to compute d component and the d component of the current error is not required to compute q component, of the converter source side reference voltage. This is expected to speed up reference voltage generation. Conventional complex power is valid only for a system in steady state with a fixed line frequency. Whereas 3-phase instantaneous power is valid during steady as well as transient states [15] and describes the total energy flow per second between two interfacing systems. Considering this, the computation of the measured Clarke’s components of the real and reactive power in the outer power loop is proposed to be based on the instantaneous power theory. The reference values of currents are first calculated using Clarke’s components and then the d-q form of the same is derived using the transformation. The model performance is validated through SIMULINK power system blockset (PSB) based simulations on the composite power system incorporating the developed controllers.

2. VSC-HVDC OPERATION

The converter phase angle can be used for the active power control. A VSC operates as a rectifier when AC voltage of the converter u_{ac} phase lags the AC network voltage e_{ac} i.e. $\delta_{ac} > 0$. The active power flows into VSC from AC system in this case as shown in Figure 1.

$$p_{ac} = \frac{e_{ac}u_{ac}}{x_{ac}} \sin \delta_{ac} \tag{1}$$

The voltage magnitude can be used to control reactive power. The converter provides reactive power support to the AC network, when the converter AC voltage $|u_{ac}|$ is higher than the AC network voltage $|e_{ac}|$.

$$Q_{ac} = \frac{e_{ac}^2}{x_{ac}} - \frac{e_{ac}u_{ac}}{x_{ac}} \cos \delta_{ac} \tag{2}$$

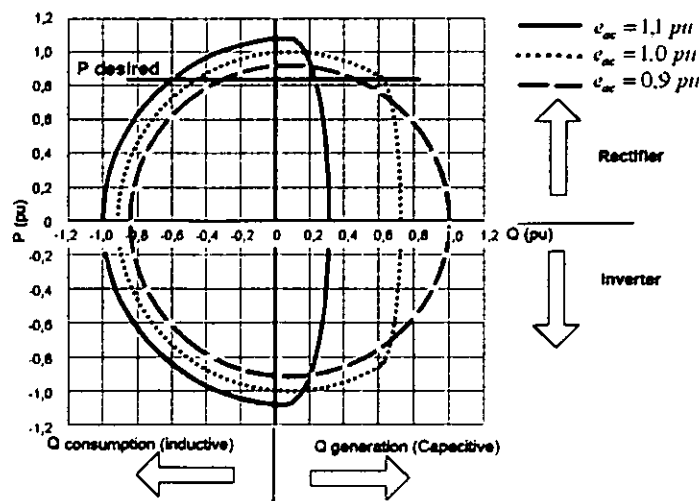


Figure 1. P-Q diagram for VSC-HVDC

Figure 1 illustrates the characteristic variation in active power, P , and reactive power, Q , capability of a VSC-HVDC link as a function of AC system voltage, measured at the network interfacing point. The reactive power delivery to the network increases with decreasing network voltage [5, 9]. Similarly, the converter reactive power absorption increases with increasing network voltage. For a given ac system voltage, the converter can be operated at any point within the P-Q circle, as required.

3. State Space Model

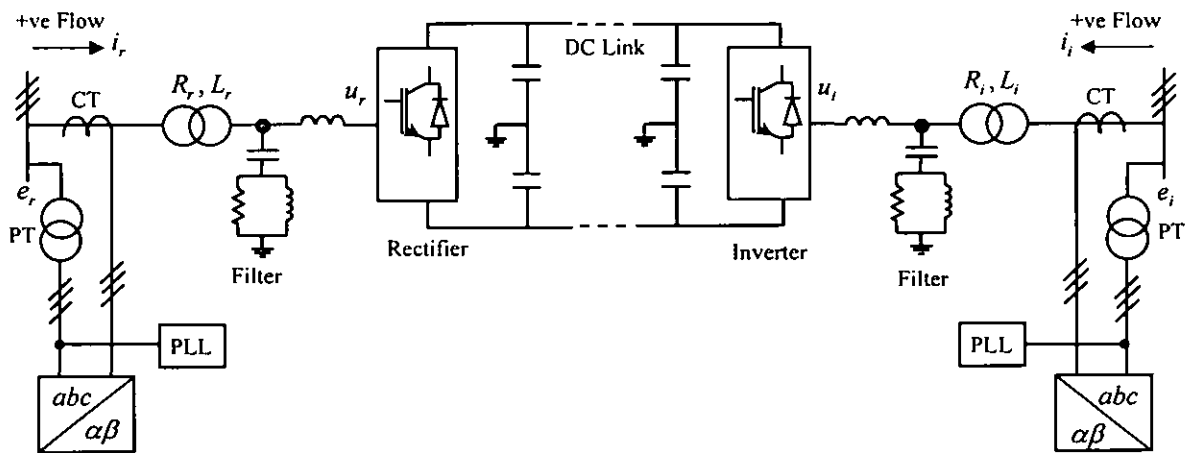


Figure 2. VSC-HVDC Power Circuit and Measurement Scheme

Assuming flows from the network to the converters at both rectifier and the inverter ends to be positive as shown in Figure 2, the voltage and current relationships at the network side of the respective coupling transformers are given by:

$$e_r^{abc} = R_r i_r^{abc} + L_r \frac{di_r^{abc}}{dt} + u_r^{abc} \quad \& \quad e_i^{abc} = R_i i_i^{abc} + L_i \frac{di_i^{abc}}{dt} + u_i^{abc} \quad (3)$$

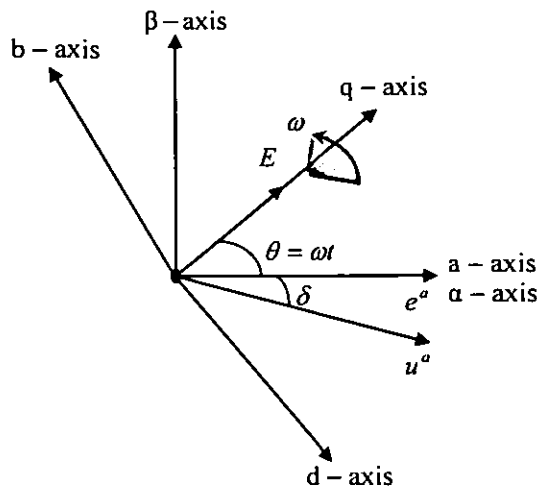


Figure 3. Inter-relationship between frames of references for VSC-HVDC

Transforming the equations in a-b-c frame of reference to a synchronously rotating reference frame as shown in Figure 3, Equations in (3) become

$$T_{dq0}^{-1} e_r^{dq0} = R_r T_{dq0}^{-1} i_r^{dq0} + L_r \frac{d(T_{dq0}^{-1} i_r^{dq0})}{dt} + T_{dq0}^{-1} u_r^{dq0} \quad (4)$$

$$T_{dq0}^{-1} e_i^{dq0} = R_i T_{dq0}^{-1} i_i^{dq0} + L_i \frac{d(T_{dq0}^{-1} i_i^{dq0})}{dt} + T_{dq0}^{-1} u_i^{dq0} \quad (5)$$

The transformation and its inverse transformation with reference to Figure 3 are given as

$$T_{dq0} = \frac{2}{3} \begin{bmatrix} \sin \theta & \sin(\theta - 120^\circ) & \sin(\theta + 120^\circ) \\ \cos \theta & \cos(\theta - 120^\circ) & \cos(\theta + 120^\circ) \\ \frac{1}{2} & \frac{1}{2} & \frac{1}{2} \end{bmatrix}, \quad T_{dq0}^{-1} = \begin{bmatrix} \sin \theta & \cos \theta & 1 \\ \sin(\theta - 120^\circ) & \cos(\theta - 120^\circ) & 1 \\ \sin(\theta + 120^\circ) & \cos(\theta + 120^\circ) & 1 \end{bmatrix}$$

Pre multiplying both sides by T_{dq0} , and expanding the 2nd term on the right hand side, Equations (4) and (5) can be written as

$$e_r^{dq0} = R_r i_r^{dq0} + L_r \left(\frac{di_r^{dq0}}{dt} + T_{dq0} \frac{dT_{dq0}^{-1}}{dt} i_r^{dq0} \right) + u_r^{dq0} \quad (6)$$

$$e_i^{dq0} = R_i i_i^{dq0} + L_i \left(\frac{di_i^{dq0}}{dt} + T_{dq0} \frac{dT_{dq0}^{-1}}{dt} i_i^{dq0} \right) + u_i^{dq0} \quad (7)$$

Equations (6) and (7) after simplification [appendix A, (A.1) and (A.2)] become

$$\begin{bmatrix} e_r^d \\ e_r^q \\ e_r^0 \end{bmatrix} = R_r \begin{bmatrix} i_r^d \\ i_r^q \\ i_r^0 \end{bmatrix} + L_r \frac{d}{dt} \begin{bmatrix} i_r^d \\ i_r^q \\ i_r^0 \end{bmatrix} + \omega_r L_r \begin{bmatrix} 0 & -1 & 0 \\ 1 & 0 & 0 \\ 0 & 0 & 0 \end{bmatrix} \begin{bmatrix} i_r^d \\ i_r^q \\ i_r^0 \end{bmatrix} + \begin{bmatrix} u_r^d \\ u_r^q \\ u_r^0 \end{bmatrix} \quad (8)$$

$$\begin{bmatrix} e_i^d \\ e_i^q \\ e_i^0 \end{bmatrix} = R_i \begin{bmatrix} i_i^d \\ i_i^q \\ i_i^0 \end{bmatrix} + L_i \frac{d}{dt} \begin{bmatrix} i_i^d \\ i_i^q \\ i_i^0 \end{bmatrix} + \omega_i L_i \begin{bmatrix} 0 & -1 & 0 \\ 1 & 0 & 0 \\ 0 & 0 & 0 \end{bmatrix} \begin{bmatrix} i_i^d \\ i_i^q \\ i_i^0 \end{bmatrix} + \begin{bmatrix} u_i^d \\ u_i^q \\ u_i^0 \end{bmatrix} \quad (9)$$

Assuming balanced operation of interfacing ac network signifying, absence of zero axis components, the d-q transformed versions of Equations in (3) are

$$\frac{1}{L_r} \begin{bmatrix} e_r^d \\ e_r^q \end{bmatrix} = \begin{bmatrix} \frac{R_r}{L_r} & 0 \\ 0 & \frac{R_r}{L_r} \end{bmatrix} \begin{bmatrix} i_r^d \\ i_r^q \end{bmatrix} + \begin{bmatrix} 0 & -\omega_r \\ \omega_r & 0 \end{bmatrix} \begin{bmatrix} i_r^d \\ i_r^q \end{bmatrix} + \frac{d}{dt} \begin{bmatrix} i_r^d \\ i_r^q \end{bmatrix} + \frac{1}{L_r} \begin{bmatrix} u_r^d \\ u_r^q \end{bmatrix} \quad (10)$$

$$\frac{1}{L_i} \begin{bmatrix} e_i^d \\ e_i^q \end{bmatrix} = \begin{bmatrix} \frac{R_i}{L_i} & 0 \\ 0 & \frac{R_i}{L_i} \end{bmatrix} \begin{bmatrix} i_i^d \\ i_i^q \end{bmatrix} + \begin{bmatrix} 0 & -\omega_i \\ \omega_i & 0 \end{bmatrix} \begin{bmatrix} i_i^d \\ i_i^q \end{bmatrix} + \frac{d}{dt} \begin{bmatrix} i_i^d \\ i_i^q \end{bmatrix} + \frac{1}{L_i} \begin{bmatrix} u_i^d \\ u_i^q \end{bmatrix} \quad (11)$$

Equations (10) and (11), with currents along d-q axes i_r^d , i_r^q and i_i^d , i_i^q as state variables, can be written in state space form $\dot{x} = Ax + Bu$ as

$$\frac{d}{dt} \begin{bmatrix} i_r^d \\ i_r^q \end{bmatrix} = \begin{bmatrix} -\frac{R_r}{L_r} & \omega_r \\ -\omega_r & -\frac{R_r}{L_r} \end{bmatrix} \begin{bmatrix} i_r^d \\ i_r^q \end{bmatrix} + \frac{1}{L_r} \begin{bmatrix} e_r^d - u_r^d \\ e_r^q - u_r^q \end{bmatrix} \quad (12)$$

$$\frac{d}{dt} \begin{bmatrix} i_r^d \\ i_r^q \end{bmatrix} = \begin{bmatrix} -\frac{R_l}{L_l} & \omega_l \\ \omega_l & -\frac{R_l}{L_l} \end{bmatrix} \begin{bmatrix} i_r^d \\ i_r^q \end{bmatrix} + \frac{1}{L_l} \begin{bmatrix} e_r^d - u_r^d \\ e_r^q - u_r^q \end{bmatrix} \quad (13)$$

Ac network voltages on rectifier and inverter sides of the dc link are assumed to be

$$\begin{bmatrix} e_r^a \\ e_r^b \\ e_r^c \end{bmatrix} = E_r \begin{bmatrix} \cos \omega_r t \\ \cos(\omega_r t - 120^\circ) \\ \cos(\omega_r t + 120^\circ) \end{bmatrix} \quad \& \quad \begin{bmatrix} e_i^a \\ e_i^b \\ e_i^c \end{bmatrix} = E_i \begin{bmatrix} \cos \omega_i t \\ \cos(\omega_i t - 120^\circ) \\ \cos(\omega_i t + 120^\circ) \end{bmatrix} \quad (14)$$

Balanced operation of interfacing ac network signifying absence of zero axis components, lead to the d-q transformed version of Equations in (14) as [appendix A, (A.3) and (A.4)]

$$\begin{bmatrix} e_r^d \\ e_r^q \end{bmatrix} = \begin{bmatrix} 0 \\ E_r \end{bmatrix} \quad \& \quad \begin{bmatrix} e_i^d \\ e_i^q \end{bmatrix} = \begin{bmatrix} 0 \\ E_i \end{bmatrix} \quad (15)$$

The relationship between the converter ac and dc voltages on rectifier and inverter sides is given by [appendix A, (A.6)]

$$\begin{bmatrix} u_r^a \\ u_r^b \\ u_r^c \end{bmatrix} = \frac{M_r V_{dcr}}{2} \begin{bmatrix} \cos(\omega_r t - \delta_r) \\ \cos(\omega_r t - \delta_r - 120^\circ) \\ \cos(\omega_r t - \delta_r + 120^\circ) \end{bmatrix} \quad \& \quad \begin{bmatrix} u_i^a \\ u_i^b \\ u_i^c \end{bmatrix} = \frac{M_i V_{dci}}{2} \begin{bmatrix} \cos(\omega_i t - \delta_i) \\ \cos(\omega_i t - \delta_i - 120^\circ) \\ \cos(\omega_i t - \delta_i + 120^\circ) \end{bmatrix} \quad (16)$$

Balanced operation of interfacing ac network signifying absence of zero axis components, lead to the d-q transformed version of Equations in (16) as [Appendix A, (A.7) and (A.8)]

$$\begin{bmatrix} u_r^d \\ u_r^q \end{bmatrix} = \frac{M_r V_{dcr}}{2} \begin{bmatrix} \sin \delta_r \\ \cos \delta_r \end{bmatrix} \quad \& \quad \begin{bmatrix} u_i^d \\ u_i^q \end{bmatrix} = \frac{M_i V_{dci}}{2} \begin{bmatrix} \sin \delta_i \\ \cos \delta_i \end{bmatrix} \quad (17)$$

The state matrices in Equations (12) and (13) can be subjected to similarity transformation [16], to obtain decoupled state space equations [Appendix C, (C.3) and (C.4)].

$$\frac{d}{dt} \begin{bmatrix} i_{rz}^d \\ i_{rz}^q \end{bmatrix} = \begin{bmatrix} -\frac{R_r}{L_r} + j\omega_r & 0 \\ 0 & -\frac{R_r}{L_r} - j\omega_r \end{bmatrix} \begin{bmatrix} i_{rz}^d \\ i_{rz}^q \end{bmatrix} + \frac{1}{2L_r} \begin{bmatrix} -u_r^d \\ E_r - u_r^q \end{bmatrix} \quad (18)$$

$$\frac{d}{dt} \begin{bmatrix} i_{iz}^d \\ i_{iz}^q \end{bmatrix} = \begin{bmatrix} -\frac{R_l}{L_l} + j\omega_l & 0 \\ 0 & -\frac{R_l}{L_l} - j\omega_l \end{bmatrix} \begin{bmatrix} i_{iz}^d \\ i_{iz}^q \end{bmatrix} + \frac{1}{2L_l} \begin{bmatrix} -u_i^d \\ E_i - u_i^q \end{bmatrix} \quad (19)$$

Whereas $i_{rz}^d, i_{rz}^q, i_{iz}^d, i_{iz}^q$ are the transformed state variables, the state variables related to the voltage i.e. u_r^d and u_r^q are the original state variables.

4. Fully Decoupled Controller Model

4.1. Inner current loop

In HVDC transmission, V_{dc} needs to be kept sufficiently high. For different operational regimes requiring real and reactive powers to be controlled independently and e_q , hence u_d and u_q need to be controlled independently. Consequently, the modulation index and also the phase shift between the modulating signal and the carrier signal in PWM module need to be varied to achieve various operational requirements. With a view to achieve dead beat control

leading to zero steady state error, using state equation (18) and defining feedback loops and PI compensation as,

$$\begin{bmatrix} x_1 \\ x_2 \end{bmatrix} = \frac{1}{2L_r} \begin{bmatrix} -u_r^d \\ E_r - u_r^q \end{bmatrix}$$

$$\text{Where, } x_1 = \left(k_p + \frac{k_i}{s}\right)(i_{rref}^d - i_r^d), \quad x_2 = \left(k_p + \frac{k_i}{s}\right)(i_{rref}^q - i_r^q)$$

Implying, $u_r^d = -2L_r x_1$ and $u_r^q = E_r - 2L_r x_2$ Thus,

$$u_r^d = -2L_r \left(k_p + \frac{k_i}{s}\right)(i_{rref}^d - i_r^d) \quad \& \quad u_r^q = E_r - 2L_r \left(k_p + \frac{k_i}{s}\right)(i_{rref}^q - i_r^q) \quad (20)$$

Similarly, from state Equation (19)

$$u_i^d = -2L_i \left(k_p + \frac{k_i}{s}\right)(i_{iref}^d - i_i^d) \quad \& \quad u_i^q = E_i - 2L_i \left(k_p + \frac{k_i}{s}\right)(i_{iref}^q - i_i^q) \quad (21)$$

Equations (20) and (21) model the inner current control loop. The control implementation involves the state variables $i_r^d, i_r^q, u_r^d, u_r^q$. However, to incorporate controller dynamics into the state matrix together with the VSC-HVDC power circuit dynamics and the interfacing ac system dynamics for carrying out modal analysis of the composite system, u_r^d, u_r^q may have to be transformed to u_{rc}^d, u_{rc}^q . Once u_r^d, u_r^q and u_i^d, u_i^q are available, required modulation index and also the phase shift between the modulating signal and the carrier signal in PWM module can be determined using the relations

$$M_r = \frac{\sqrt{u_r^{d^2} + u_r^{q^2}}}{V_{dcr}/2}, \quad \delta_r = \tan^{-1}\left(\frac{u_r^q}{u_r^d}\right) - \theta_r, \quad M_i = \frac{\sqrt{u_i^{d^2} + u_i^{q^2}}}{V_{dci}/2}, \quad \delta_i = \tan^{-1}\left(\frac{u_i^q}{u_i^d}\right) - \theta_i \quad (22)$$

4.2. Outer loop

The outer loop comprises of controllers such as the DC voltage controller, the active power controller and the reactive power controller. These controllers provide reference values of the respective direct and quadrature axis currents to the inner current control loop, implemented in d-q frame.

4.2.1. DC voltage controller

Inverter side is set to control the DC link voltage. A control equation for the direct axis current reference for the inner loop on the inverter side is implemented for the purpose. This outer controller is much slower than the inner loop current controller, to ensure stability. i_{iref}^d being in rotating d-q frame, yields dc component in steady state and is synonymous to the active current, assuming no power losses in the converter.

$$i_{iref}^d = (V_{dciref} - V_{dci}) \left(k_p + \frac{k_i}{s}\right) \quad (23)$$

4.2.2. Active power controller

The reference value of the active part of the converter current for the inner loop is supplied from the outer active power loop. The reference value i_{rref}^d being in rotating d-q frame, yields dc component in steady state. The control of active power combines both open loop and the feedback loop as shown in Equation (24). For implementation of the feedback loop, error

between the desired dc power to be transferred and the active power measured on the interface bus is computed in the loop itself using

$$\Delta P_r = P_{rord} - P_r \quad \& \quad P_{rref} = P_{rord} + \Delta P_r \left(k_p + \frac{k_i}{S} \right) \quad (24)$$

4.2.3. Reactive power controller

The reference value of the reactive part of the converter current for the inner loop is supplied from the outer reactive power loop. The reference values i_{rref}^q at the rectifier and i_{iref}^q at the inverter ends being in rotating d-q frame, yield dc component in steady state. The control of reactive power combines both open loop and the feedback loop as shown in Equations (25) and (26). For implementation of the feedback loop, error between the desired reactive power to be exchanged between the ac network and the dc link and the reactive power measured on the interface bus is computed in the loop itself.

$$\Delta Q_r = Q_{rord} - Q_r \quad \& \quad Q_{rref} = Q_{rord} + \Delta Q_r \left(k_p + \frac{k_i}{S} \right) \quad (25)$$

$$\Delta Q_i = Q_{iord} - Q_i \quad \& \quad Q_{iref} = Q_{iord} + \Delta Q_i \left(k_p + \frac{k_i}{S} \right) \quad (26)$$

4.3. Processing of Measurements

Using instantaneous power theory, phase current and voltage measurements on the network can be transformed to Clarke variables.

$$e_\alpha = \frac{2}{3} \left(e_a - \frac{1}{2} e_b - \frac{1}{2} e_c \right) \quad \& \quad e_\beta = \frac{2}{3} \left(\frac{\sqrt{3}}{2} e_b - \frac{\sqrt{3}}{2} e_c \right) \quad (27)$$

Instantaneous real and reactive power measured on the rectifier side, and the reactive powers measured on the inverter side, in terms of the respective Clarke's components are [15]

$$P_r = e_r^\alpha i_r^\alpha + e_r^\beta i_r^\beta \quad (28)$$

$$Q_r = e_r^\beta i_r^\alpha - e_r^\alpha i_r^\beta \quad (29)$$

$$Q_i = e_i^\beta i_i^\alpha - e_i^\alpha i_i^\beta \quad (30)$$

The measured value of the rectifier end active power and the reactive power both ends are used to implement open and feedback control in the outer power loop.

4.4. Estimating Reference Values Of Currents for inner Current Control Loop

Usually rectifier side is set to control both real and reactive powers. Instantaneous active and reactive currents on the rectifier side [15] are given as

$$i_r^{\alpha p} = \frac{e_r^\alpha}{e_r^{\alpha^2} + e_r^{\beta^2}} p_{rref} \quad i_r^{\beta p} = \frac{e_r^\beta}{e_r^{\alpha^2} + e_r^{\beta^2}} p_{rref}$$

$$i_r^{\alpha q} = \frac{e_r^\beta}{e_r^{\alpha^2} + e_r^{\beta^2}} q_{rref} \quad i_r^{\beta q} = \frac{-e_r^\alpha}{e_r^{\alpha^2} + e_r^{\beta^2}} q_{rref}$$

Instantaneous active and reactive reference currents on the rectifier side are now computed as

$$i_{rref}^\alpha = i_r^{\alpha p} + i_r^{\alpha q} \quad \& \quad i_{rref}^\beta = i_r^{\beta p} + i_r^{\beta q} \quad (31)$$

Usually inverter side is set to control DC voltage and reactive power. The d-axis reference current is directly derived from the reference and measured values of DC voltages.

$$i_{iref}^d = (V_{dciref} - V_{dci}) \left(k_p + \frac{k_i}{S} \right) \quad (32)$$

Instantaneous active and reactive currents on the inverter side are given as

$$\begin{aligned} i_i^{\alpha p} &= \frac{e_i^\alpha}{e_i^{\alpha^2} + e_i^{\beta^2}} P_{iref} & i_i^{\beta p} &= \frac{e_i^\beta}{e_i^{\alpha^2} + e_i^{\beta^2}} P_{iref} \\ i_i^{\alpha q} &= \frac{e_i^\beta}{e_i^{\alpha^2} + e_i^{\beta^2}} Q_{iref} & i_i^{\beta q} &= \frac{-e_i^\alpha}{e_i^{\alpha^2} + e_i^{\beta^2}} Q_{iref} \end{aligned}$$

Instantaneous reactive reference current on the inverter side is give as

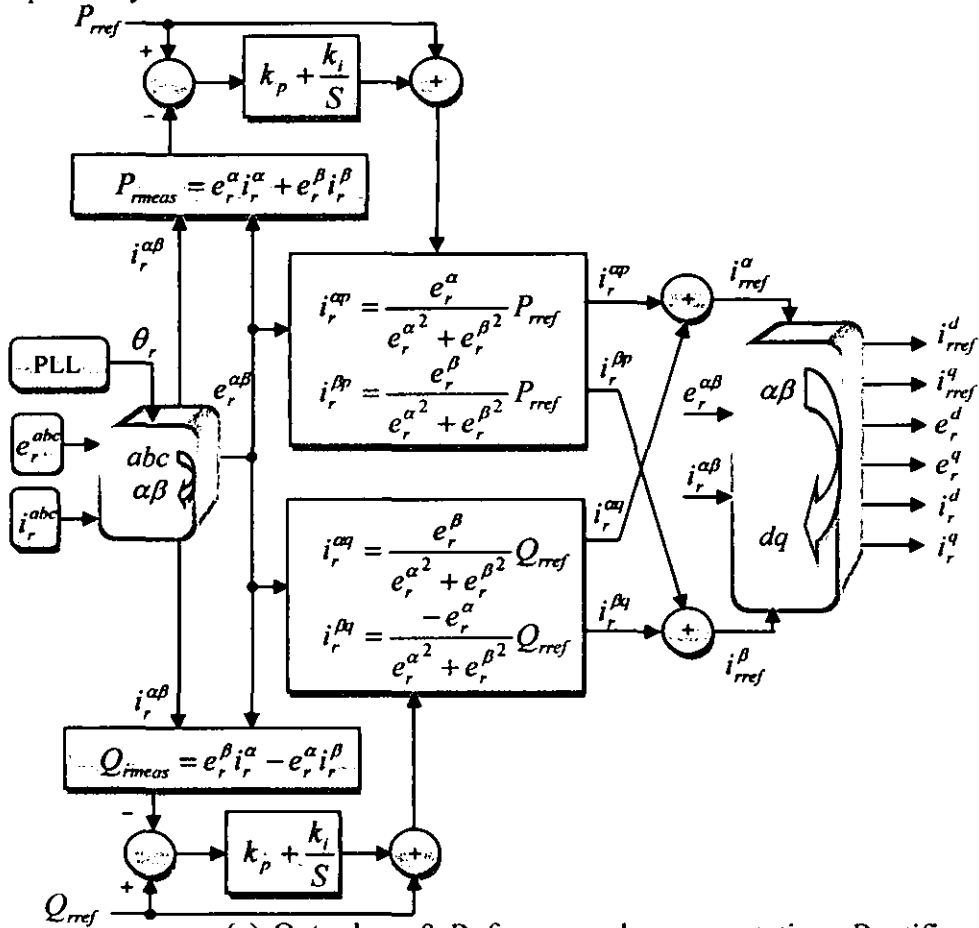
$$i_{iref}^\alpha = i_i^{\alpha p} + i_i^{\alpha q} \quad \& \quad i_{iref}^\beta = i_i^{\beta p} + i_i^{\beta q} \quad (33)$$

The d-q variables can now be derived from the Clarks variables from Equations (27), (31), and (33) using the relationships as shown in Equations (34) and (35). The transformation angle θ is available as the output of the phase locked loop.

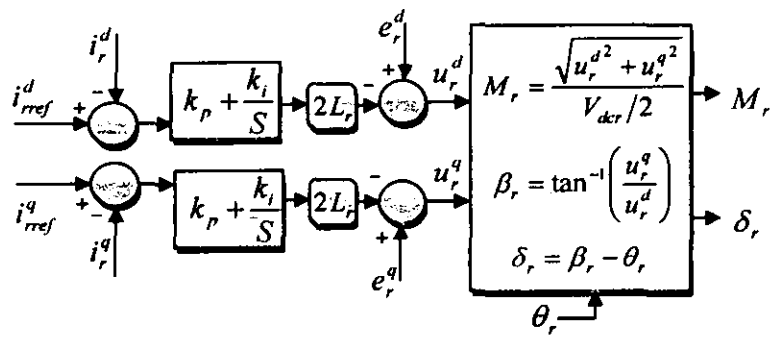
$$e^d = e^\alpha \cos \theta + e^\beta \sin \theta \quad \& \quad e^q = -e^\alpha \sin \theta + e^\beta \cos \theta \quad (34)$$

$$i^d = i^\alpha \cos \theta + i^\beta \sin \theta \quad \& \quad i^q = -i^\alpha \sin \theta + i^\beta \cos \theta \quad (35)$$

The complete model of the rectifier and the inverter side controllers are shown in Figure 4 and Figure 5 respectively.

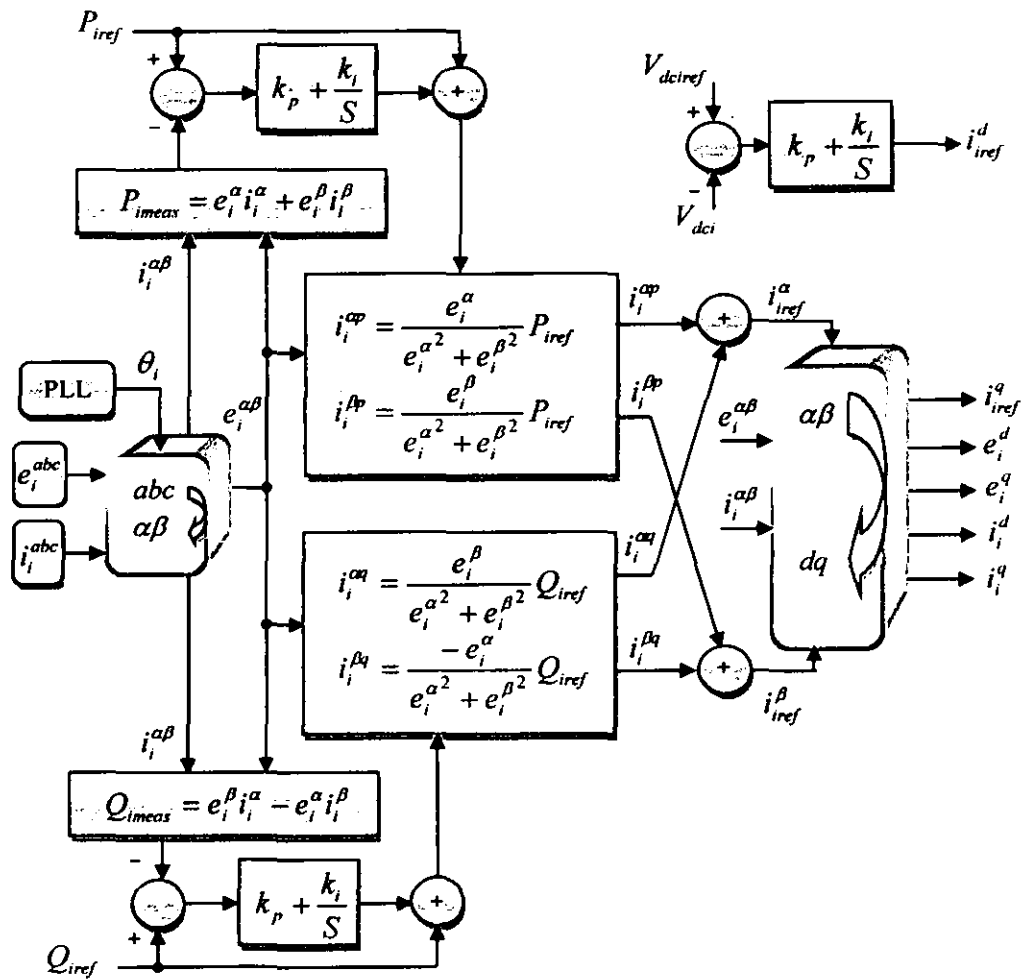


(a) Outer loop & Reference value computation– Rectifier side

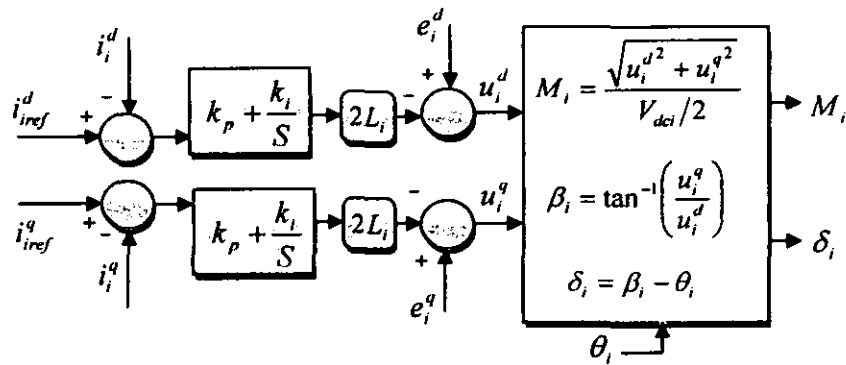


(b) Inner current loop – Rectifier side

Figure 4. VSC-HVDC RECTIFIER CONTROLLER



(a) Outer loop & Reference value computation– Inverter side



(b) Inner current loop – Inverter side

Figure 5. VSC-HVDC INVERTER CONTROLLER

5. Controller Model Performance Assessment

The system and the scenario descriptions are presented in Tables 1 & 2 respectively. Total simulation time is 3.0 sec, carrier frequency is 1350 Hz and the integration time step is 7.407 μ sec

5.1. Comparative Performance Assessment

In the scenario considered to evaluate the performance of the developed model, the short circuit level at both rectifier and inverter end AC system buses is 2000MVA i.e. the source impedance 26.45 Ω is less than the converter transformer impedance 39.675 Ω . The inverter end controls are activated at t = 0.1 second and the rectifier end controls are activated at t = 0.3 sec. Figure 6 shows the ac network voltage at the rectifier end bus. The dynamic over voltage is 3%. Since real and reactive power controls at this end are activated and the ac voltage controller is inactive, ac voltage is 4% lower than the rated one.

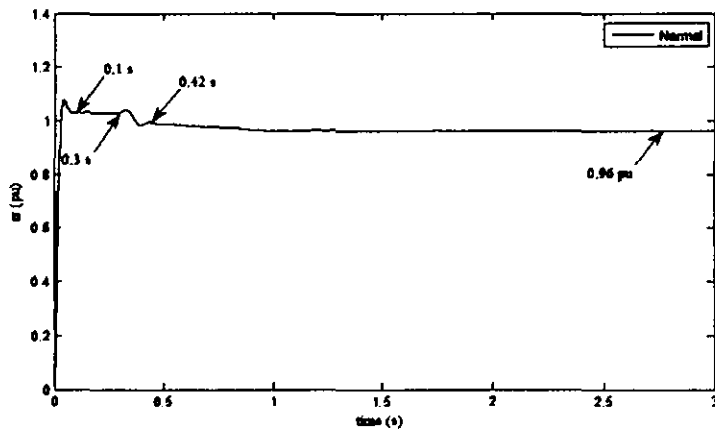


Figure 6. AC Network Bus voltage - Rectifier side

Figure 7 shows the ac network voltage at the inverter end bus. Only dc link voltage and the reactive power flow control are activated at this end and ac voltage control remains inactive.

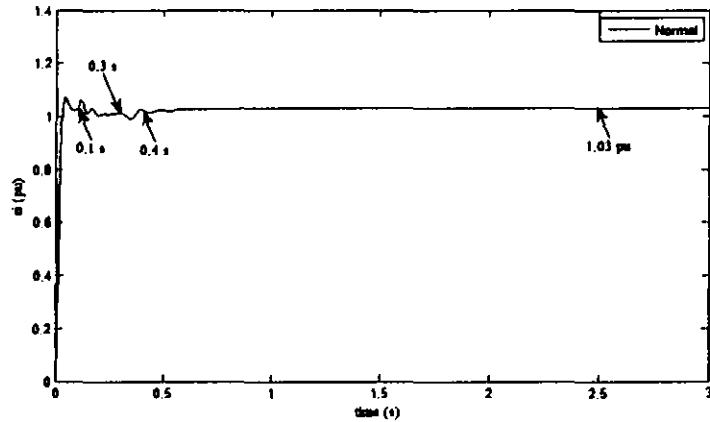


Figure 7. AC Network Bus voltage - Inverter side

Figure 8 shows the real power flow into DC link on rectifier side. Real power controller is activated at the rectifier side at $t=0.3$ sec. Figure 9 shows the reactive power flow into DC link on rectifier side. The rectifier end has the reactive power controller activated at $t=0.3$ sec. Q import or export is set at zero. Taking reactive power flow from network to the converter at both the ends as positive, it shows that the Q flow is indeed controlled to its set value with some amount of oscillations within acceptable limits.

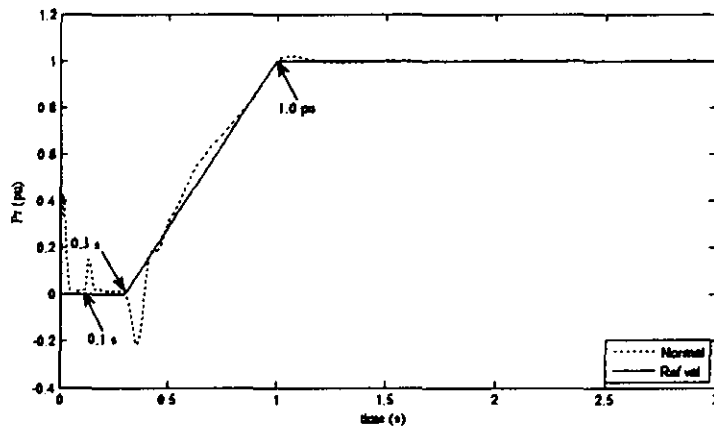


Figure 8. Real Power Flow into DC Link -Rectifier side

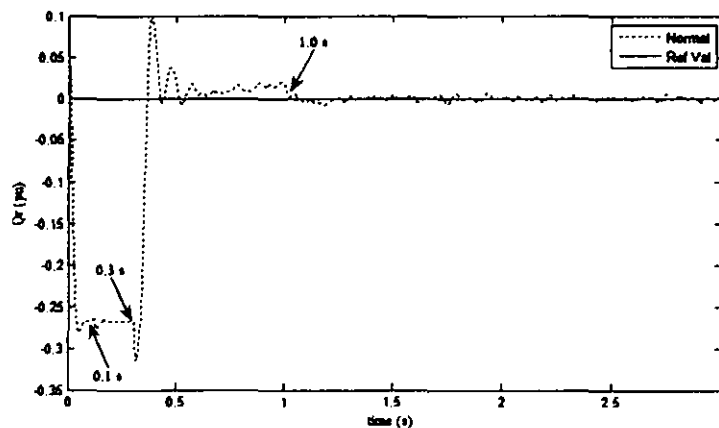


Figure 9. Reactive Power Flow into DC Link- Rectifier side

Figure 10 shows the DC link voltage at the inverter side wherein the DC voltage controller is activated at 0.1 sec. Figure 11 presents the inverter side reactive power flow from the interfacing ac network into the inverter.

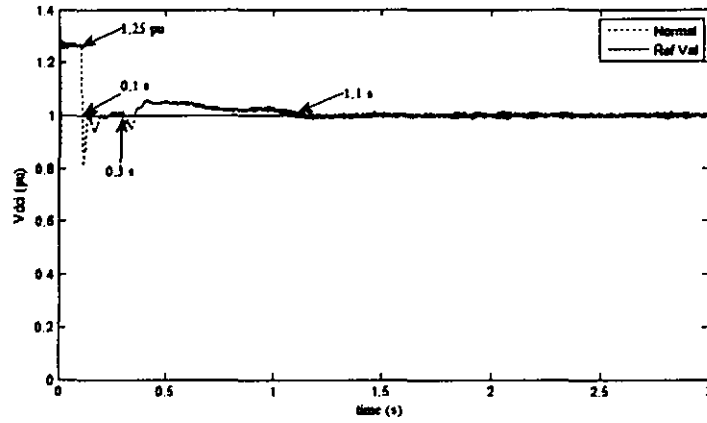


Figure 10. DC Link Voltage Measured on Inverter side

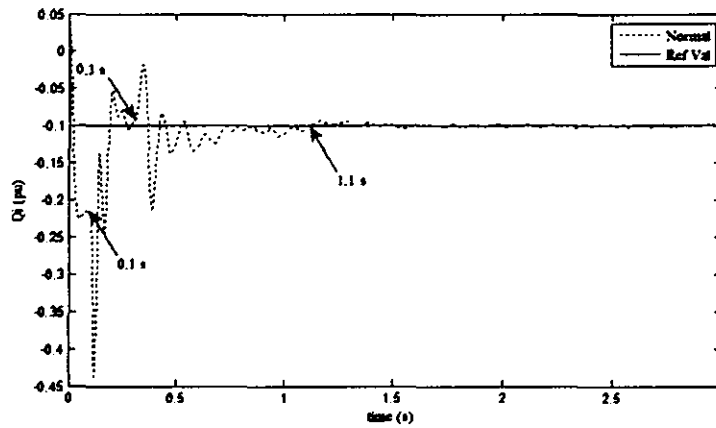


Figure 11. Reactive Power Flow into DC Link- Inverter side

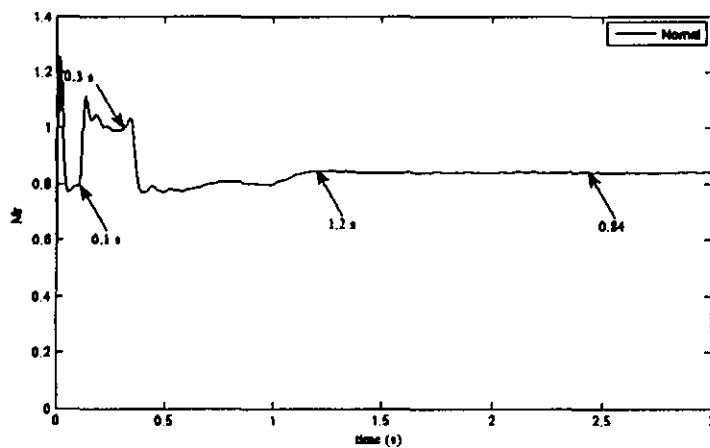


Figure 12. Modulation Index – Rectifier side

Figure 12 shows the variation of the modulation index at the rectifier end.

6. Conclusion

Instantaneous power theory is advantageous for measuring real and reactive power, as it is suitable for steady and transient states as well as for non sinusoidal waveforms, a distinct possibility in presence of power electronics related harmonics, during system operation. Similarity transformation can be used to obtain a fully decoupled model for the inner current control loop. Control circuit implementation involves original current and voltage state variables. However, to facilitate small signal stability assessment of a composite system comprising of VSC-HVDC link as well as interfacing ac system, the variables need to be transformed while framing the state matrix.

7. LIST OF SYMBOLS AND ABBREVIATIONS

7.1. SYMBOLS

u	ac voltage of the converter
e	ac network voltage
i	ac network current
R	resistance of the transformer
L	inductance of the transformer
ω	angular velocity corresponding to the rated system frequency
V_{dc}	dc link voltage
P	real power
Q	reactive power
Suffix r, i	indicate rectifier and inverter sides respectively
Suffix $a-b-c$	three phase reference frame
Suffix α, β	Clarke's stationary frame
Suffix d, q	Synchronously rotating reference frame
M	modulation index
δ	phase shift between modulating signal and carrier signal in PWM module
θ	phase angle obtained through phase locked loop

7.2. ABBREVIATIONS

VSC	Voltage-Sourced Converter
HVDC	High-Voltage Direct Current transmission
IGBT	Insulated Gate Bipolar Transistor
PWM	Pulse Width Modulation
CSC	Current-Sourced Converter
PT	potential Transformer
CT	Current Transformer
PLL	Phase locked loop circuit

Appendix A

Noting that in Equations (6) and (7),

$$T_{dq0} \frac{d}{dt} T_{dq0}^{-1} = \frac{2}{3} \begin{bmatrix} \sin \omega t & \sin(\omega t - 120^\circ) & \sin(\omega t + 120^\circ) \\ \cos \omega t & \cos(\omega t - 120^\circ) & \cos(\omega t + 120^\circ) \\ \frac{1}{2} & \frac{1}{2} & \frac{1}{2} \end{bmatrix} \begin{bmatrix} \omega \cos \omega t & -\omega \sin \omega t & 0 \\ \omega \cos(\omega t - 120^\circ) & -\omega \sin(\omega t - 120^\circ) & 0 \\ \omega \cos(\omega t + 120^\circ) & -\omega \sin(\omega t + 120^\circ) & 0 \end{bmatrix}$$

$$T_{dq0} \frac{d}{dt} T_{dq0}^{-1} = \omega \begin{bmatrix} 0 & -1 & 0 \\ 1 & 0 & 0 \\ 0 & 0 & 0 \end{bmatrix}$$

Equations (6) and (7) reduce to

$$\begin{bmatrix} e_r^d \\ e_r^q \\ e_r^0 \end{bmatrix} = R_r \begin{bmatrix} i_r^d \\ i_r^q \\ i_r^0 \end{bmatrix} + L_r \frac{d}{dt} \begin{bmatrix} i_r^d \\ i_r^q \\ i_r^0 \end{bmatrix} + \omega_r L_r \begin{bmatrix} 0 & -1 & 0 \\ 1 & 0 & 0 \\ 0 & 0 & 0 \end{bmatrix} \begin{bmatrix} i_r^d \\ i_r^q \\ i_r^0 \end{bmatrix} + \begin{bmatrix} u_r^d \\ u_r^q \\ u_r^0 \end{bmatrix} \quad (\text{A.1})$$

$$\begin{bmatrix} e_i^d \\ e_i^q \\ e_i^0 \end{bmatrix} = R_i \begin{bmatrix} i_i^d \\ i_i^q \\ i_i^0 \end{bmatrix} + L_i \frac{d}{dt} \begin{bmatrix} i_i^d \\ i_i^q \\ i_i^0 \end{bmatrix} + \omega_i L_i \begin{bmatrix} 0 & -1 & 0 \\ 1 & 0 & 0 \\ 0 & 0 & 0 \end{bmatrix} \begin{bmatrix} i_i^d \\ i_i^q \\ i_i^0 \end{bmatrix} + \begin{bmatrix} u_i^d \\ u_i^q \\ u_i^0 \end{bmatrix} \quad (\text{A.2})$$

Relationship related to the rectifier side in Equation (14) can be written as

$$T_{dq0}^{-1} \begin{bmatrix} e_r^d \\ e_r^q \\ e_r^0 \end{bmatrix} = E_r \begin{bmatrix} \cos \omega_r t \\ \cos(\omega_r t - 120^\circ) \\ \cos(\omega_r t + 120^\circ) \end{bmatrix}$$

Pre-multiplying both sides by T_{dq0}

$$T_{dq0} T_{dq0}^{-1} \begin{bmatrix} e_r^d \\ e_r^q \\ e_r^0 \end{bmatrix} = E_r T_{dq0} \begin{bmatrix} \cos \omega_r t \\ \cos(\omega_r t - 120^\circ) \\ \cos(\omega_r t + 120^\circ) \end{bmatrix}$$

$$\begin{bmatrix} e_r^d \\ e_r^q \\ e_r^0 \end{bmatrix} = \frac{2}{3} E_r \begin{bmatrix} \sin \omega t & \sin(\omega t - 120^\circ) & \sin(\omega t + 120^\circ) \\ \cos \omega t & \cos(\omega t - 120^\circ) & \cos(\omega t + 120^\circ) \\ \frac{1}{2} & \frac{1}{2} & \frac{1}{2} \end{bmatrix} \begin{bmatrix} \cos \omega_r t \\ \cos(\omega_r t - 120^\circ) \\ \cos(\omega_r t + 120^\circ) \end{bmatrix}$$

$$\begin{bmatrix} e_r^d \\ e_r^q \\ e_r^0 \end{bmatrix} = \begin{bmatrix} 0 \\ E_r \\ 0 \end{bmatrix} \quad (\text{A.3})$$

Similarly, relationship related to the inverter side in Equation (14) becomes

$$\begin{bmatrix} e_i^d \\ e_i^q \\ e_i^0 \end{bmatrix} = \begin{bmatrix} 0 \\ E_i \\ 0 \end{bmatrix} \quad (\text{A.4})$$

The switching functions describing state of an IGBT in rectifier and inverter end converters, and assuming a sinusoidal signal modulating the carrier input in the PWM based IGBT gating module are given by

$$\begin{aligned}
\begin{bmatrix} S_r^a \\ S_r^b \\ S_r^c \end{bmatrix} &= \begin{bmatrix} \frac{1}{2} + \frac{M_r}{2} \cos(\omega_r t - \delta_r) \\ \frac{1}{2} + \frac{M_r}{2} \cos(\omega_r t - \delta_r - 120^\circ) \\ \frac{1}{2} + \frac{M_r}{2} \cos(\omega_r t - \delta_r + 120^\circ) \end{bmatrix} && \&& \begin{bmatrix} S_i^a \\ S_i^b \\ S_i^c \end{bmatrix} = \begin{bmatrix} \frac{1}{2} + \frac{M_i}{2} \cos(\omega_i t - \delta_i) \\ \frac{1}{2} + \frac{M_i}{2} \cos(\omega_i t - \delta_i - 120^\circ) \\ \frac{1}{2} + \frac{M_i}{2} \cos(\omega_i t - \delta_i + 120^\circ) \end{bmatrix} \\
\begin{bmatrix} u_r^a \\ u_r^b \\ u_r^c \end{bmatrix} &= \begin{bmatrix} S_r^a \\ S_r^b \\ S_r^c \end{bmatrix} V_{dcr} - \left(\frac{V_{dcr}}{3} \right) \sum_{k=a,b,c} S_r^k && \&& \begin{bmatrix} u_i^a \\ u_i^b \\ u_i^c \end{bmatrix} = \begin{bmatrix} S_i^a \\ S_i^b \\ S_i^c \end{bmatrix} V_{dci} - \left(\frac{V_{dci}}{3} \right) \sum_{k=a,b,c} S_i^k
\end{aligned} \tag{A.5}$$

Using Equations in (A.5), the relationship between the converter ac side and dc side voltages on rectifier and inverter sides is given by

$$\begin{bmatrix} u_r^a \\ u_r^b \\ u_r^c \end{bmatrix} = \frac{M_r V_{dcr}}{2} \begin{bmatrix} \cos(\omega_r t - \delta_r) \\ \cos(\omega_r t - \delta_r - 120^\circ) \\ \cos(\omega_r t - \delta_r + 120^\circ) \end{bmatrix} \quad \& \quad \begin{bmatrix} u_i^a \\ u_i^b \\ u_i^c \end{bmatrix} = \frac{M_i V_{dci}}{2} \begin{bmatrix} \cos(\omega_i t - \delta_i) \\ \cos(\omega_i t - \delta_i - 120^\circ) \\ \cos(\omega_i t - \delta_i + 120^\circ) \end{bmatrix} \tag{A.6}$$

Rectifier related expression in Equation (A.6) can be written as

$$T_{dq0}^{-1} \begin{bmatrix} u_r^d \\ u_r^q \\ u_r^0 \end{bmatrix} = \frac{M_r V_{dcr}}{2} \begin{bmatrix} \cos(\omega_r t - \delta_r) \\ \cos(\omega_r t - \delta_r - 120^\circ) \\ \cos(\omega_r t - \delta_r + 120^\circ) \end{bmatrix}$$

Pre-multiplying both sides by T_{dq0} yields

$$\begin{aligned}
T_{dq0} T_{dq0}^{-1} \begin{bmatrix} u_r^d \\ u_r^q \\ u_r^0 \end{bmatrix} &= \frac{M_r V_{dcr}}{2} T_{dq0} \begin{bmatrix} \cos(\omega_r t - \delta_r) \\ \cos(\omega_r t - \delta_r - 120^\circ) \\ \cos(\omega_r t - \delta_r + 120^\circ) \end{bmatrix} \\
\begin{bmatrix} u_r^d \\ u_r^q \\ u_r^0 \end{bmatrix} &= \frac{2 M_r V_{dcr}}{3} \begin{bmatrix} \sin \omega t & \sin(\omega t - 120^\circ) & \sin(\omega t + 120^\circ) \\ \cos \omega t & \cos(\omega t - 120^\circ) & \cos(\omega t + 120^\circ) \\ \frac{1}{2} & \frac{1}{2} & \frac{1}{2} \end{bmatrix} \begin{bmatrix} \cos(\omega_r t - \delta_r) \\ \cos(\omega_r t - \delta_r - 120^\circ) \\ \cos(\omega_r t - \delta_r + 120^\circ) \end{bmatrix} \\
\begin{bmatrix} u_r^d \\ u_r^q \\ u_r^0 \end{bmatrix} &= \frac{M_r V_{dcr}}{2} \begin{bmatrix} \sin \delta_r \\ \cos \delta_r \\ 0 \end{bmatrix}
\end{aligned} \tag{A.7}$$

Similarly at the inverter end

$$\begin{bmatrix} u_i^d \\ u_i^q \\ u_i^0 \end{bmatrix} = \frac{M_i V_{dci}}{2} \begin{bmatrix} \sin \delta_i \\ \cos \delta_i \\ 0 \end{bmatrix} \tag{A.8}$$

Appendix B

Eigen values of the state matrix in Equation (12) can be determined by solving the characteristic equation given by $A - \lambda_r I = 0$

$$\begin{bmatrix} -\frac{R_r}{L_r} & \omega_r \\ -\omega_r & -\frac{R_r}{L_r} \end{bmatrix} - \lambda_r \begin{bmatrix} 1 & 0 \\ 0 & 1 \end{bmatrix} = 0 \tag{B.1}$$

Equation (B.1) yields two Eigen values

$$\lambda_{r1} = -\frac{R_r}{L_r} - j\omega_r \text{ and } \lambda_{r2} = -\frac{R_r}{L_r} - j\omega_r$$

Eigen vector corresponding to λ_{r1} , $V_1 = \begin{bmatrix} v_{11} \\ v_{21} \end{bmatrix}$, can be determined from $|A - \lambda_{r1}I|V_1 = 0$

$$\left\{ \begin{bmatrix} -\frac{R_r}{L_r} & \omega_r \\ -\omega_r & -\frac{R_r}{L_r} \end{bmatrix} - \lambda_{r1} \begin{bmatrix} 1 & 0 \\ 0 & 1 \end{bmatrix} \right\} \begin{bmatrix} v_{11} \\ v_{21} \end{bmatrix} = 0 \quad (\text{B.2})$$

Substituting $\lambda_{r1} = -\frac{R_r}{L_r} + j\omega_r$ in (B.2) yields

$$-\left[\frac{R_r}{L_r} - \frac{R_r}{L_r} + j\omega_r \right] v_{11} + \omega_r v_{21} = 0 \quad \& \quad -\omega_r v_{11} - \left[\frac{R_r}{L_r} - \frac{R_r}{L_r} + j\omega_r \right] v_{21} = 0$$

Or $-j\omega_r v_{11} + \omega_r v_{21} = 0 \quad \& \quad -\omega_r v_{11} - j\omega_r v_{21} = 0 \quad (\text{B.3})$

Treating v_{11} as the free variable in equation (B.3) and assigning an arbitrary value of 1 yields

$$V_1 = \begin{bmatrix} v_{11} = 1 \\ v_{21} = j1 \end{bmatrix}$$

Eigenvector corresponding to λ_{r2} , $V_2 = \begin{bmatrix} v_{12} \\ v_{22} \end{bmatrix}$ can be determined from $|A - \lambda_{r2}I|V_2 = 0$

$$\left\{ \begin{bmatrix} -\frac{R_r}{L_r} & \omega_r \\ -\omega_r & -\frac{R_r}{L_r} \end{bmatrix} - \lambda_{r2} \begin{bmatrix} 1 & 0 \\ 0 & 1 \end{bmatrix} \right\} \begin{bmatrix} v_{12} \\ v_{22} \end{bmatrix} = 0 \quad (\text{B.4})$$

Substituting $\lambda_{r2} = -\frac{R_r}{L_r} - j\omega_r$ in equation (B.4) yields

$$-\left[\frac{R_r}{L_r} - \frac{R_r}{L_r} - j\omega_r \right] v_{12} + \omega_r v_{22} = 0 \quad \& \quad -\omega_r v_{12} - \left[\frac{R_r}{L_r} - \frac{R_r}{L_r} - j\omega_r \right] v_{22} = 0$$

Or $j\omega_r v_{12} + \omega_r v_{22} = 0 \quad \& \quad -\omega_r v_{12} + j\omega_r v_{22} = 0 \quad (\text{B.5})$

Treating v_{22} as the free variable in Equation (B.5) and assigning an arbitrary value of 1

yields $V_2 = \begin{bmatrix} v_{12} = j1 \\ v_{22} = 1 \end{bmatrix}$

Modal matrix of the state matrix in Equation (12) is given as $P = [V_1 \ V_2] = \begin{bmatrix} 1 & j1 \\ j1 & 1 \end{bmatrix}$ and it's

inverse $P^{-1} = \frac{1}{2} \begin{bmatrix} 1 & -j1 \\ -j1 & 1 \end{bmatrix}$

Similarity transformation $P^{-1}AP$ of state matrix in Equation (12), which is of the form,

$$\dot{x} = Ax + Bu \text{ is given by } P^{-1}AP = \frac{1}{2} \begin{bmatrix} 1 & -j1 \\ -j1 & 1 \end{bmatrix} \begin{bmatrix} -\frac{R_r}{L_r} & \omega_r \\ -\omega_r & -\frac{R_r}{L_r} \end{bmatrix} \begin{bmatrix} 1 & j1 \\ j1 & 1 \end{bmatrix} \text{ leading to,}$$

$$P^{-1}AP = \begin{bmatrix} -\frac{R_r}{L_r} + j\omega_r & 0 \\ 0 & -\frac{R_r}{L_r} - j\omega_r \end{bmatrix} \quad (\text{B.6})$$

Appendix C

To facilitate modal analysis of a composite power system incorporating VSC-HVDC link, using the transformation $x = Px_z$, the state matrix in Equation (12), which is of the form,

$\dot{x} = Ax + Bu$ can be written as

$$P\dot{x}_z = APx_z + Bu \quad \text{or} \quad \dot{x}_z = P^{-1}APx_z + P^{-1}Bu \quad (\text{C.1})$$

Modal matrix and its inverse for the state matrix are given as $P = \begin{bmatrix} 1 & j1 \\ j1 & 1 \end{bmatrix}$ and

$$P^{-1} = \frac{1}{2} \begin{bmatrix} 1 & -j1 \\ -j1 & 1 \end{bmatrix}$$

Substituting these into the state equation and also substituting rectifier related expression in Equation (15),

$$\frac{d}{dt} \begin{bmatrix} i_{rz}^d \\ i_{rz}^q \end{bmatrix} = \frac{1}{2} \begin{bmatrix} 1 & -j1 \\ -j1 & 1 \end{bmatrix} \begin{bmatrix} -\frac{R_r}{L_r} & \omega_r \\ -\omega_r & -\frac{R_r}{L_r} \end{bmatrix} \begin{bmatrix} 1 & j1 \\ j1 & 1 \end{bmatrix} \begin{bmatrix} i_{rz}^d \\ i_{rz}^q \end{bmatrix} + \frac{1}{2} \begin{bmatrix} 1 & -j1 \\ -j1 & 1 \end{bmatrix} \left\{ \frac{1}{L_r} \begin{bmatrix} 0 \\ E_r \end{bmatrix} - \frac{1}{L_r} \begin{bmatrix} u_r^d \\ u_r^q \end{bmatrix} \right\}$$

The equation after using Equation (B.6) reduces to,

$$\frac{d}{dt} \begin{bmatrix} i_{rz}^d \\ i_{rz}^q \end{bmatrix} = \begin{bmatrix} -\frac{R_r}{L_r} + j\omega_r & 0 \\ 0 & -\frac{R_r}{L_r} - j\omega_r \end{bmatrix} \begin{bmatrix} i_{rz}^d \\ i_{rz}^q \end{bmatrix} + \frac{1}{2L_r} \begin{bmatrix} -jE_r \\ E_r \end{bmatrix} - \frac{1}{2L_r} \begin{bmatrix} u_r^d - ju_r^q \\ u_r^q - ju_r^d \end{bmatrix} \quad (\text{C.2})$$

jE_r , ju_r^q and ju_r^d in Equation (C.2) are the projections of E_r , u_r^q , u_r^d on their respective orthogonal axes in an orthogonal system of coordinates and reduce to zero. Equation C.2 can be written as

$$\frac{d}{dt} \begin{bmatrix} i_{rz}^d \\ i_{rz}^q \end{bmatrix} = \begin{bmatrix} -\frac{R_r}{L_r} + j\omega_r & 0 \\ 0 & -\frac{R_r}{L_r} - j\omega_r \end{bmatrix} \begin{bmatrix} i_{rz}^d \\ i_{rz}^q \end{bmatrix} + \frac{1}{2L_r} \begin{bmatrix} -u_r^d \\ E_r - u_r^q \end{bmatrix} \quad (\text{C.3})$$

Similarly the state Equation (13) reduces to,

$$\frac{d}{dt} \begin{bmatrix} i_{iz}^d \\ i_{iz}^q \end{bmatrix} = \begin{bmatrix} -\frac{R_l}{L_l} + j\omega_r & 0 \\ 0 & -\frac{R_l}{L_l} - j\omega_r \end{bmatrix} \begin{bmatrix} i_{iz}^d \\ i_{iz}^q \end{bmatrix} + \frac{1}{2L_l} \begin{bmatrix} -u_l^d \\ E_l - u_l^q \end{bmatrix} \quad (\text{C.4})$$

Whereas $i_{rz}^d, i_{rz}^q, i_{iz}^d, i_{iz}^q$ are not the original state variables, the state variables related to the voltage i.e. u_r^d and u_r^q are the original state variables.

References

- [1] Bahrman MP. Overview of HVDC transmission. Proceedings of 2006 IEEE Power Systems Conference and Exposition (PSCE), 2006; 18–23.
- [2] Asplund G. Application of HVDC Light to power system enhancement. Proceedings of the IEEE PES 2000 winter meeting, 2000; 4: 2498–2503.
- [3] Eriksson K. HVDC Light and development of Voltage Source Converters. Proceedings of IEEE/PES T and 2002 Latin American Conference, Sao Paulo, Brazil, 2002; 1–5.
- [4] Skytt AK, Holmberg P, Juhlin L.E. HVDC Light for connection of wind farms. Proceedings of the 2nd International Workshop on Transmission Networks for off shore Wind Farms Royal Institute of Technology Stockholm, Sweden, 2001.
- [5] Andersen BR. VSC transmission. CIGRE B4. HVDC and Power Electronics HVDC Colloquium, Oslo, 2006.
- [6] Schettler F, Huang H, Christl N. HVDC Transmission Systems using Voltage Sourced Converters- Design and Application. Proceedings of the IEEE PES 2000 summer meeting, 2000, 2: 715–720.
- [7] Stretch N, Kazerani M, Shatshat REI. A Current-Sourced Converter-based HVDC Light Transmission System. Proceedings of 2006 IEEE International Symposium on Industrial Electronics (ISIE), Canada, 2006; 3: 2001–2006.
- [8] Ye Y, kazerani M, Quintana VH. Current-Source Converter Based STATCOM: Modeling and Control. IEEE Transactions Power Delivery, 2005; 20 (2): 795 – 800.
- [9] Bahrman M, Edris AA, Haley R. Asynchronous back-to-back HVDC link with the voltage source converters. Presented at Minnesota Power Systems Conference, USA, 1999; 1–7.
- [10] Schauder C, Mehta H. Vector analysis and control of advanced static VAR compensators. IEE Proceedings Generation, Transmission and Distribution, 1993; 140 (4): 299–306.
- [11] Du C, Sannino A, Bollen M. Analysis of the Control Algorithms of Voltage-Source Converter HVDC. Proceeding of 2005 IEEE Russia Power Tech, 2005; 1–7.
- [12] Nikkhajoei H, Iravani R. Dynamic Model and Control of AC–DC–AC Voltage-Sourced Converter System for Distributed Resources. IEEE Transactions Power Delivery, 2007; 22 (2): 1169–1178.
- [13] Lindberg A, Lindberg L. Inner current loop for large voltage source converters operating at low switching frequency. Proceedings of 5th International Conference on Power Electronics and Variable-Speed Drives IEE, 1994; 217–222.
- [14] Lindberg A, Larsson T. PWM and control of three level voltage source converters in an HVDC back-to-back station. Proceedings of 6th International Conference on AC–DC Power Transmission IEE, 1996; 297 – 302.
- [15] Akagi H, Kanazawa Y, Nabae A. Instantaneous reactive power compensators comprising switching devices without energy storage components. IEEE Transactions Industry Applications, 1984; IA-20 (3) 625–630.
- [16] Mahjoub A, Mukerjee R. Modeling of Controller for Voltage Sourced Converter based HVDC Transmission System. Proceedings of IEEE 2nd International Power and Energy Conference (PECon 08), Johor Baharu, Malaysia, 2008; 849–854.

Tables

Table 1. System Description

Converter Transformer	200 MVA, 0.15 p.u.	230kV/100kV
DC Link Rating	200 MW	$\pm 100\text{Kv}$
AC Side Harmonic Filters	40 MVAR	Quality Factor = 15
27 th High Pass Damped	18 MVAR	
54 th High Pass Damped	22 MVAR	
Outer Loop Controllers		
P controller	$K_p=0.0$	$K_i=20.0$
Q controller	$K_p=0.0$	$K_i=20.0$
V_{dc} controller	$K_p=2.0$	$K_i=40.0$
Inner loop current controller	$K_p=4.0$	$K_i=40.0$

Table 2. Scenario Description

Case Study Description	Normal Fault Level
AC network Short Circuit Level	
Rectifier Side	2000 MVA
Inverter Side	2000 MVA
Rectifier Side Controller	P, Q
Active controllers activated at	$t = 0.3 \text{ sec}$
P_{ref}	1.0 p.u.
Q_{ref}	0.0 p.u.
Inverter Side Controller	V_{dc}, Q
Active controllers activated at	$t = 0.1 \text{ sec}$
P_{ref}	1.0 p.u.
V_{dciref}	1.0 p.u.
Q_{iref}	-0.1 p.u.